IMAGE PROCESSING AND EXPERIMENTAL TECHNIQUES TO CHARACTERIZE THE HYDRAULIC PERFORMANCE OF GRATE INLETS

This Doctoral Thesis dissertation concerns two main research topic: the analysis of the flow velocity pattern in the nearness of a grate inlet through Surface Flow Image Velocimetry (SFIV) technique and the study of overflow of surcharged sewer system through grate inlets.

Concerning the first main issue, a methodology able to reproduce the velocity field and, consequently, the flow distribution around the grate inlet, has been proposed. This methodology can be used by inlet manufacturers to improve the design of their products in order to collect as much water as possible in case of storms. In fact, water is collected by two main mechanisms: the frontal flow where the amount of water is intercepted through the upper part of the inlet (orthogonal to the flow direction), and the lateral flow where the flow is intercepted through the lateral side of the inlet (parallel to the main flow direction). As demonstrated and discussed in this thesis, this lateral inflow, due to the transversal component of the flow, is around a 20 - 30% respect to the 70 - 80% of the frontal flow.

The second main issue treated in this thesis has been the behavior of the overflow by grate inlet due to pressured sewer systems. The estimation of grate inlet discharge coefficients and the head energy loss in this kind of situation could be very important to provide useful values to be used by commercial numerical code that nowadays use common default values assuming orifice or weir approaches.

The experimental campaigns related to the two main topics were carried out using a physical model in real scale located in the Hydraulic Laboratory of the Technical University of Catalonia. It is important to consider that the SFIV technique method could be also extrapolated to other applications in the fields of hydraulic engineering like rivers and costal engineering.

flumen Dinàmica fluvial i enginyeria hidrològica

UPC

CIMNE

2019

IMAGE PROCESSING AND EXPERIMENTAL TECHNIQUES TO CHARACTERIZE THE HYDRAULIC PERFORMANCE OF GRATE INLETS Author: Jackson David Tellez Alvarez

UPC

IMAGE PROCESSING AND EXPERIMENTAL TECHNIQUES TO CHARACTERIZE THE HYDRAULIC PERFORMANCE OF GRATE INLETS

THIS DISSERTATION IS SUBMITTED FOR THE DEGREE OF DOCTOR OF PHILOSOPHY

Author: Jackson David Tellez Alvarez

April 2019

SUPERVISORS:
Manuel Gómez Valentín
Beniamino Russo

flumen Dinàmica fluvial i enginyeria hidrològica

UPC

CIMNE

UNIVERSITAT POLITÈCNICA DE CATALUNYA BARCELONATECH

Image processing and experimental techniques to characterize the hydraulic performance of grate inlets

Jackson David Tellez Alvarez

TECHNICAL UNIVERSITY OF CATALONIA

BARCELONATECH

DOCTORATE PROGRAM IN CIVIL ENGINEERING

DOCTORAL THESIS

"IMAGE PROCESSING AND EXPERIMENTAL TECHNIQUES TO CHARACTERIZE THE HYDRAULIC PERFORMANCE OF GRATE INLETS"

Author:

Jackson David TELLEZ ALVAREZ

(Identify ORCID :0000-0009-1428-9872)

Supervisors:

Professor Manuel GÓMEZ VALENTÍN

Professor Beniamino RUSSO

A thesis submitted in fulfilment of the requirements for the degree of Doctor of Philosophy in the

FLUMEN INSTITUTE

DEPARTMENT OF CIVIL AND ENVIRONMENTAL ENGINEERING

E.T.S. d'Enginyers de Camins, Jordi Girona 1-3, D1, 08034 Barcelona – www.flumen.upc.edu

April 2019, Barcelona

Acknowledgments / Agradecimientos

Mi más profundo agradecimiento a toda mi familia, en especial a mi madre Roxana por el gran apoyo emocional y el sacrificio que han ayudado a que esta tesis se haga realidad. A mi Padre Guido, por darme su apoyo y a mis hermanos Kristian, Guido, Rolando y Roxana por apoyarme siempre e incentivarme a terminar este documento.

Gracias a mis asesores, el Prof. Manuel Gómez y el Prof. Beniamino Russo por darme la oportunidad de realizar mi tesis doctoral. Para ellos gracias por la paciencia y la libertad para realizar este trabajo de investigación.

Un profundo agradecimiento especial al Prof. Manuel Gómez, por incluirme en algunos proyectos y trabajos en el Instituto Flumen. Además, por la guía constante en esta tesis doctoral, dándome un gran soporte académico y personal durante esta investigación.

Gracias al Prof. Beniamino Russo, que ha dedicado su tiempo en consejos para realizar este documento, y por su disponibilidad siempre que fue necesario y por el seguimiento de este trabajo.

Gracias al Prof. Jose M. Redondo, por los momentos de conferencias y algún proyecto que hemos compartido y que me han servido para adquirir conocimientos en otras áreas.

Quiero expresar mi sincero agradecimiento al Profesor Ilias Sibgatullin por permitirme aprender y compartir conocimientos en la Facultad de Mecánica y Matemáticas de la Universidad de Moscú Lomonosov. De igual manera extiendo mi agradecimiento al Dr. Sergei Strijhak, Dr. Matvey Kraposhin, Arina Kryuchkova, Victoria Korchagova que forman parte del equipo del Instituto de Sistemas de Programación de la Academia de Ciencias Rusas, su apoyo fue fundamental durante el período de estancia de investigación. Asimismo, amplío mi gratitud al Profesor Yuli Chashechkin y Andrey Ilynyh, quienes me permitieron colaborar en el Laboratorio de Mecánica de Fluidos del Instituto de Problemas en Mecánica de la Academia de Ciencias Rusas.

A las personas que trabajan en el Laboratorio de Hidráulica, especialmente a Jaime, Juan Pomares, Xavi y Marcos que me han ayudado y brindado su soporte técnico durante las campañas experimentales.

A mis compañeros del Instituto Flumen del Departamento de la UPC, que hemos pasado momentos lindos: Eduardo Martínez, Eduard Galvis, Jose Luis Aragón, Esteban Sánchez, Hans Sánchez, Gonzalo Olivares, Jordi Prats, Marcos Sanz, Jeannette Zambrano, Georgina Corestein, Úrsula, Rodrigo Concha, Rodrigo Ugarte, Carlos Caro, Soledad Estrella, Belén Martí, Anaïs Ramos, Marina Arbat, Arnau Triadú, Jeannette Zambrano, Pablo Sánchez, Georigina Corestein, Irene Seco, Klaudia Horváth, Victor Rendon, Santos Trinidad y Chiara Cosco. Y por último un gran agradecimiento a Waiteng por sus correcciones de este documento.

También agradezco a los Profesores Ernest Bladé, Marti Sánchez, Josep Dolz y Daniel Niñerola por integrarme en el departamento de Hidráulica siendo amables, disponibles en colaborar y haber hecho más llevadero este trabajo.

Gracias a otros compañeros como son Cristina Fernandez, Andrés Díaz, Carolina Leyton y Gustavo Agredo, con quienes he compartido bonitos momentos en la UPC. Y por último a Cesca Torrella, Ceferino Robledo y Silvia Aranda, por su amabilidad y soporte en la UPC.

Abstract

This Doctoral Thesis dissertation concerns two main research topic: the analysis of the flow velocity pattern in the nearness of a grate inlet through Surface Flow Image Velocimetry (SFIV) technique and the study of overflow of surcharged sewer system through grate inlets.

Concerning the first main issue, a methodology able to reproduce the velocity field and, consequently, the flow distribution around the grate inlet, has been proposed. This methodology can be used by inlet manufacturers to improve the design of their products in order to collect as much water as possible in case of storms. In fact, water is collected by two main mechanisms: the frontal flow where the amount of water is intercepted through the upper part of the inlet (orthogonal to the flow direction), and the lateral flow where the flow is intercepted through the lateral side of the inlet (parallel to the main flow direction). As demonstrated and discussed in this thesis, this lateral inflow, due to the transversal component of the flow, is around a 20 - 30% respect to the 70 - 80% of the frontal flow.

The second main issue treated in this thesis has been the behavior of the overflow by grate inlet due to pressured sewer systems. The estimation of grate inlet discharge coefficients and the head energy loss in this kind of situation could be very important to provide useful values to be used by commercial numerical code that nowadays use common default values assuming orifice or weir approaches.

The experimental campaigns related to the two main topics were carried out using a physical model in real scale located in the Hydraulic Laboratory of the Technical University of Catalonia. It is important to consider that the SFIV technique method could be also extrapolated to other applications in the fields of hydraulic engineering like rivers and costal engineering.

Keywords

Grate inlet, Surface Flow Image Velocimetry (SFIV), image processing, overflow of surcharged sewers, discharge coefficients.

Resumen

Esta tesis doctoral trata dos temas principales: el análisis del patrón de velocidad de flujo en la proximidad de una reja de alcantarillado a través de la técnica de la velocimetría por imagen del flujo de superficie (en inglés Surface Flow Image Velocimetry, SFIV) y la salida de un flujo por una reja producido por la entrada en carga de un sistema de alcantarillado.

En cuanto a la primera cuestión, se propuso una metodología capaz de reproducir el campo de velocidad y, consecuentemente, la distribución del caudal alrededor del sumidero. Esta metodología puede ser utilizada por los fabricantes de rejas de alcantarillado para poder mejorar el diseño de sus productos y así poder recoger la mayor cantidad de agua posible durante eventos de lluvia. De hecho, el agua es interceptada a través de dos mecanismos principales: el flujo frontal donde la cantidad de agua es interceptada a través de la parte aguas arriba de la reja (lado ortogonal a la dirección del flujo), y el flujo lateral donde el flujo es interceptado a través del lado lateral de la reja (lado paralelo a la dirección principal del caudal). Como se demuestra y se discute en esta tesis, esta afluencia lateral, debido al componente transversal del flujo, es alrededor de un 20-30% respecto al 70-80% del flujo frontal.

La segunda cuestión principal tratada en esta tesis ha sido el comportamiento del flujo producido por la entrada en carga de un colector de alcantarillado y la salida de dicho flujo al exterior a través de una reja de alcantarillado. La estimación de los coeficientes de descarga de la reja y la pérdida de energía hidráulica en estas condiciones podrían ser muy importantes para proporcionar valores útiles para ser utilizados por códigos numéricos comerciales que hoy en día utilizan valores predeterminados comunes asumiendo enfoques hidráulicos de tipo orificio o vertedero.

Las campañas experimentales relacionadas con los dos temas principales se llevaron a cabo utilizando un modelo físico en escala real ubicado en el laboratorio hidráulico de la Universidad Politécnica de Cataluña. Es importante tener en cuenta que el método de la técnica SFIV podría ser también extrapolado a otras aplicaciones en los campos de la ingeniería hidráulica como la ingeniería de ríos o la ingeniería costera.

Palabras clave

Reja de alcantarillado, Velocimetría por Imagen del Flujo Superficial (SFIV), procesamiento de imágenes, entrada en carga de un colector de alcantarillado, coeficientes de descarga.

Symbols and abbreviations

Latin letters

$\boldsymbol{A}$	cross-section flow area.
A_1	area of interrogation domain.
$A_{i,j}$	velocity gradient tensor.
A'	area of a small segment that divides STI into a number of portions.
A_{est}	area estimate of the section.
A_g	minimum area that includes all the voids in the grate inlet.
A_h	grate hole's area.
B	water spread.
B_t	distance from the tank.
c, d	constants from each device provided by the manufacturer.
c_τ	constant that depends on the ability of the analysis procedure to determine the displacement between the images.
$\boldsymbol{C}$	tracer number density / value of coherency.
C_d	discharge coefficient including all the effects of energy losses through the grate, effect of approaching velocity, etc.
d_t	distance between two consecutive position of the tracers during δt.
d_τ	particle image diameter.
d_p	particle diameter.
E	efficiency of the grate inlet between 0 and 1.
E'	inlet efficiency related to a width of half roadway x=3 m.
$Framerate_{camera}$	framerate of camera.
g	gravitational acceleration (9.81 m/s^2).
g(x,t)	grey level intensity.

$\boldsymbol{I}$	normalized image intensity.
I_x	street transversal slope.
I_y	street longitudinal slope.
$\boldsymbol{J}$	appropriate orientation vector of STIV method.
k	coefficient related to the street geometric conditions and to the flow depth.
k_r	adjustment coefficient for large-scale roughness flow in rivers (k_r=0.85, recommend the literature).
K	energy loss coefficient.
l_x, l_y	dimensions of the image in x and y direction.
L	length of the grate inlet.
L_X, L_Y	linear dimensions of the recording medium.
m	value corresponding to the total number of paths identified for each case.
M_0	paraxial image magnification.
n	number of turns of current meter.
n_d	number of diagonal bars.
n_i	total number of positions along the channel.
n_l	number of longitudinal bars.
n_t	number of transversal bars.
n_0	nominal refractive index of the medium.
N_I	mean number of particles per interrogation volume in the fluid
p	ratio between the void area and A_g.
p_0	Intensity of image.
$p(X)$	position-dependent sensitive of the pixel.
$\overrightarrow{p_1}$	position vector of the target at instant t_1.
$\overrightarrow{p_2}$	position vector of the target at instant t_2.
P_{ij} (t)	intensity for the perturbed density field.
Q	approaching discharge on the UPC platform of 3 meters width.
Q_{est}	discharge.
Q_F	frontal flow rate.

Q_I	inflow.
Q_{Int}	discharge intercepted by the grate inlet.
$Q_{outflow}$	outflow discharge from surcharge flow through the grate inlet.
$\mathrm{Q_0}$	outflow /carryover of the grate
$\mathrm{Q_{Out}}$	outflow.
$Q_{roadway}$	flow approaching to an inlet related to half roadway
Q_s	lateral flow rate.
Q_t	total flow rate of SFIV technique.
Q_1	outflow (1).
Q_2	outflow (2).
Q_3	outflow (3).
t	time exposed by the light pulse.
t	time.
t_1	time 1
t_2	time 2
T	matrix of LSPIV method.
u	velocity.
$\mathrm{u_{max}}$	full-scale velocity.
$\vec{u}$	mean velocity vector of the target.
U_x, V_y	components of velocity on a surface.
v	flow velocity.
$v_{outflow}$	velocity of surcharge flow through the grate inlet ($v_{outflow} = \frac{Q_{outflow}}{A_h}$)
V_i	instantaneous velocity for two consecutive time.
$\overline{V_j}$	mean velocity obtained by averaging each of the instantaneous velocities.
$V_{Mean\ velocity}$	mean velocity.
$\mathrm{V_s}$	velocity field using SFIV technique.
V_s^*	mean surface velocity obtained for each case by averaging the mean velocity of each tracer or particles.
$(V_m)_{est}$	is the estimated mean velocity.

$V_{(\frac{Pixel}{Frame})}$	framerate of camera (Pixel/Frame).
W	width of the grate inlet.
W_t	is the width of the tank.
x	width of the road (generally a half of roadway).
x	horizontal coordinate.
$x_p(t)$	position of the particles in the fluids as function of time t
x_i, z_j	location of the centre of the window.
X	position vector in image domain.
X,Y	in-plane coordinates of **X**.
$X_{i,j}$	location of its center.
$X_p(t)$	position of the image on the camera as a function of time t.
y	flow depth or water depth / Vertical coordinate.
y_{est}	flow depth estimated.
z_o	object distance from the Z=0 plane to the effective center of the lens.
Z_0	image distance from the effective center of the lens to the image plane.

Greek letters

αη or (1- α)η	alternating black and white region of widths.
β	equal to $\beta = \left(\frac{\rho_0}{n_0}\right)\left(\frac{d_n}{d_\rho}\right) \approx 0.184.$
δ_t	Increased time for image capture.
δz	depth of field.
Δh	water level above the grate.
Δh_k	difference of water level above the grate.
$\Delta\xi$	displacements in the x direction along the tank.
$\Delta\zeta$	displacements in the vertical z direction along the tank.
Δx	displacement of the marker, located at x at time t.
$\Delta x_{p,\,max}$	particle displacement associated with the full-scale velocity.
$\Delta x^*, \Delta z$	representation of the size of the region.
Δy	displacement of the marker, locater at y at the time t.

Δz_0	thickness of the light sheet.
$\Delta_{size\ IA}$	Size of interrogation area (IA).
Δt	time interval, separating observations of the marker images.
$\Delta_{t\ camera}$	interval of time.
ε	Exposure time.
η	spacing of the lines on the mask.
θ	angle of the platform.
λ	light wavelength.
ρ_0	nominal reference density (1000 kgm^{-3}).
$\boldsymbol{\sigma_{\Delta X}}$	root mean square displacement error.
τ_0	low-pass-filter time constant.
$\emptyset$	orientation angle of STIV method.
$\overline{\emptyset}$	mean orientation angle of STIV method.

Abbreviation

CCD	charge-coupled device (image sensor).
DVR	dynamic velocity range.
DSR	dynamic spatial range.
HID	high image density.
LID	low image Density.
PIV	particle image velocimetry.
PTV	particle tracking velocimetry.
RMS	root mean square.
SFIV	surface flow image velocimetry.

List of Figures

List of Tables

Contents

Chapter 1 Introduction to visualization technique. Main objectives of the thesis

1.1 Introduction of visualization technique

In the last decades, the flow visualization techniques started to study more deeply to quantify the flow measurements in hydraulic applications where it has gone of the hand of the evolution of the technology. Besides, many techniques were developed according to the principle of Particle Image Velocimetry (PIV) with specific objectives of researchers.

The visualization techniques for hydraulic applications were applied in the hydraulic research because it is possible to quantify the flow measure in a non-intrusive way for a large domain and capable to reproduce the velocity field while other methods only provide values in a single point.

Besides, many lines of research are focussed on measures of the river flow discharge through visualization techniques, because this is a non-intrusive technique capable to reproduce the behavior of the approaching flow in rivers. However, in urban areas, it is difficult to do hydraulic measures during floods too. For this reason, the challenge of the thesis was to develop a methodology of the technique called Surface Flow Image Technique (SFIV) to reproduce the field velocities in two directions and the distribution of the flow with application in urban hydrology as the flow behavior near grate inlets.

1.2 Motivation

To prevent flooding caused by inadequate sewer systems has become an important issue in urban drainage. Potential damage from prolonged flooding in urban areas can easily arrive to millions of euros. Normally the residents of the cities pay services fees and they expect that the urban drainage system operates effectively without fear of failure due to weather conditions. The drainage systems designed to cope with the most extreme storm conditions would be too expensive to build and operate and it is better to do a balance with the technical conditions and economic restrictions of the cities (**Schmitt et al. 2004**).

In the catalogues of grates, there are many different types and shapes. Some of them capture flow better than others or have a greater area of voids, some have diagonal bars, others transversal bars, etc., such a variety of grates depends not only on their functionality but also on aesthetics reasons. New designs are decided in response to grates dimensions, shapes, integration in street furniture and design, etc. The suppliers and manufacturers provide extensive data on structural behavior but rarely provide information about the hydraulics behavior of the grate, especially about its captured flow capacity.

The hydraulic efficiency of surface drainage structures depends at the same time on the rate of water removal from the gutter and on the amount of water that can enter into the storm system. In this field, the general problem of the urban drainage cannot consider separately the two following components (**Smith 2006**):

1. The surface system composed of streets, ditches, and various natural and artificial channels;
2. The subsurface storm sewer network.

For this reason, the study of the surface drainage system is a basic requirement for the correct behavior of a drainage system, because in case of flooding, hazard criteria are generally related to the surface runoff produced during the storm event. The geometry of the gutter, physical features of the surface and type of road drainage inlets have an influence on the hydraulics parameters of a stream circulating in urban areas. For this reason, in this thesis propose a methodology to measure surface velocity field through image processing technique obtaining the distribution of the flow around the grate inlet and the behavior of surcharge flow through the grate inlet.

1.3 Aim of study

The aim of the conducted research is to develop techniques able to predict the behavior of the flow around the grate inlet and the distribution of the intercepted flow rate on the grate. The idea is to generate the velocity field in the vicinity of some grates and compare these velocities and flow near the inlet, with the intercepted flow rate measured on the platform for the same grates in the Laboratory of Hydraulics of the Technical University of Catalonia (UPC).

1.4 Objectives of the thesis

The main objective of this thesis is to estimate the velocity field through the technique of digital image processing, the so-called Surface Flow Image Velocimetry (SFIV). In particular, the first stage of this technique has been applied to determine the velocity field and the distribution of the flow near the grate inlet and the second stage was to study the behavior of surcharged flow through the grate inlet and estimate the discharge coefficient.

The dissertation is divided into some specific objectives as follows:

- To perform an experimental campaign in the Laboratory of Hydraulics of the Technical University of Catalonia in the real-scale platform that can simulate the hydraulic behavior of a traffic lane developing a methodology of SFIV technique to generate the field velocities and distribution of flow rate around the grate inlet. We will take videos with a high-resolution camera, and from the image, we are going to reproduce the velocity patterns. At the same time, we are measuring the intercepted flow by the inlet.

- To validate the methodology of SFIV technique, this includes comparisons of the field velocities and distribution of the flow with two different software as Digiflow developed by the Department of Applied mathematics and Theoretical Physics at the University of Cambridge versus PIVlab that is a toolbox of MATLAB.

- To validate the methodology of SFIV technique, comparing the intercepted flow estimated from the images with the measured intercepted flow in the laboratory of hydraulics using the platform for three different grates.

- To develop a second experimental campaign to study the behavior of grate inlet under pressure flow conditions and estimate the discharge coefficient of the outflow for a range of flow from 10 to 50 l/s. Moreover, we will obtain the distribution of flow rate around the grate, and the field velocities using the SFIV technique.

1.5 Thesis structure

The rest of this document is organized as follows:

Chapter 2 presents the state-of-the-art of the description of the surface flow image velocimetry technique and software packages as well as some applications of image processing techniques in hydraulics engineering.

In Chapter 3, the experimental campaign performed for this dissertation and the research activities previously conducted in the Laboratory of Hydraulics of UPC are described. Moreover, the flow velocity pattern in the vicinity of the sewer grate, and the development of the Surface Flow Image Velocity technique are applied to calculate a balance of mass on the grate and estimates the frontal and lateral flow rate of the grate inlet.

Chapter 4 presents the second experimental campaign focused in the outflow from sewers in case of pressure flow conditions and calculate the discharge coefficients for sewer grates, also the distribution of the flow and velocity field around the grate inlet through SFIV technique.

Chapter 5, presents the conclusions, achieved results and give some suggestions for future works.

Chapter 2 State of the Art about high resolution techniques for velocity measurements

This chapter describes different measurement techniques capable to measure the flow velocities, where the methods of measuring can be classified in velocity measure in a single point or in more than one. These techniques are specially used for measuring velocities in problems of hydraulics, fluid mechanics and other engineering applications.

Basically, this chapter collects the state of the art of different schemes and methods about measurement techniques developed. Showing the review of some techniques to measure the flow in the physical model of urban drainage located in the Laboratory of Hydraulics of the Technical University of Catalonia as Acoustic Doppler Velocimetry (ADV), and some image processing techniques to measure the velocity of surface flow for engineering applications.

2.1 Measurement techniques

In order to investigate the traditional measurements and methods used to determine the velocities in a fluid, it requires a technique that allows simultaneous measurement of fluid velocity and the distribution of the discharge in a section. In the advances of traditional measurements and methods that are present in bibliography like Laser Doppler Velocimetry, Image based velocimetry techniques, Electro-magnetic measurement techniques, etc., some processes are more interesting to be used in the platform of grate inlet with this type of flow approaching. Therefore, this chapter studies and compares some instruments, techniques and methods available in the market such as Acoustic Doppler Velocimeter, Propeller Type Water Current meter and image based velocimetry techniques as Particle Image Velocimetry.

2.1.1 Propeller Type Water Current meter

The propeller type current meter is used to measure point velocity of water flow directly in m/s (**Figure 2:1**). This is used for flow measurement by mechanical effects from the rotor current meter. These equipments are based on the counting of number of rotations of a propeller, where an electronic signal is transmitted by the meter on each revolution allowing the total number of revolutions to be counted and timed. Because the rate at which the propeller rotates is directly related to the velocity of the water, the timed revolutions are used to determine the water velocity. Furthermore, these instruments are more used as oceanographic device or river discharge measurement.

This type of instrument is classified in mechanic propeller and electromagnetic propeller. where the mechanic propeller is divide in four types:

- Type of collector: helix. The propeller type is helical.
- Type of size instrument: Mini propeller (laboratory application), Counter balanced water current propeller, water current propeller Salmon and universal propeller (rivers and channels)

- Type of control box: accountant and chronometer and automatic counter
- Type of floats: bars, gangways and border.

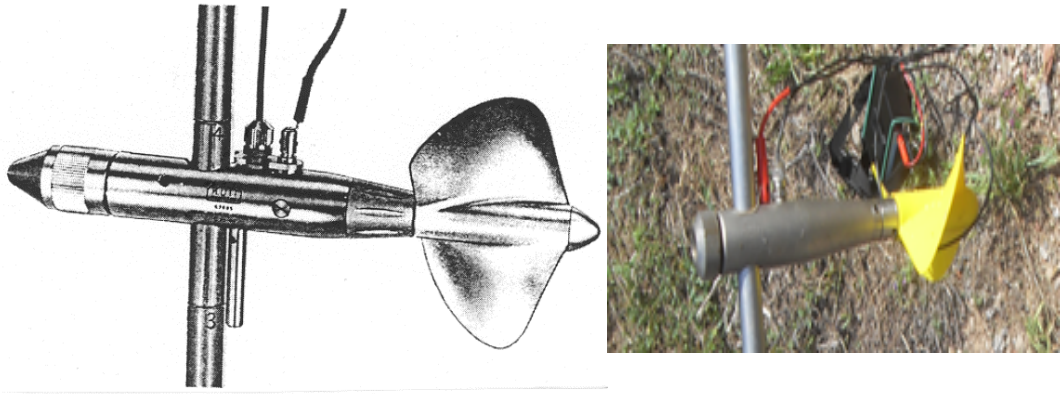

Figure 2:1 Current meter equipment.

Current meter consists of a propeller, attached to a shaft which rotates driven by the fluid stream. The measure is to compare the number of turn's makes the propeller per unit time (n) and this value is related to the water velocity (v) following an **Equation *[2:1]*** of the form:

$$\boldsymbol{v = c + dn} \qquad \textbf{[2. 1]}$$

Where: v : is the velocity (m/s)

c, d : are constants from each device provided by the manufacturer

n : number of turns of current meter (units/time)

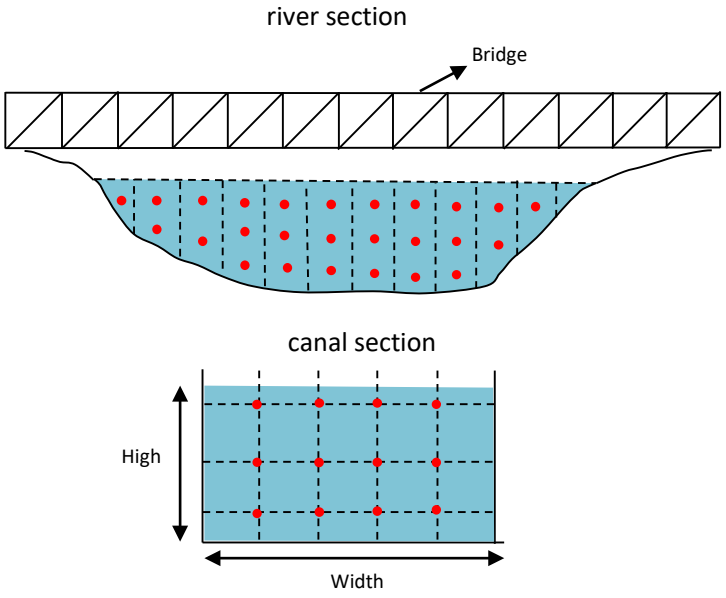

Figure 2:2 Measure with current meter.

The way of counting turns can be mechanical or electronic. These instruments provides the integration of the velocity corresponding to the diameter of the propeller. Using the micro-current propeller is possible to measure velocity in flow with few centimeters of depth (around 20 cm), considering that velocity is measured in a single one point. Flow measurement with current meter is basically measuring the velocity at various points of a cross section. To make a correct flow measurement is not enough to measure the velocity at a single point, is necessary to divide the section into several subsections. The method has the following four steps: The first is determine the section of study, and second is define the set of points of measurement, regularly spaced with more density of points where there is a velocity gradient high, the third is convert the number of turns of the propeller per unit of time in velocity (m/s), and finally with the velocity profile, the area of diagram of velocity is measured to obtain the flow rate of the section (m^3/s) (**Figure 2:2**). It is only used in steady flow conditions.

2.1.2 Acoustic Doppler Velocimeter (ADV)

The Doppler effect (or Doppler shift), named after the Austrian mathematician and physicist Christian Doppler who proposed it in 1842 (**Doppler, 1842**), is the change in frequency and wavelength of a wave for an observer moving relative to the source of the waves. The received frequency is increased (compared to the emitted frequency) during the approach, it is identical at the instant of passing by, and it is decreased during the recession.

Velocities can be measured in any body of water containing suitable acoustic scatters, or scattering particles may be added to the flow. Scatters are particles in the flow (typically suspended sediment) that reflect acoustic signals back to the probe receivers. The ADV probe actually measures the velocity of the scatters in the flow, but these small particles move with the same average speed as the water – the velocity it measures is consequently the velocity of the water.

Acoustic Doppler Velocimeter Vectrino from Nortek AS

This type of instrument is developed normally by the group SonTek or Nortek, where the price is around 15 000 Euros. In our laboratory of the Technical University of Catalonia we have the Nortek with the special software to store the data.

The Vectrino uses the Doppler Effect to measure current velocity by transmitting short pairs of sound pulses, listening to their echoes and, ultimately, measuring the change in pitch or frequency of the returned sound. Sound does not reflect from the water itself, but rather from particles suspended in the water. The particles are typically suspended sediment or air bubbles (**Nortek AS 2004**).

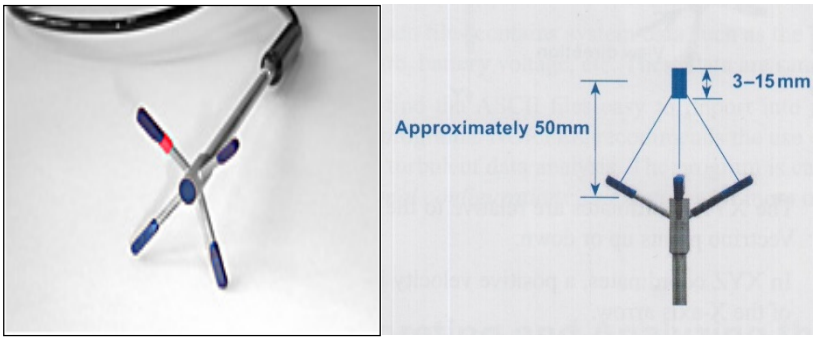

Figure 2:3 Down-looking cable probe close-up.

In contrast to standard Doppler profilers and current meters, an Acoustic Doppler Velocimeter Vectrino is a biostatic sonar. This means that it uses separate transmit and receive beams. It transmits through a central beam

and receives through four beams, each mounted inside a receiver arm and all focused on the same volume, to obtain the three velocity components from that volume. Two main types of beam configurations exist, a side-looking probe and a down-looking probe where the main difference is the orientation of the transmitter and receiver beams (**Figure 2:3 and Figure 2:4**).

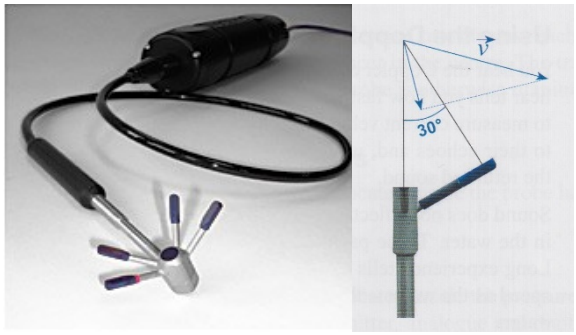

Figure 2:4 Side-looking cable probe.

Coordinate systems: The vectrino measures velocity components parallel to its three beams. Vectrino is more sensitive to the Z-velocity than it is to the X or Y velocity. Consequently, the Z-velocity component yields a lower measurement uncertainty. (**Figure 2:5**).

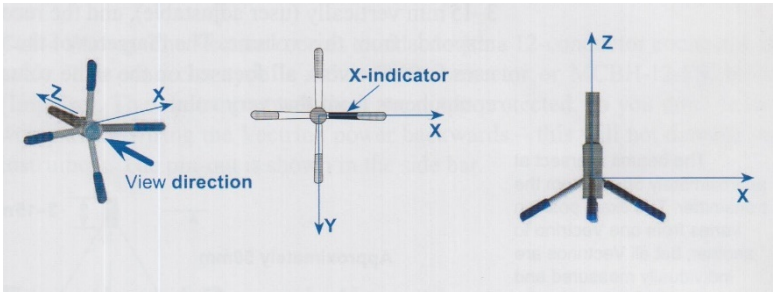

Figure 2:5 Definition of XYZ coordinates.

While the output sampling rate is between 1 and 200 [Hz], the internal sampling rate goes from 200 to 5000 [Hz]. The Doppler uncertainty (or noise) at 25 [Hz] equates 1 [%] of the velocity range (**Nortek AS, 2004**).

Although the probe is inserted into the flow, the sensing volume is several centimeters away from all physical parts of the probe, so the presence of the probe generally does not distort too much the measurement, except for supercritical flow conditions. All acoustic transducers should be submerged during data collection. Operating with the transducers out of water will not cause damage, but the obtained data will be meaningless.

2.1.3 Basics principles of Particle Image Velocimetry (PIV)

The first visualization by Leonardo da Vinci (1452 – 1519) sketched various flow fields over objects in a flowing stream (**Gad-el-Hak et al. 1998**). The scientist Ludwig Prandtl in 1904 propelled the investigation of flows a great step forward by making it possible to replace passive observations of nature with experiments carefully planned to extract information about the flow using visualization techniques.

However, at that time only a qualitative description of the flow field was possible. No quantitative data about flow velocity, etc., could be achieved.

The year 2014 marked the 30th anniversary of the term "Particle Image Velocimetry" (PIV) where the state of the art was started by some papers by (**Ian Grant, 1994**), the bibliography of PIV (**Adrian, 1996**) and some very good books on PIV by Raffel and Westerwel (**Raffel et al., 1998; 2007; Adrian and Westerweel, 2011**).

The first research to achieve such measurements employed the method of laser speckle for solid mechanics, that consist in the displacement of speckle patterns as a substitute of tracers of images (particles), where the light created by the interference pattern of the laser is represented in bright and dark areas and it is called speckles, considering that it could be applied to the measurements of fluid velocity fields. In 1997, the laser speckle phenomenon was applied to fluid flow by measuring the parabolic profile in laminar tube flow (**Barker and Fourney, 1977; Dudderar and Simpkins, 1977; Grousson and Mallick, 1977**). In 1983, Ph.D. student working at the Von Karman Institute showed practical measurements for laminar flow and turbulent flow of liquids and gases using laser speckle velocimetry (LSV), stirring up more interest within the fluid mechanics community (**Meynart, 1980a; 1980b; 1982a; 1982b; 1983b; 1983a**).

In 1991 Adrian showed the importance of particle images techniques for experimental fluid mechanics **(Adrian, 1991**). Many types of research became interested in PIV since because these techniques permit studying the structure of turbulence flows. Hence, a successful measurement techniques must be able to measure over a wide dynamic range of scales in length and velocity (**Adrian, 2004; 2005**)

Flow visualization is useful to understand the mechanics of a particular flow field and the information provided is invaluable for rapid feedback during experimental development (**Adrian and Westerweel, 2011**). This may be particularly important when a single camera for PIV provides a 2D image of the real complex flows.

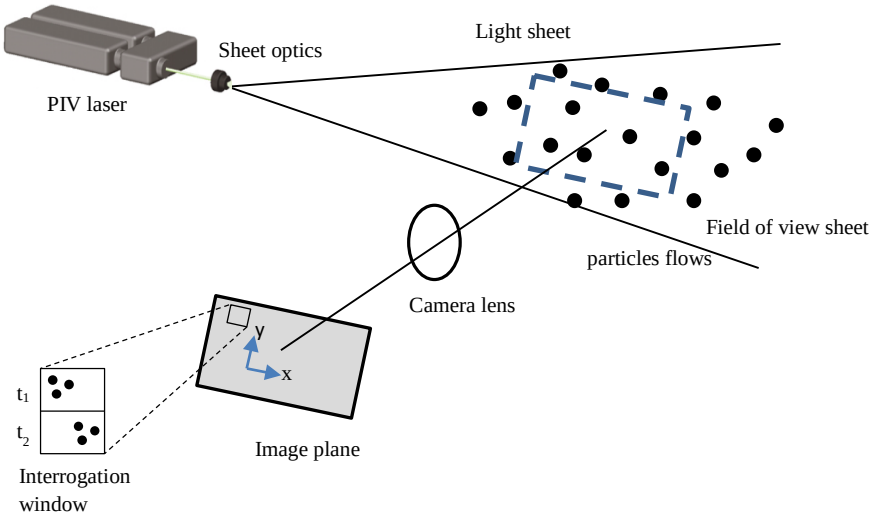

Figure 2:6 PIV laboratory systems.

In general, the Particle Image Velocimetry method (PIV) is a classical velocity measurement through the video camera that returns instantaneous fields of the vector velocity by the fundamental definition of velocity and estimate the local velocity u from the **Equation *[2:1]*** (**Figure 2:6**)

$$\boldsymbol{u(x,t) = \frac{\Delta x(x,t)}{\Delta t}} \qquad \textbf{[2:1]}$$

Where: u : is the velocity (m/s)

Δx : is a the displacement of the marker, located at x at time t (m)

Δt : is the over short time interval, separating observations of the marker images (s)

The **Figure 2:6**, show a scheme of typical PIV systems used to obtain instantaneous velocity measurement for fluids. The mechanism is based in the addition of particles in the fluid (tracers) following on a stream. The analyzed region is illuminated by a laser that synchronizes with a camera (normally digital camera CCD). For the post-process of image sequence, it is used a software of PIV. Through the software it is possible to follow the particles using a cross-correlation between two consecutive images.

2.2 PIV fundamentals

Before going into details of the PIV technique, some general steps in the procedure for determining the velocity field are shown in **Figure 2:7**. PIV is a non-intrusive velocity measurement, in contrast to techniques for the measurement of flow velocities employing probes such as pressure tubes or hot wires, the PIV technique being an optical technique works non-intrusively, where in the flow should be seeded particles as tracers, the size of particles need to been small enough to follow the fluid acceleration and capable to be visualize by the camera. Also, PIV technique is an indirect velocity measurement as it measures the velocity of a fluid element indirectly by means of the measurement of the velocity of tracer particles within the flow, which in most applications, have been added to the flow before the experiment starts. Besides, PIV is a whole field technique which allows the recording of images of large parts of flow fields in a variety of applications in gaseous and liquid media and extraction of the velocity information out of these images. The spatial resolution of PIV is large, whereas the temporal resolution (frame rate of recording PIV images) is limited due to current technological restrictions.

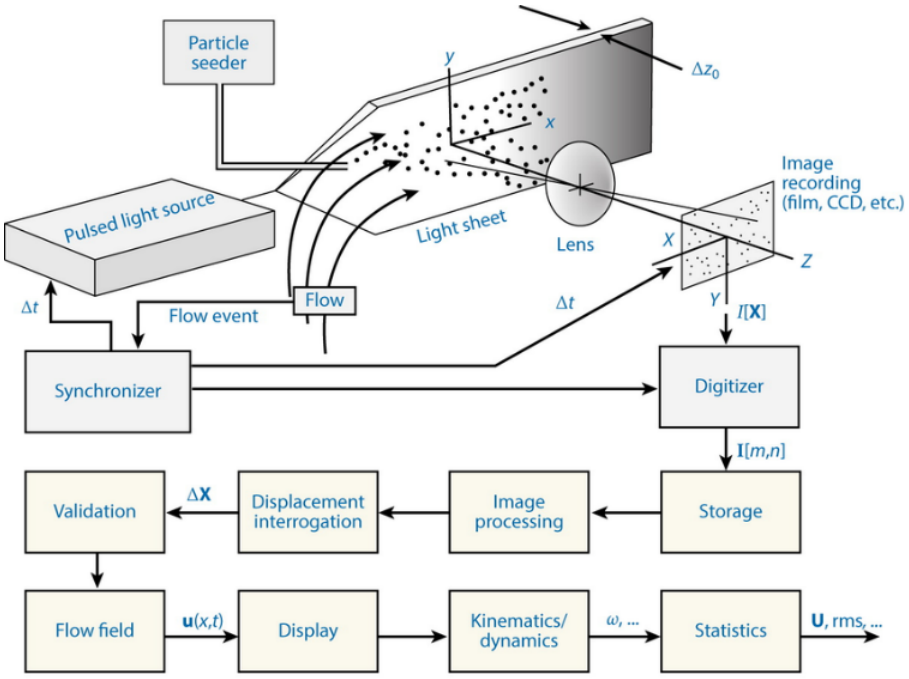

Figure 2:7 Procedure of data processing (**Adrian and Westerweel, 2011**).

Furthermore, a theoretical understanding of the basic principles of the PIV techniques has improved significantly. Simulations of the recording and evaluation process give useful information on many parameters important for the layout of an experiment utilizing PIV (**Raffel et al. 1998**).

The 2D standard PIV scheme has main components including laser sheet, digital video camera recorder, computer, synchronizer, pulsed laser, as shown in **Figure 2:8**.

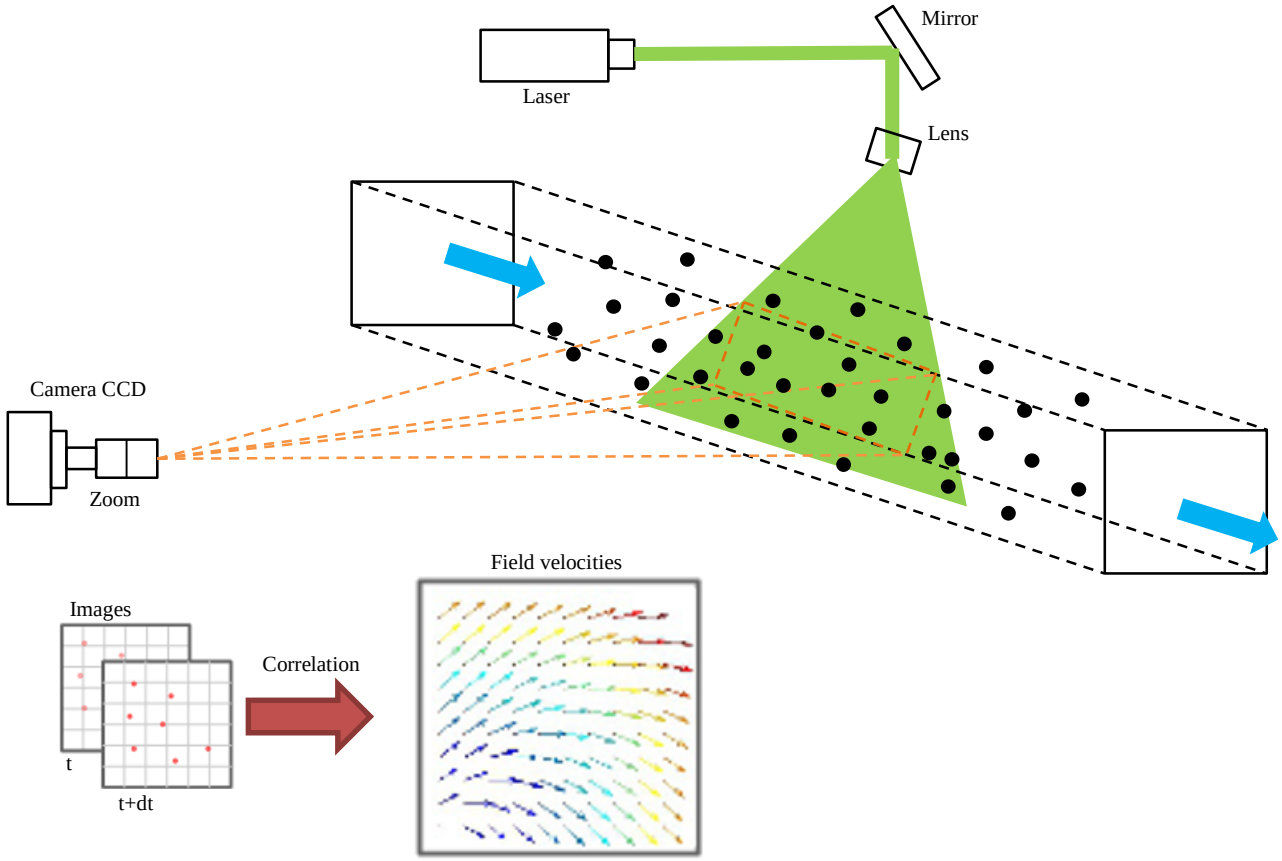

Figure 2:8 A scheme of a 2D standard PIV systems.

2.2.1 Illumination

The area should be sufficiently illuminated to achieve good visualization of the particles or tracers. It is desirable that the lighting be even and diffused to avoid shadows and reflections, and thus ensure proper identification of the particles or tracers. In the point measurement technique of PIV, the laser is used as a source of bright illumination. PIV image acquisition should be done using short light pulses to prevent particle image streaking. Hence, pulsed lasers become obvious choices for PIV work (**Dabiri, 2006**). Currently, solid-state Nd: YAG lasers using frequency-doubling crystals to produce pulses at 532 mm are used widely.

The illumination is characterized by the time Δt between the exposures and the duration δt of the exposure. The ratio of the exposure duration relative to the exposure time delay, $\delta t / \Delta t$, determines the degree to which the motion of the tracer particles is frozen (**Adrian and Westerweel, 2011**). Considering that the illumination has two important parameters, namely the duration of the illumination pulse, called exposure time, and the delay time between two successive pulses. These parameters have to be fixed depending on the type of the flow of study. The first parameter of exposure time has to be sufficiently short to guarantee a good illumination of tracers; while the delay time is the most changeable parameter during the recording phase. In conclusion, the exposure time and delay time parameters have to be carefully fixed, considering the character of the flow under study (**Di Cristo, 2011**).

Xenon lamps can produce several hundred joules in pulses as short as 1 μs, considering that only a small fraction of this energy can be used to form a thin, high-quality light sheet owing to inherent limits on collimating light from an extended source.

2.2.2 Camera and Imaging

Since the appearance of the PIV technique, this system has evolved tremendously as a result of various technological advances. The evolution of computer equipment allowed for greater speed and capacity of processing. In addition, Couple Charge Device (CCD) sensors have developed with increasing resolution, replacing the method of very slow and laborious video-recording by CCD cameras.

CCD cameras have as a main component an electronic semiconductor plate of photosensitive silica with hundreds of filaments ordered in mesh, creating millions of tiny light-sensitive photodiodes defining the basic element of the image: the pixel (Picture Element), which when stimulated by light energy, release electrons that produce an electrical charge, which once registered can encode the image.

The digital image is the result of converting analog data into digital. The light strikes the digital sensor and generates electrical signals to a processor, the Analog-Digital device will convert in digital code by creating an image file. The digital image is composed of elements called pixels which are arranged in a frame called bitmap. Each pixel is the combination of values of color and brightness in a certain position that be recorded numerically.

Computers use the binary number system consisting of only two digits which are the 0 and 1. Considering that the number of possible combinations to increase the number of bits equal 2^n, where n is the number of bits. The greyscale images are created with a palette of eight bits with 256 tones ranging from black (0) to white (255); 254 intermediate shades of gray are enough for the human eye to not detect abrupt transitions.

The objective aperture corresponds to the diameter of the diaphragm located inside the objective; a larger diameter lighter reaches the sensor surface. It is expressed with a series of numbers f/ called diaphragms or diaphragm points. The most common are: f/1.4, f/2, f/2.8, f/4, f/5.6, f/8 and f/22.

The speed of shutter controls the time the shutter blades remain open; the more time, more light reaches the film. This speed value is expressed in fractions of second called exposure time. The same exposure of the film can be achieved by varying the parameters of openness and speed. If the speed is increased, it has to be compensated with an increased diameter of the diaphragm. **Figure 2:9** shows the visualization of particles or tracers with the PIV camera.

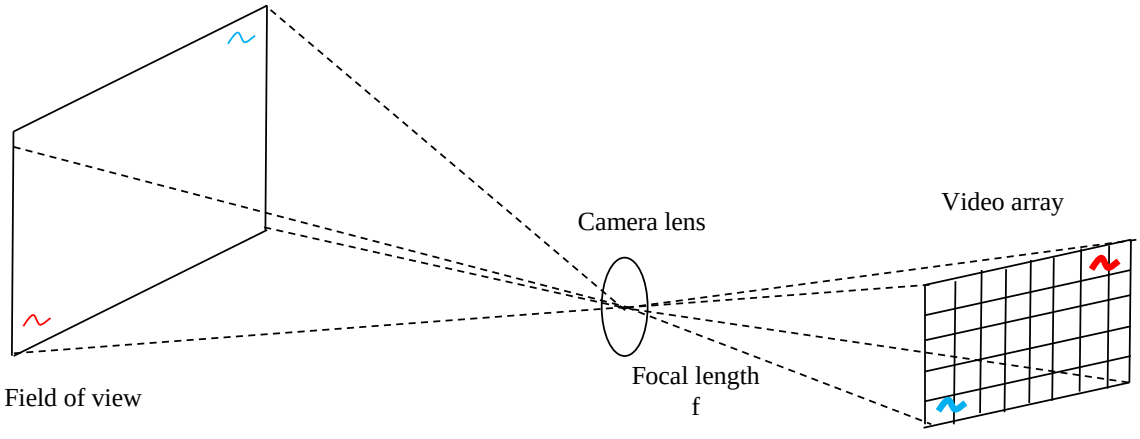

Figure 2:9 Camera visualization.

The lens of the cameras have the function to locate the particles or tracers in the fluids as $x_p(t)$, and the location of the image on the camera is defined as $X_p(t)$. **Figure 2:10** shows the behavior of simple geometry of the differents planes of the PIV method, where the the plane of particles or tracers have a plane of coordinates (x,y,0), which are mapped on the plane (X,Y), according to **Equation *[2:2]*** of projection of the camera and **Equation *[2:3]*** of Mo.

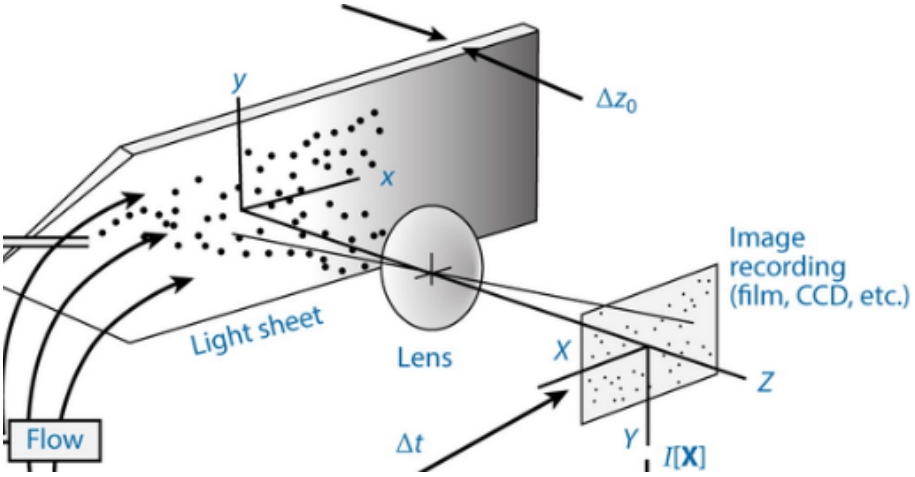

Figure 2:10 Discretization of viasulation of particles or tracers (**Adrian and Westerweel, 2011**).

$$\begin{pmatrix} X \\ Y \end{pmatrix} = M_0 \begin{pmatrix} x \\ y \end{pmatrix} \qquad [\ 2:2\ ]$$

$$M_o = \frac{Z_0}{z_0} \qquad [\ 2:3\ ]$$

Where: M_0 : is the lateral magnification

z_o : is the object distance from the z=0 plane to the effective center of the lens

Z_0 : is the image distance from the effective center of the lens to the image plane

An image may be defined as a two-dimensional function, f(x,y), where x and y are spatial (plane) coordinates, and the amplitude of f at any pair of coordinates (x,y) is called the intensity or gray level of the image at that point. A digital image is a numerical representation of an object. It is composed of a finite number of elements; each such element is called a picture element or pixel. When x, y, the amplitude f(x,y) of an image are all finite, discrete quantities, an image is called a digital image.

2.2.3 Image Digitization

The elements of a digitizer are a sampling aperture, mechanism for scanning the image, light senor, quantitizer and output storage medium. The characteristic of an image digitizer depends on the pixel size, image size, local property measured, linearity and noise.

Digitization is a process of converting a physical image to a digital image as spatial sampling or rectangular sampling. Digitalizing an image means turning it into a file that can be manipulated by computer, that is to say, set of bits. To digitalize an image, it is necessary to divide it into discrete units, each of which is called a pixel. Once

divided the image is assigned a value to each of the pixels. Important change in PIV technique was to change to digital recording called Digital-PIV, influencing also the recording modes (**Willert and Gharib, 1991**).

The resolution in digital photography refers to the amount or density of pixels that form the image and the number of colors. The resolution in digital photography refers to the amount or density of pixels that form the image and the number of colors. The number of pixels is specified by indicating the total number of pixels or indicating the number of pixels that are in each of the dimensions of the image (first the horizontal and then the vertical). An image of 3.3 million pixels can be referred to as an image of 2,048 x 1536 pixels.

The charge-coupled devices (CCDs) and complementary metal oxide semiconductor (CMOS) arrays, consist of rectangular or square arrays of pixel sensors that convert the light energy in the image plane into electrical signals in the form of either electrical charge held in the electron storage wells of a CCD or voltages from the active pixel sensors of a CMOS (**Adrian and Westerweel, 2011**). These two types of sensors provide some signals proportional to the light energy that enters each pixel during the exposure time δt following Digitization **Equation *[2:4]***:

$$\boldsymbol{I[i,j] = \int_{A_{i,j}} \int_{\delta t} p\left(X - X_{i,j}\right) I(X,t)\, dX dt = \int_{A_{i,j}} p\left(X - X_{i,j}\right) \varepsilon(X)\, dX} \qquad \textbf{[2:4]}$$

Where: i, j : are the row and column numbers of the pixel

$X_{i,j}$: is the location of its center

$p(X)$: is the position-dependent sensitive of the pixel

ε : is the exposure

The process of converting a continuous image intensity field into a two dimensional array of analog pixel reading is called pixelization. The CCD camera or PIV cameras have capability to transfer the charge created by the first exposure from each pixel to an adjacent charge storage well, where the transfer process is very fast, of order 1 μs. allowing the pixel sensor to record the second exposure nearly at once. The time of transfer of all the charges determine the frame rate of the camera.

2.2.4 Digital Image Processing

The initial interest of digital image processing stems from two interest areas firstly, improvement of pictorial information for human interpretation and secondly, processing of image data for storage, transmission, and representation for autonomous machine perception (**González and Woods, 2002**).

From the sixties and the development of computers, digital image processing has advanced to impressive steps and algorithms were first used in a wide range of applications as geologists studying contamination with satellite or aerial images, archaeologists restoring old photographs of ancient artifacts destroyed over time, applications in astronomy, biology, defense, industry, character recognition, quality control, fluids mechanics, etc.

Around 30 years ago, the advances in digital image processing initiated a quantitative analysis of flow visualization pictures and have led to new measurement techniques such as particle image velocimetry (PIV) with digital images developed by Hesselink (**1988**).

An image can be defined mathematically as a two-dimensional function f(x, y), where x and y are polar coordinates (in a plane), and f in any pair of coordinates is the intensity or level of gray of the image in this coordinate. When the coordinates (x, y) and the values of f are all finite, discrete quantities, the image is a digital image. A digital

image is composed of a finite number of elements, each a specific place and value. These elements are called pixels. The field of digital image processing refers to processing digital images by means of a digital computer.

There are basic methods for implementing the general measurement scheme as low image density PIV called particle tracking velocimetry (PTV), high image density PIV called particle image velocimetry (PIV) and Laser Speckle velocimetry (LSV).

PTV or Low Image Density is a technique that requires low concentration of particles to have a good performance, and the results of PTV vector fields tend to be sparse. A priority is to define the image interrogation spot A_1, which needs to be enough large to contain the maximum particle image displacement, where N_I is the image density, and a crucial term in PIV as shown in **Equation of image density *[2:5]***:

$$N_I = \frac{CA_1 \Delta z_0}{M_0^2} \ll 1 \qquad \textit{[2:5]}$$

The interrogation volume is the intersection between the interrogation spot and the light sheet thickness. Also the value of N_I represents the mean number of particles per interrogation volume in the fluid.

High Image density or PIV is a technique that increases the number of vector fields but at the same time increases the number of particles or tracers and uses a statistical method to track displacement of small groups of particles or tracers. The most common approach is space-time cross-correlation of the images of the particles with small interrogation spots or windows.

To do a cross-correlation of two consequence images, an image at the time t exposed by a light pulse is recorded on one frame of the video camera, as defined in **Equation of image I_1 *[2:6]***:

$$I_1(X) = I(X,t) = \int \delta(z)\tau_0 \left[X - F(x)\right] g\left[x - x_p(t)\right] dx \qquad \textit{[2:6]}$$

And the images from t+Δt are exposed and recorded on a second frame, following the **Equation *[2:7]***:

$$I_2(X) = I(X,t+\Delta t) = \int \delta(z)\tau_0 \left[X - F(x)\right] g\left[x - x_p(t+\Delta t)\right] dx \qquad \textit{[2:7]}$$

The method of cross-correlation estimates the velocity field with a correlation between image (I_1) and image (I_2) (**Equation *[2:6]* and *[2:7]***), with the location of W_1, following the **Equation *[2:8]*** of cross-correlation image:

$$R(s) = \int_{W_1} I_1(x) I_2(X+s) dX \qquad \textit{[2:8]}$$

Digital particle image velocimetry called DPIV has a procedure of digital PIV cross-correlation to estimate the mean displacement of the particles or tracers in an interrogation area. Furthermore, to compute the cross-correlation the large peak value is usually the best approximation of the displacement of the particle or tracers in the windows. This information about the displacement and the time between two consecutive images allow computing the mean velocity in one interrogation area as show in the **Figure 2:11**:

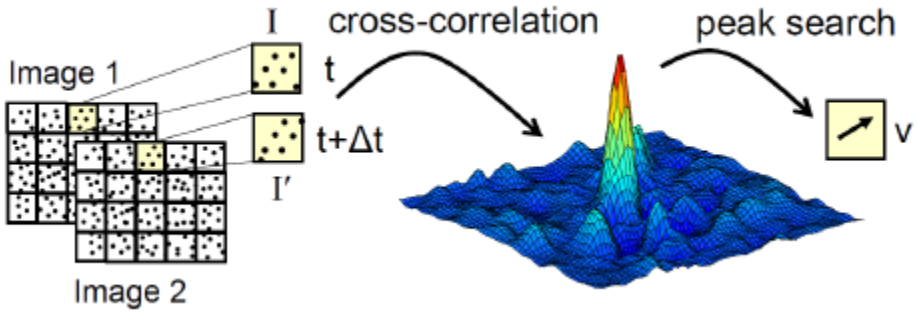

Figure 2:11 Cross-correlation procedure (**Willert, 1997**).

The cross-correlation method between two interrogation areas from successive images or frames and successive times is used as Fast-Fourier transform (FFT's). Applying the FFT in the PIV image processing reduces the time required for the necessary operation to produce a velocity field (**Willert and Gharib, 1991; Keane and Adrian, 1992**).

2.2.5 Postprocessing

This step proceeds after the definition of the interrogation spot of PTV or PIV. The displacement data are converted to a real velocity by dividing the displacement by the pixels per unit length and by the exposure time delay. These results can be represented in a map of vector of field velocities and the turbulences of the flows in units as meters per second or centimeters per second. **Figure 2:12** shows a typical output field velocities vector for reproduce the behavior of the flow around the cylinder and the effect of turbulence. The flow is flowing from right to left.

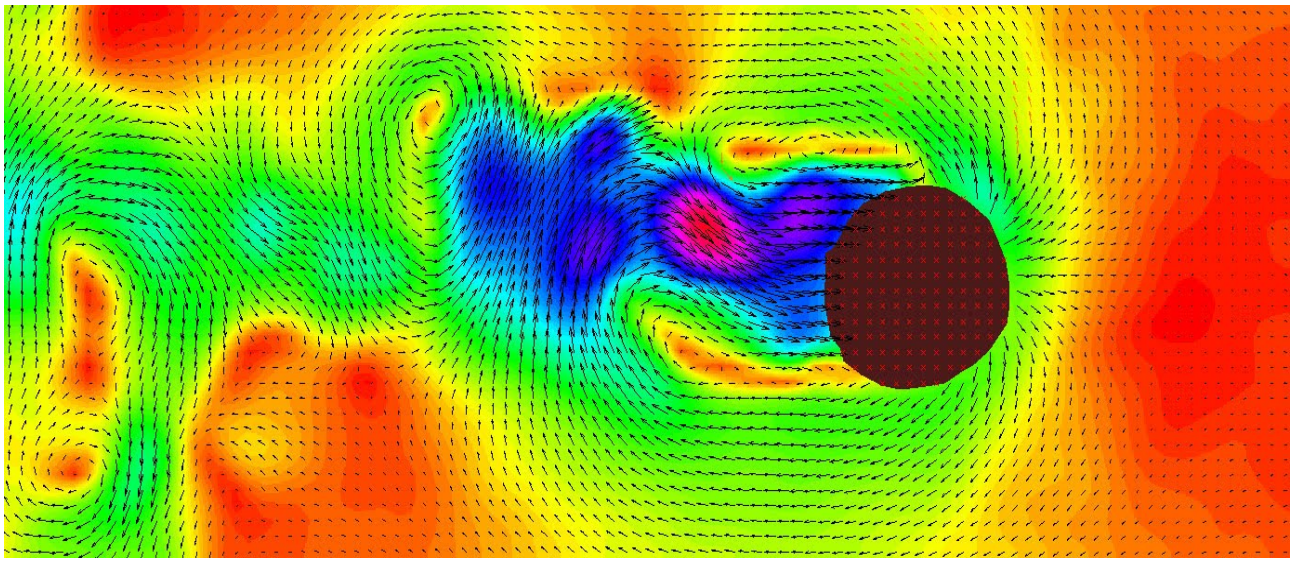

Figure 2:12 Field velocities vector around cilinder. Source: **www.pivlab.blogspot.de.**

Post-Processing of PIV data is characterized by validation of the raw data, replacement of incorrect data, data reduction, analysis of the information and presentation and animation of the information. The first step is the validation of the raw data which require a special algorithm to be developed in order to detect these incorrect data. The second step is the replacement of incorrect data, which refers to complete data fields similar to the case of study for numerically obtained data. Next it is important to reduce the data because is difficult to analyse several hundred velocity vector maps that describe their fluid mechanical feature. Fourthly, the information is analyzed,

where this is the most difficult task for the users of PIV. And finally the information is presented using special software for the graphical presentation of the PIV field data. Animation is also used for better understanding of the comparison between experiments and simulations of field velocities. (**Raffel et al., 1998**).

It is possible to correct the velocity field of PIV method on velocity field maps using a software package proposed by Nogueira et al. (**2001**) also established the limits on the resolution of correlation PIV through the paper that focuses on the fundamentals of spatial resolution for correlation-based PIV (**Nogueira *et al.*, 2005**).

2.2.6 Accuracy, resolution and performance of PIV

The measurement of displacement between two consecutive images with some tracers of particles present in the fluid has to be considered, because the performance may not be sufficiently accurate and the fluid motion may not be represented correctly, especially when the fluid has strong temporal and spatial accelerations (**Westerweel et al., 2013**).

The priority is to consider the parameters that can possibly degrade the image, for instance, illumination, representation of the tracers or particles on the sensor, the digital camera device, inappropriate particle location and pixilation of the image.

Besides, the dubiety of the result as a consequence of image processing, interrogation area, analyst of image and data reconstruction are other problems in the performance of the PIV. As a result, the image can reproduce some noise in the recording medium.

To determine the displacement of the centroid of the particle image is possible through the root mean square called rms error ($\sigma_{\Delta x}$), where x represents the position in the fluid and X represents the position in the image plane. Subtracting the error of Δt the error of the velocity measurement is determine by the **Equation *[2:9]*** of rms error of the velocity measurement:

$$\boldsymbol{\sigma_u = \frac{\sigma_{\Delta x}}{\Delta t} = \frac{\sigma_{\Delta u}}{M_0 \Delta t}} \qquad \textbf{[2:9]}$$

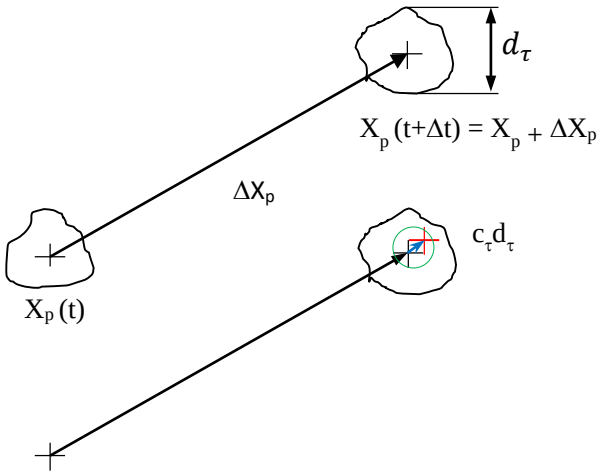

Figure 2:13 Despacement of particle image.

Where the value of M_0 is the image magnification. To analyse the measurement of the displacement between two images of the same particle is represented in the **Figure 2:13**, where is important to take in account the noise in

the image processing because the result of correlation of two images consequence depend of the center of the particles, and it could be affect to the position of the particles.

Previous studies demonstrate that in basics principle of displacements it is easier to locate the center of a small image than a large image (**Adrian, 1986**), where these author proposed **Equation *[2:10]*** of rms error:

$$\sigma_{\Delta X} = c_\tau d_\tau \qquad \textit{[2:10]}$$

Where: c_τ : is a constant that depends on the ability of the analysis procedure to determine the displacement between the images

d_τ : is the particle image diameter (**Adrian, 1997**)

Furthermore **Equation *[2:11]*** of d_τ by Offutt, is useful when we subtract the f-number of the lens in favor of the depth of field δz because the depth of field is normally a restriction imposed on the system (**Offutt, 1995**)

$$d_\tau = M_0\left[1.5\delta z\lambda + d_p^2\right]^{\frac{1}{2}} \qquad \textit{[2:11]}$$

Consider that the relation of particle displacement associated with the full-scale velocity is $\Delta x_{p,\,max}$, the dynamic velocity range (DVR) is defined as the ratio of the maximum velocity to the minimum resolvable velocity following **Equation *[2:12]***

$$DVR = \frac{u_{max}}{\tau_u} = \frac{M_0 \Delta x_{p,max}}{c_\tau d_\tau} \qquad \textit{[2:12]}$$

Where: u_{max} : is the full-scale velocity defined as the Equation ***[2:13]***

$$u_{max} = \frac{\Delta x_{p,max}}{\Delta_t} \qquad \textit{[2:13]}$$

In the recording plane the format of the recording have two dimensions as L_x and L_Y, but in fluid the filed view is given by the **Equation *[2:14]*** and **Equation *[2:15]***:

$$l_x = \frac{L_X}{M_0} \qquad \textit{[2:14]}$$

$$l_y = \frac{L_Y}{M_0} \qquad \textit{[2:15]}$$

For this reason, the definition of dynamic spatial range (DSR) follows **Equation *[2:16]*** where the minimum scale are less than $\Delta x_{p,\,max.}$

$$DSR = \frac{l_x}{\Delta x_{p,max}} = \frac{L_X/M_0}{\Delta x_{p,max}} \qquad \textit{[2:16]}$$

The product of DVR by DSR define the performance of the PIV as show in the **Equation *[2:17]***:

$$DVR\ x\ DSR = \frac{L_X}{c_\tau d_\tau} \qquad [\ 2{:}17\ ]$$

the parameter of **Equation *[2:17]*** should be high values to be suitable for turbulence approximation and measurements in high Reynolds number flows (**Adrian and Westerweel, 2011**).

Prasad et al.(**1992**) studied the effect of resolution on the speed and accuracy of particle image velocimetry interrogation; while in the last decades the effect of resolution, speed, performance and accuracy of the image processing in PIV was studied by many authors like (**Liu et al., 1991; Westerweel et al., 1997; Fouras and Soria, 1998; Keane and Adrian, 1998; Nogueira et al., 1999; Nogueira et al., 2001; Foucaut and Stanislas, 2002; Lecuona *et al.*, 2002; McKenna S. P., 2002; Scarano, 2003; Nogueira *et al.*, 2005**).

2.2.7 Advanced techniques of PIV

In fluids mechanics the general measurement method implemented frequently in experiments are low image density PIV (PTV), high image density PIV (PIV) and Laser Speckle velocimetry (LSV) (**Figure 2:14**). These three methods have different characteristics because they work with different types of image, different methods of interrogation and reproduce different characteristics of the vector fields, with the main difference being the concentration of particles or tracers. A brief description of these methods is provided.

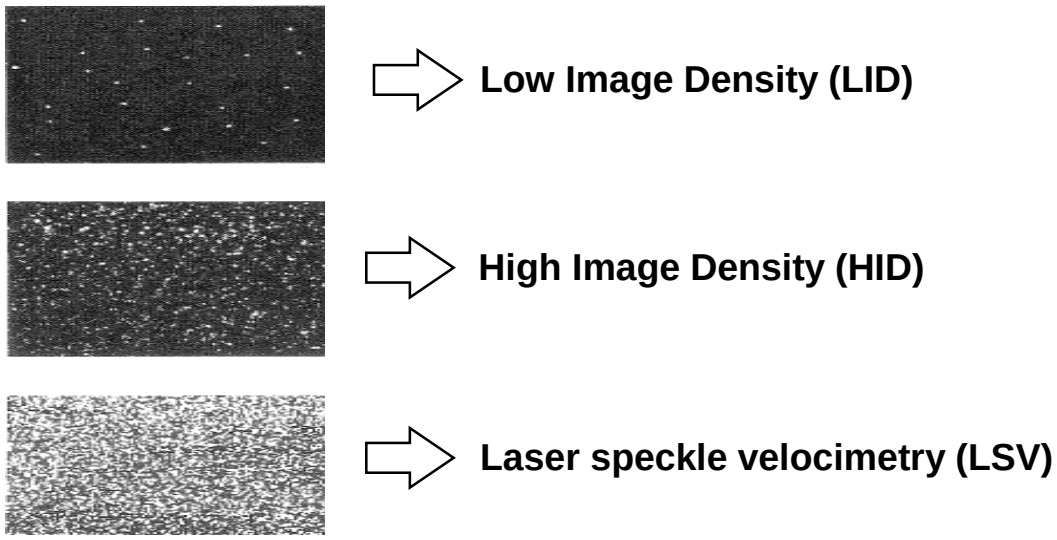

Figure 2:14 Types of flow visualization.

2.2.7.1 Low Image Density (LID)

The first visualization of motion of fluids using this techniques was developed by Prandtl in 1957 **(Prandtl and Tierjens, 1957; Antman *et al.*, 2003; Oertel, 2010**), but in recent times Flór and van Heijst (**1996**) used to analyse the motion of vortices in a stratified fluid. To make a map of velocity field it is necessary to know the direction and magnitude of the fluid velocity by measuring the orientation and the length of the streaks. Moreover, Particle Tracking Velocimetry present a low source density of particles in the area of study ($N_I << 1$) as show in the **Figure 2:15.**

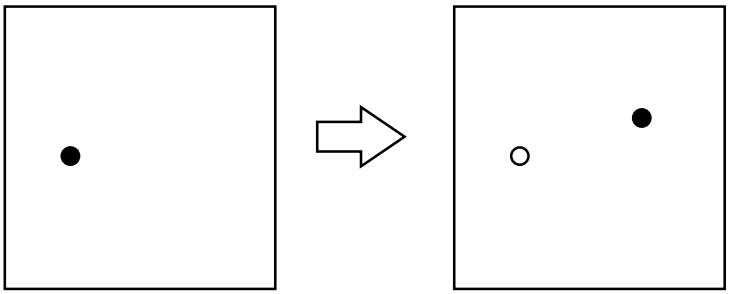

Low image density

$N_I << 1$

Figure 2:15 Despacement of Particle tracking velocimetry.

The displacement method of PTV requires the flow to be seeded with tracer particles of very low concentration, and a very low image number intensity in frames or video recording. Also only a single particle can be identified in image recording. Particle tracking is possible frame to frame and with low information density in the measurement plane. The disadvantages of PTV is the low concentration of particles being the restriction to increase the number of density of vector that can be measured.

2.2.7.2 High Image Density (HID)

High Image Density (HID) is a whole flow field technique providing instantaneous velocity vector measurements in a cross section of a flow. The use of modern digital cameras and dedicated computing hardware, results in real time velocity maps. In PIV, the velocity vectors are derived from sub sections of the target area of the particle-seeded flow by measuring the movement of particle between two light pulse following **Equation *[2:1]*** described in the section **2.1.3.**

The visualization of vector field of the PIV method requires the flow seeded with tracer particles of high concentration, a high image number density in photo or video recording. Particle image tracking is impossible from frame to frame due to high information density in measurement plane. Also, Particle Image Velocimetry present a high source density of particles in the area of study ($N_I >> 1$) as show in the **Figure 2:16**.

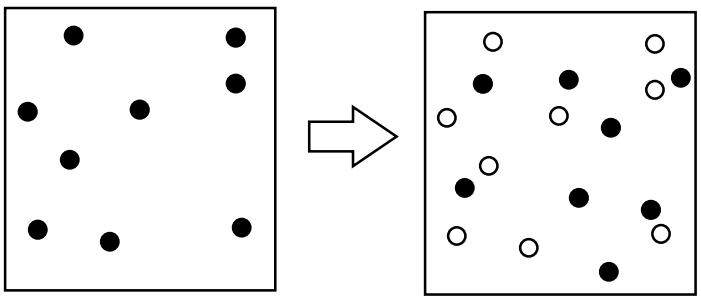

High image density

$N_I >> 1$

Figure 2:16 Despacement of high image density.

Hence, the motion of the fluid can be determined by measuring the particle displacements through evaluation of the PIV recordings, where the recorded images are divided into small interrogation areas and analyzed by means of a correlation method. Furthermore, with the PIV technique quantitative two-dimensional information of the fluid velocity is obtained. Comprehensive descriptions and explanation on the principle of the PIV technique have been provided by Raffel et al. (**1998; 2007**). Furthermore this method was extended in three-dimensional flows by Malik et al. (**1993**).

2.2.7.3 Laser Speckle Velocimetry (LSV)

The Laser speckle velocimetry (LSV) requires the flow seeded with tracer particles of very high concentration, a very high image number density in photo or video recording. The single particle cannot be identified in image recording; thus particle image tracking is impossible from frame to frame due to high information density in the measurement plane.

Furthermore, LSV is very similar to PIV method, with this technique focusing on the displacement of speckle patterns instead of particle images (**Fomin, 1998**). The first experiment of this techniques was in solid mechanics, but was extended to some application in laminar pipe flow (**Barker and Fourney, 1977; Dudderar and Simpkins, 1977; Grousson and Mallick, 1977**). Iwata et al. (**1978**) did some measurement of flow velocity by multiple exposure speckle photography; Meynart also applied LSV in complex flows in gases and liquids, in laminar and turbulent regime and also used to analyse the convective flow field (**Meynart, 1980b; 1982a; 1982b**).

2.2.8 Algorithm code "Digiflow"

This section describes the algorithm used for image processing. Advanced image processing software Digiflow developed by Dalziel Research Partners at the Department of Applied Mathematics and Theoretical Physics (DAMTP), at the University of Cambridge, provides a range of image processing features designed especially for studying the measurement of fluids flows.

The history of the Digiflow started in 1988 with the first version called DigImage, published the first commercial version in 1992, being the first tools of image processing in fluids mechanics. After in 1994 began the development of Digiflow where the first commercial version was published in February 2005 with the development of synthetic schlieren.

Synthetic schlieren is a novel technique for producing qualitative visualizations of density fluctuations and for obtaining quantitative whole-field density measurements in two dimensional density-stratified flows (**Dalziel, 2012**). The principal techniques of Digiflow is "pattern matching refractrometry" that provides accurate quantitative measurements of two dimensional density field, being these techniques are based on the same optical principles as the classical schlieren method, but have the advantages of being much easier to setup and of being adaptable to much larger domains (**Dalziel et al., 2000**).

The origins of synthetic schlieren is in the classical schlieren and moiré fringe techniques, where the synthetic schlieren have inside four techniques as qualitative synthetic schlieren, line refractrometry, dot tracking refractrometry and pattern matching refractometry.

The basics optics of the four techniques described before depends on the same optical phenomenon. The principal parameters for the optics visualization are the density "p" and the refractive index "n" that have relationship among them. Furthermore **Figure 2:17** show the optical sketch of the synthetic schlieren where the apparent movements are given by **Equation *[2:18]*** of $\Delta\xi$ and **Equation *[2:19]*** of $\Delta\zeta$:

$$\Delta\xi = \frac{1}{2} W_t (W_t + 2B_t) \frac{1}{n_0} \frac{\partial n'}{\partial x} \qquad [\ 2{:}18\ ]$$

$$\Delta\zeta = \frac{1}{2} W_t (W_t + 2B_t) \frac{1}{n_0} \frac{\partial n'}{\partial x} \qquad [\ 2{:}19\ ]$$

Where: W_t : is the width of the tank

B_t : is the distance from the tank to the mask

$\Delta\xi$: is the displacements in the x direction along the tank

$\Delta\zeta$: is the displacements in the vertical z direction along the tank

n_0 : is the nominal refractive index

(Also the light rays are nominally parallel to the cross-tank coordinate y)

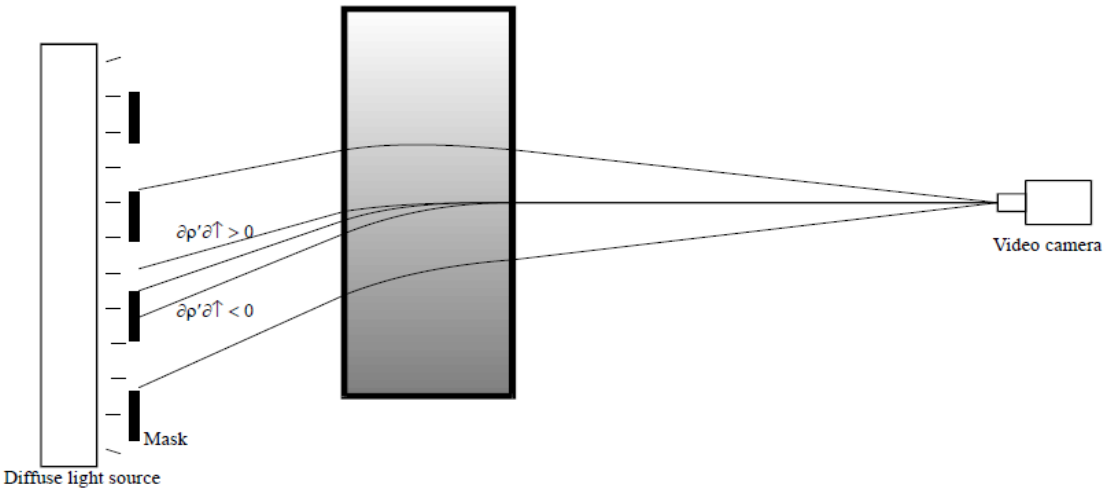

Figure 2:17 Sketch of basics setup of synthetic schlieren (Dalziel, 2012).

If we have salt water, the relationship between salinity, density and refractive index are approximately linear following the Equation *[2:20]*:

$$\nabla n = \frac{dn}{d\rho} \nabla\rho = \beta \frac{n_0}{\rho_0} \nabla\rho \qquad [\ 2{:}20\ ]$$

Where: β : is equal to $\beta = \left(\frac{\rho_0}{n_0}\right)\left(\frac{d_n}{d_\rho}\right) \approx 0.184$

For the description of quantitative mode of the method synthetic schlieren was necessary to use a typical video camera with a CCD sensor capable to obtain a digital image that provide a rectangular pixels represent by a signal $P_{ij}(t)$, where it need to be proportional to the spatial of the light intensity falling on the surface p(x,z;t), describe in the Equation *[2:21]*.

$$P_{ij}(t) = \frac{1}{\Delta x^* \Delta z} \int_{x_i - \frac{\Delta x^*}{2}}^{x_i + \frac{\Delta x^*}{2}} \left[\int_{x_j + \frac{\Delta z}{2}}^{x_j + \frac{\Delta z}{2}} p(x, z; t) dz \right] dx \qquad [\ 2{:}21\ ]$$

Where: $\Delta x^*, \Delta z$: is the representation of the size of the region of the mask imaged by individual pixels.

The representation of a mask resulting in the image horizontal lines oriented parallel to the x axis. If the lines are perfectly black (p=0) and perfectly white (p=1), the intensity p_0 in **Equation *[2:22]*** represent the intensity produced by the mask under quiescent conditions.

$$p_0(x, z) = \begin{cases} 0 & 0 \le z \bmod \eta < \alpha \\ 1 & otherwise \end{cases} \qquad [\ 2{:}22\ ]$$

The intensity of the corresponding digitized image will be described in the **Equation *[2:23]*** of p_{ij}:

$$p_{i,j;0} = \begin{cases} 0 & \frac{1}{2}\Delta z \le z_j \bmod \eta < \alpha\eta - \frac{1}{2}\Delta z \\ 1 & \alpha\eta + \frac{1}{2}\Delta z \le z_j \bmod \eta < \eta - \frac{1}{2}\Delta z \\ \frac{1}{2} + \frac{z_j \bmod \eta - \alpha\eta}{\Delta z} & \alpha\eta - \frac{1}{2}\Delta z \le z_j \bmod \eta < \eta + \frac{1}{2}\Delta z \\ \frac{1}{2} - \frac{z_j \bmod \eta - \alpha\eta}{\Delta z} & \eta - \frac{1}{2}\Delta z \le z_j \bmod \eta < \frac{1}{2}\Delta z \end{cases} \qquad [\ 2{:}23\ ]$$

Where: η : is the spacing of the lines on the mask

$\alpha\eta$ or $(1-\alpha)\eta$: is the alternating black and white region of widths

An expression similar to **Equation *[2:23]*** holds when the density field is perturbed. Provided the perturbations are small such that $\Delta\zeta < \eta$, where $\Delta\zeta$ is given by **Equation *[2:19]***, and variations in $\Delta\zeta$ occur over a length scale large compared with η, then η may be replaced in **Equation *[2:23]*** with η-$\Delta\zeta$ (**Dalziel et al., 2000**). Qualitative mode synthetic schlieren works by calculating $|Pij\ (t) - Pij;0|$, this difference simply being $|\Delta\zeta|$ and is proportional to $\left|\frac{\partial \rho'}{\partial z}\right|$ for pixels which contain an edge in both the Pij;0 and Pij (t) images (**Dalziel et al., 1998**).

The qualitative mode of the techniques synthetic schlieren developed three variations based on different approaches to measuring the apparent motion of the mask called line refractrometry, dot tracking refractrometry and pattern matching refractrometry.

Line refractrometry. - is when the intensities P_{ij} (t) for the perturbed density field are compared with the interpolated base state to determine the apparent displacement normal to the line as in **Equation *[2:24]*** of $\Delta\zeta$. To obtain the quantitative information through this approximation is necessary to introduce the intensity by the sensor CCD located in the digital video camera.

$$\Delta\zeta = \left[\frac{(P - P_0)(P - P_{-1})}{(P_1 - P_0)(P_1 - P_{-1})} - \frac{(P - P_0)(P - P_1)}{(P_{-1} - P_0)(P_{-1} - P_1)} \right] \Delta z \qquad [\ 2{:}24\ ]$$

Additional parameters are define as $P= P_{ij}$ (t), $P_0= P_{ij;0}$, $P_{-1}=P_{i,j-1;0}$ and $P_1= P_{i,j+1;0}$. Furthermore this method was used in experiment of internal waves by Sutherland et al. (**1999**).

Dot tracking refractrometry. - It is a regular array of dots. The basic principle of the technique is the location of the intensity-weighted centroid relative to a position of each dot. Where the centroids of the dots are found first for the base flow, and then for each flow containing a density perturbation to be analyzed (**Dalziel et al., 2000**). Furthermore the difference in these two centroids locations gives the two components $\Delta\xi$ and $\Delta\zeta$ for each dot (i,j) related to the in-plane density gradient $\Delta\rho'_{ij}$ through **Equation *[2:18]*** and ***[2:19]***.

Pattern matching refractrometry. – These kind of techniques has its origins in the Particle Image velocimetry (PIV) techniques. The principle function of this techniques is to show the motion of the displacement of the pattern of dot through of the measure of the difference between comparable interrogation windows in the quiescent image and the image at the time Δt. Cross-correlation function is the way to measure the difference between shifted windows.

Many research focusing on PIV frequently use **Equation *[2:25]*** of $f_{cross}(\Delta\xi, \Delta\zeta; x_i, z_j)$ to analyse the motion of fluids through the cross correlation using Fast Fourier Transforms. Furthermore, **Equation *[2:26]*** of $f_{abs}(\Delta\xi, \Delta\zeta; x_i, z_j)$ and **Equation*[2:27]*** of $f_{sq}(\Delta\xi, \Delta\zeta; x_i, z_j)$ are functions to help the performance of the processing of images in the CPU.

$$f_{cross}(\Delta\xi, \Delta\zeta; x_i, z_j) = -\frac{\langle \boldsymbol{P}(x+\Delta\xi, z+\Delta\zeta; t)\boldsymbol{P_0}(x,z)\rangle - \langle \boldsymbol{P}(x+\Delta\xi, z+\Delta\zeta; t)\boldsymbol{P_0}(x,z)\rangle}{[\langle \boldsymbol{P}(x+\Delta\xi, z+\Delta\zeta; t)^2\rangle - \langle \boldsymbol{P}(x+\Delta\xi, z+\Delta\zeta; t)^2\rangle]^{\frac{1}{2}}[\langle \boldsymbol{P_0}(x+z)^2\rangle - \boldsymbol{P_0}(x,z)^2\rangle]^{\frac{1}{2}}} \qquad \textbf{[2:25]}$$

$$f_{abs}(\Delta\xi, \Delta\zeta; x_i, z_j) = \langle |\boldsymbol{P}(x+\Delta\xi, z+\Delta\zeta; t) - \boldsymbol{P_0}(x,z)| \rangle \qquad \textbf{[2:26]}$$

$$f_{sq}(\Delta\xi, \Delta\zeta; x_i, z_j) = \langle [\boldsymbol{P}(x+\Delta\xi, z+\Delta\zeta; t) - \boldsymbol{P_0}(x,z)]^2 \rangle \qquad \textbf{[2:27]}$$

The Digiflow software is the most accurate, but computationally expensive, as it uses powerful pattern-matching techniques to determine the apparent displacement as accurately as possible: the design of this part of the system has concentrated more on accuracy than speed (**Dalziel, 2012**).

2.3 Hydraulic engineering applications for free surface flow

The literature review confirms some techniques that the engineers began to use as a tool to evaluate the velocity fields and flow discharge fluxes in hydraulics applications, derived from fundamental research in fluids mechanics laboratories. In the 1980s, some researchers started to develop instruments and techniques such as acoustic velocimetry, laser Doppler velocimetry, thermal anemometry, radar and particle image velocimetry (PIV), etc. (**Muste et. al, 2010**). Both Eulerian and Lagrangian methods were used and particle seeding image techniques for experimental fluids mechanics was very popular for measurements of extensive regions where the pattern of the instantaneous velocity field was necessary (**Adrian, 1991**). Also, PIV and particle tracking velocimetry (PTV) were developments with a lot of application in complex and turbulence flows (**Westerweel et al., 2013**), where the analysis of the velocity has been developed in two and three dimensions In the area of fluids mechanics (**Kloosterzielt and Heijst, 1991; Dalziel, 1992; Keane and Adrian, 1992; Malik et al., 1993; Adrian et al, 2000; Adrian and Westerweel, 2011**).

Some studies of large scale flows specific for hydraulics applications are reported by Stevens et al. (**1994**) with application for laboratory experiments, another application for measuring flow velocity in porous media by Dill et al. (**1995**) and research to determine the flow field downstream of hydraulic jump by Hornung et al. (**1995**) and Lennon et al. (**2006**), also some developed to detect unsteady surface-velocity field measurement by Lloyd et al.

(1995) and Muller et al. (2002). Other applications were developed by Ettema et al. (1997) to measure the field velocities of ice and in experiments of bubble plume (Lindken and Merzkirch, 2001; Seol *et al.*, 2007). Furthermore, a novel technique to quantitative detection of rain intensity from video camera was proposed by Allamano et al. (2015).

Large-Scale particle tracking velocimetry techniques called LSPTV is a tool developed with the basic principle of Particle Tracking Velocimetry (PTV) to study unsteady flows (Sokoray-Varga and Józsa, 2008). This, in the last advanced of techniques, was developed using multi-channel CCD cameras (Li *et al.*, 2013) with some application in sediment transport.

2.3.1 Space-Time Image Velocimetry (STIV)

Non-intrusive techniques Space-Time Image Velocimetry (STIV) was proposed to measure river surface. Tracers are used to indicate the brightness or color distribution in river surface in the STIV techniques, from which the sequence of image capture on the river is converted to surface velocity field. Furthermore, it is possible to measure the orientation angle of the pattern to the mean flow direction with Space-Time Image (STI) (Fujita and Tsubaki, 2002; Fujita et al., 2007).

Regarding the correction of the orientation angle of the vectors, the description of the space-time image (STI) is important in order to apply to the STIV image techniques. Figure 2:18 shows how to construct the STI system for image processing and correction of the orientation angle of the mean flow direction. Firstly it is important to identify the relation between the display coordinates (x,y) and the physical coordinates (X,Y,Z) by establishing mark points coordinates before measurement (Fujita *et al.*, 2012). The relation described before can be demonstrated following Equation *[2:28]* of x and y coordinates and the reverse form following Equation *[2:29]*, where these equations describe the physical coordinates along “L”. where “L” is the physical length of the search line.

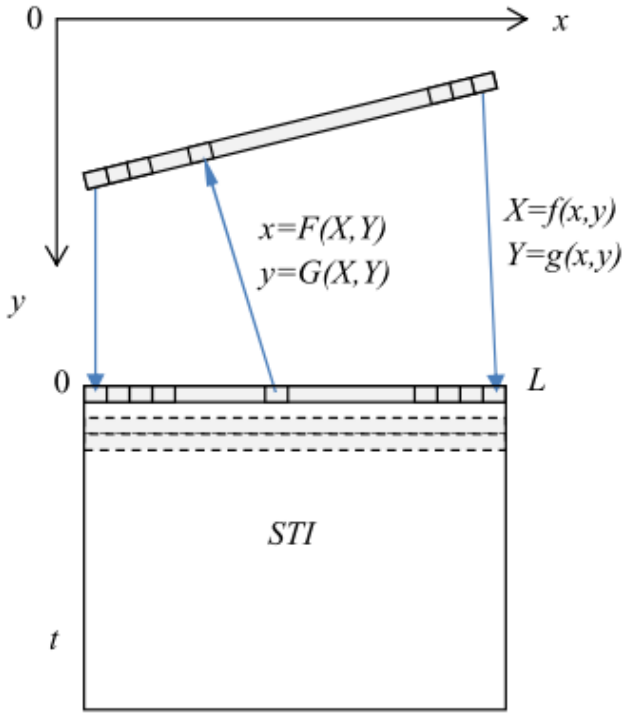

Figure 2:18 Sketch of STI constr ution (Fujita *et al.*, 2012).

$$x = F(X,Y), \qquad y = G(X,Y) \qquad [\ 2{:}28\ ]$$

$$X = f(x,y), \qquad Y = g(x,y) \qquad [\ 2{:}29\ ]$$

The distribution of intensity of the image is a search time placed parallel to the mean flow direction, where the orientation angle can be obtained by the following **Equation *[2:30]*** (**Fujita et al., 2007**):

$$tan2\emptyset = \frac{2J_{xt}}{J_{tt} - J_{xx}} \qquad [\ 2{:}30\ ]$$

Where the values of "J" can be calculate following the **Equation *[2:31]***, **Equation *[2:32]*** and **Equation *[2:33]***:

$$J_{xx} = \int_{A'} \frac{\partial g}{\partial x}\frac{\partial g}{\partial x} dxdx \qquad [\ 2{:}31\ ]$$

$$J_{xt} = \int_{A'} \frac{\partial g}{\partial x}\frac{\partial g}{\partial t} dxdt \qquad [\ 2{:}32\ ]$$

$$J_{tt} = \int_{A'} \frac{\partial g}{\partial x}\frac{\partial g}{\partial x} dtdt \qquad [\ 2{:}33\ ]$$

Where: g(x,t) : is the grey level intensity

A' : is the area of a small segment that divides STI into a number of portions

In the processing, the value of coherency is the main value of orientation angle for each small segment as shown in **Equation *[2:34]***, used as a weighting function.

$$C = \frac{\sqrt{(J_{tt} - J_{xx})^2 + 4J_{xt}^2}}{J_{xx} + J_{tt}} \qquad [\ 2{:}34\ ]$$

Equation *[2:35]* defines the mean orientation angle as:

$$\overline{\emptyset} = \frac{\int \emptyset C(\emptyset) d\emptyset}{\int C(\emptyset) d\emptyset} \qquad [\ 2{:}35\ ]$$

The STIV techniques analyse the flow measurement of the Uji River located in the city of Uji, Japan as shown in **Figure 2:19**. This river divides the city of Uji into two parts for the community's frequent use for repose and recreation.

Figure 2:19 Visualization of Uji River upstream.

The section of the river that was studied through STIV techniques is 135 m long and 65 m wide. **Figure 2:20** shows the measured streamwise velocity distribution in the river Uji. This vialization was analyzed with thirty seconds of consecutive image recorded, which is a total of 900 frames recorded with the camera capture rate of 30 frames per second.

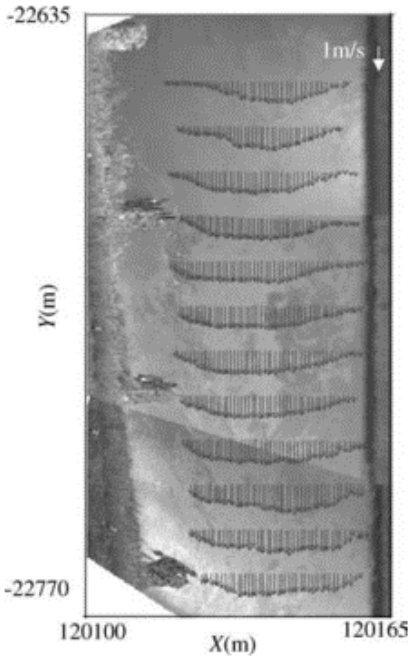

Figure 2:20 Visualization of velocity field of Uji River using STIV techniques (**Fujita et al., 2007**).

Additionally, another study that some researchers did with the space-time image velocimetry was the case of Uono river located in Japan. The river has a width of about 100 m as shown in **Figure 2:21**, having results from a flow velocity of around 3.5 m/s. Because the velocity is high there is only one mean direction of flow.

Another river surface measurement was performed in 2011 in the Kinu River in Japan, where the image size was 1920 x 1080 pixels. These experiments were evaluated with two cameras located one on the right bank and the other on the left bank of the river Kinu in order to analyse the difference of the camera positions. The conclusion was that the velocity distribution measured from the two angles showed agreeably good results.

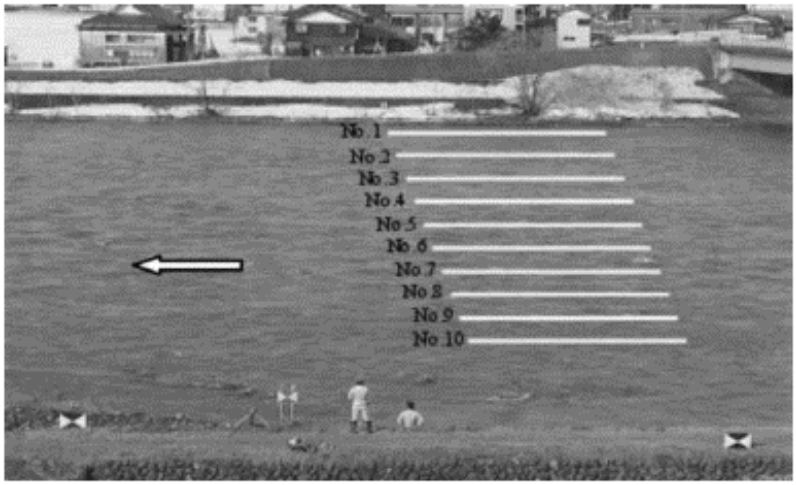

Figure 2:21 Visualization of surface flow image of Uono River (**Fujita et al., 2007**).

2.3.2 Unmanned Aerial Vehicle (UAV)

This method consists of measuring the surface velocity distribution of the river with video images obtained from an unmanned aerial vehicle (UAV) as shown in **Figure 2:22**. The description of the structure of the systems of aerial STIV developed some tools to correct the vibration of UAV through intelligent processing techniques such as Rotation Invariant Phase Only Correlation called RIPOC and Scale Invariant Feature Transform called SIFT (**Fujita and Notoya, 2015**).

Figure 2:22 Equitment of UAV.

The first step of the technique is to apply the RIPOC algorithm developed by Takita et al. (**2003, 2004**) in order to detect the background displacement between the images, parallel displacement length, rotation angle and change of image size. The second step is the detection of feature points using SIFT algorithm (**Lowe, 2004; Bay *et al.*, 2008**). To be more efficienct in the process and have a good performance, Library Approximate Nearest Neighbors (FLANN) developed by Muja et al. (**Muja and Lowe, 2009, 2014**) was used. As the image still has some errors of vibration, the application of Random sample consensus method (RANSAC) (**Fischler and Bolles, 1981; Hast et al., 2013**) is important to avoid outlier data for the image transformation process in the third step corresponding to the application of STIV techniques developed by Fujita et al. (**2007**).

Furthermore, a test was performed on the Saint Joseph river in Indiana, USA, reproducing instantaneous velocity maps of flow and demonstrating the power of the method (**Blois *et al.*, 2016**). Another study was in Thur River, Switzerland (**Detert and Weitbrecht, 2015**), where the image processing was done with MATLAB-based open source software PIVlab developed by Thielicke et al. (**2014**). Another research implemented a similar technique called remotely piloted aircraft system (RPAS), that has application only for low surface velocity and small discharge described by (**Bolognesi *et al.*, 2016**).

2.3.3 The Variance Image (VI) and Threshold Segmentation with Path Discretization (TSPD)

This method to capture the surface flow velocities and the discharge volumes with the application of video-based techniques and digital image processing for data collection was developed by Osorio-Cano et al. (**2013**). The validation of this method was through laboratory measurements in the UISA hydraulics channels in the Universidad Nacional de Colombia (UNAL) as shown in **Figure 2:23**.

The authors describe two techniques based on digital image processing – Variance Image (VI) Techniques and Threshold Segmentation and Path Discretization. Both techniques are compared with results from conventional instruments. For both techniques 12 variance images were captured with a group of 20 photograms recorded every 1 second (δt).

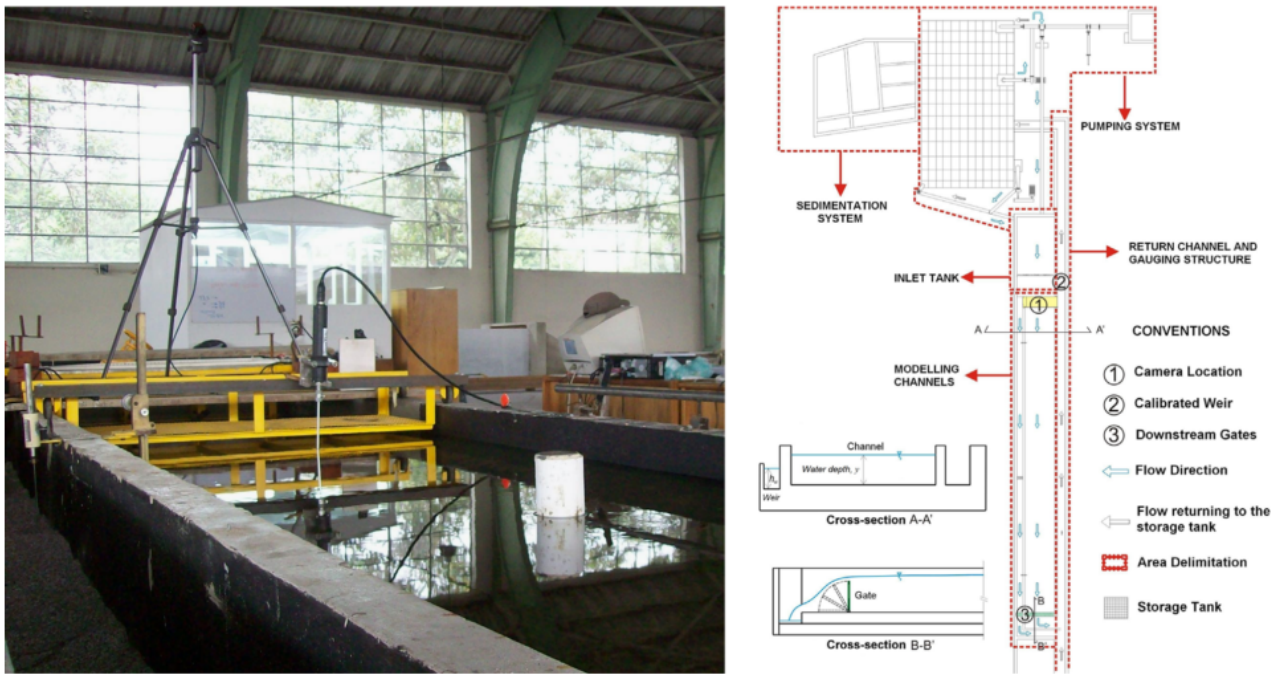

Figure 2:23 Sketch of UISA Hydraulics channels (**Osorio-Cano, Osorio and Medina, 2013**)

The Variance Image technique (VI)

The principle objective of the techniques is to measure the variance of the pixel intensity of a group of stored images where paths or routes of possible tracers or particles traveling on the surface flow are detected (**Osorio-Cano et al., 2013**).

Matlab tools were used to correct the variance at some point by the function ginput, transform the velocity field (u and v) in coordinates of the image to (x,y,z) and correct the effect of the angle from the camera using the Pinhole model (Direct Linear Transform, DLT), where the projection of matrix H was built as shown in **Equation *[2:36]*** of Pinhole model:

$$V_i = \frac{d}{t}\begin{bmatrix} w_i u_i \\ w_i v_i \\ w_i \end{bmatrix} = \begin{bmatrix} h_{11} & h_{12} & h_{13} & h_{14} \\ h_{21} & h_{22} & h_{23} & h_{24} \\ h_{31} & h_{32} & h_{33} & 1 \end{bmatrix}\begin{bmatrix} x_i \\ y_i \\ z_i \\ 1 \end{bmatrix} = H \begin{bmatrix} x_i \\ y_i \\ z_i \\ 1 \end{bmatrix} \qquad [\ 2{:}36\ ]$$

Considering that for these studies the value of z is constant, the values (x,y) are represented for every point in the image. Furthermore, the instantaneous velocity for two consecutive time is generated with the following **Equation *[2:37]***:

$$V_i = \frac{d_t}{t} = \frac{\sqrt{(x_{i+1} - x_i)^2 - (y_{i+1} - y_i)^2}}{t} \qquad [\ 2{:}37\ ]$$

Where: d_t : is the distance between two consecutive position of the tracers during δt

n_i : is the total number of positions along the channel

i : is equal to 1,2,…,n_i-1

The mean velocity is obtained by averaging each of the instantaneous velocities using **Equation *[2:38]***:

$$\overline{V_j} = \frac{1}{n_i - 1}\sum V_i \qquad [\ 2{:}38\ ]$$

Where: m : is value corresponding to the total number of paths identified for each case

j : is equal to 1,2,…,m

i : is equal to 1,2,…,n_i-1

And as the final result, the mean surface velocity is obtained for each case by averaging the mean velocity of each tracer or particles following **Equation *[2:39]***:

$$V_s^* = \frac{1}{m}\sum \overline{V_j} \qquad [\ 2{:}39\ ]$$

Where: j : is equal to 1,2,…,m

Consequently the mass conservation equation is used to obtain the discharge through the channel UISA in the laboratory of hydraulics of UNAL, as shown in **Equation *[2:40]*** of discharge:

$$Q_{est} = \frac{(V_m)_{est}}{A_{est}} = (k_r V_s)(b y_{est}) \qquad [\ 2{:}40\ ]$$

Where: $(V_m)_{est}$: is the estimated mean velocity

y_{est} : is the estimated flow depth

k_r : is the adjustment coefficient for large-scale roughness flow in rivers (k_r=0.85, recommend the literature).

Threshold segmentation and path discretization (TSPD) technique

This technique is similar to the variance of image techniques described before. For the analysis the video recorder captures frames with small area between 400 by 600 pixels at a velocity of 10 frame per second with a duration of 1 minute, with a total of 6 cases of study.

The description of the Threshold Segmentation and Path Discretization (TSPD) techniques are divided in 3 steps: namely, binarization of raw video data, data grouping by labeling and filtration and path discretization. The first step corresponds to sensitive analyzes of the performance, focusing on the transformation of RGB binary image in grayscale intensity value of the image with the range of 0 to 255. The idea is to assign the value 1 (white dots) to a value equal or greater to 230, and value 0 (white dots) less than 230 to the binary image. The second step is the identification the white element on the binary image. The accuracy of the techniques depends of the size of the objects and the connectivity of the objects, because the objects of the binary image correspond to tracers moving as surface flow. Lastly, the third step was to build the surface velocities with the Threshold segmentation and path discretization (TPSD) and Variance Image (VI) Techniques.

2.3.4 Large-scale particle image velocimetry (LSPIV)

The developed Large-Scale particle Image Velocimetry (LSPIV) was previously studied by Fujita and Komura (**1994**) and Fujita et. al (**1997**). LSPIV techniques have similar algorithm to conventional PIV but with special treatment for flow illumination, flow tracing and removal of the spatial distortion of the recorded images due to lens aberrations and imaging at oblique angles (**Fujita et al., 1998**).

LSPIV Velocimetry techniques used a CCD or Charge-coupled device camera located in a position with angle of 90^0 to the flow for the image capture as shown in Figure 2:24. The LSPIV techniques used a conventional system for image recorded and the image resolution is 640 by 480 or 512 by 512 pixel with 8 bit image of gray level. The important tasks for the image processing of LSPIV are match flow seeding, image recording and processing variables to the flow structures to be captured (**Fujita et al., 1998**).

In order to consider that in the image process, the results present some image distortion that is possible to correct through the procedure for correction of distorted images with some parameters described by Fujita et al. (**1997**). Two coordinates systems are used: cathode-ray tube (CRT) coordinates (xyz) and the physical coordinates (XYZ), both of which are related through a transformation matrix. The transformation equation from CRT-coordinates to the physical coordinates follow the **Equation *[2:41]***:

$$X = \frac{b_1 x + b_2 y + b_3}{b_4 x + b_5 y + 1}, \quad Y = \frac{b_6 x + b_7 y + b_8}{b_4 x + b_5 y + 1} \qquad [\,2{:}41\,]$$

Where: b_i (i=1,8) : are the transformation coefficients determinate by the least square method using N pairs of points of know coordinates, (x_1,y_1), $X_1,Y_1),\ldots(x_N,y_N),(X_N,Y_N)$.

Also, the transformation equation can be generated using the **Equation *[2:42]***:

$$TB = Z \qquad [\,2{:}42\,]$$

Where T is equal to the matrix as show in the **Equation *[2:43]***:

$$T = \begin{bmatrix} x_1 & y_1 & 1 & -x_1X_1 & -y_1Y_1 & 0 & 0 & 0 \\ . & . & . & . & . & . & . & . \\ . & . & . & . & . & . & . & . \\ . & . & . & . & . & . & . & . \\ x_N & y_N & 1 & -x_NX_N & -y_NY_N & 0 & 0 & 0 \\ 0 & 0 & 0 & -x_1Y_1 & -y_1Y_1 & x_1 & y_1 & 1 \\ . & . & . & . & . & . & . & . \\ . & . & . & . & . & . & . & . \\ . & . & . & . & . & . & . & . \\ 0 & 0 & 0 & -x_NY_N & -y_NY_N & x_N & y_N & 1 \end{bmatrix} \quad [\ 2{:}43\ ]$$

And B and Z follow the **Equation** *[2:44]* and **Equation** *[2:45]*

$$B = [b_1, b_2, \dots b_8]^T \quad [\ 2{:}44\ ]$$

$$Z = [X_1, X_2, \dots X_N, Y_1, Y_2, \dots Y_N]^T \quad [\ 2{:}45\ ]$$

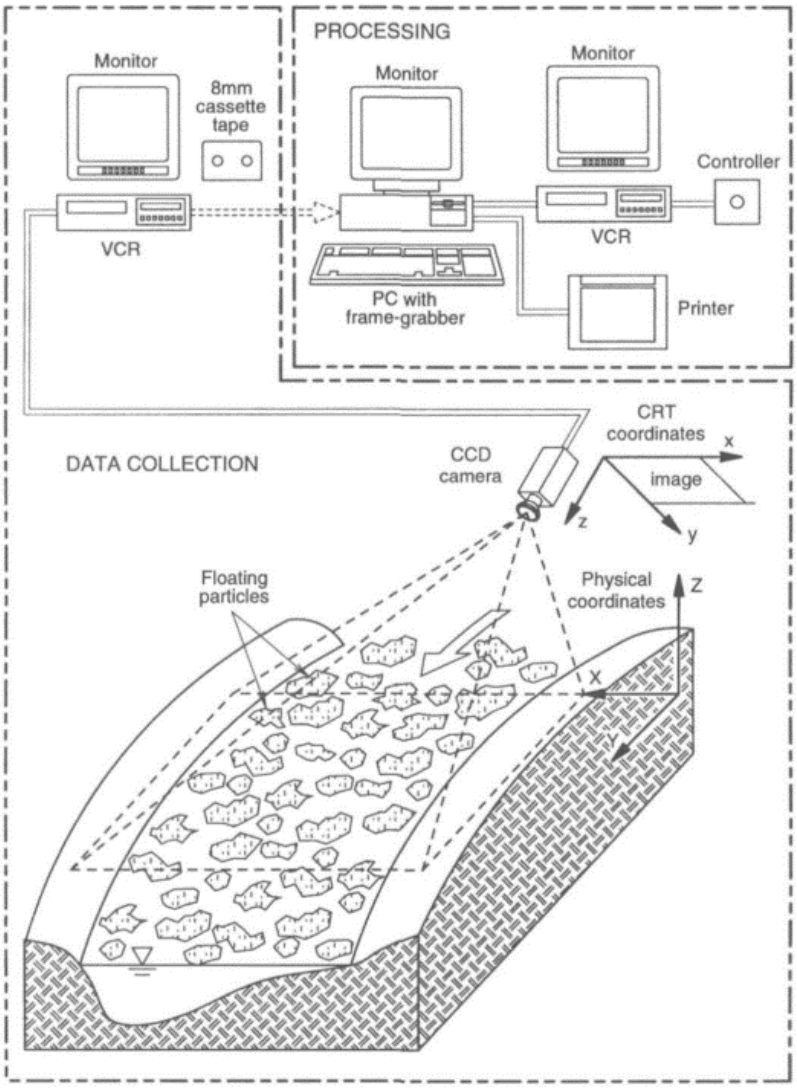

Figure 2:24 Diagram of Large-Scale Particle Image Velocimetry (**Fujita et al., 1998**)

Consequently, the LSPIV techniques include some additional steps in the procedures to build field velocities through LSPIV method as shown in **Figure 2:25**. In fact, the output of the LSPIV measurement is the instantaneous velocity vector for the area of study. The seeding and illumination of the LSPIV image techniques are significantly different from the standard PIV.

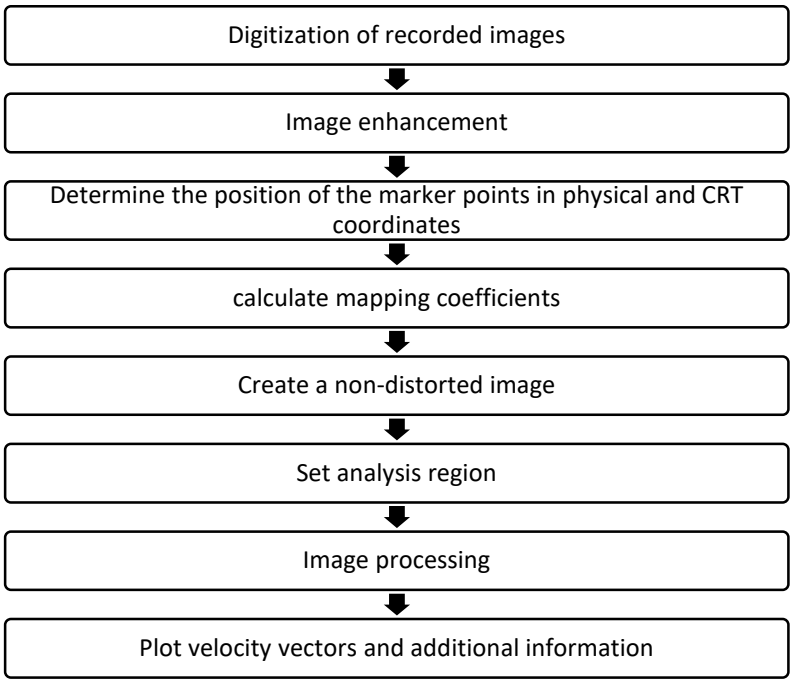

Figure 2:25 Steps of LSPIV techniques (**Fujita et al., 1998**)

The particles located in the free surface are used as tracer, but are sometimes not well distributed in the area of study and additional seeding particles is necessary in the domain to have a good correlation and reproduce the velocity field (**Ismail and Ulrich, 2007; Di Cristo, 2011**). But in some cases of rivers, the domain of study is very large and foams and straw on the free surface are usually used as tracers. The velocity field using this kind of tracers present significant error in the flow velocity. Admiraal et al. (**2004**), developed a new method to reduce the error of visualization of tracers in a real case of study in the Lake Ogallala in Nebraska, United States of America method. For this reason, Admiral et al. proposed methods to reduce the effect of the tracers with the case study of the Lake Ogallala in Nebraska, U.S.A. Furthermore, the effect of tracers, seeding procedure and concentration are further investigated by Muste et al. (**2004**).

Another important factor is the illumination, that in LSPIV techniques is lesser compared to the standard PIV that requires high intensity. This technique usually uses halogen, sodium-vapor or other types of lamps located in a suitable position to produce uniform illumination in the area of study.

LSPIV was used in some applications in fluvial hydraulics like surface of shallow water flows in hydraulics structures described by Weibrecht et al. (**2002**), and laboratory experiments on mass exchange between river and dead water zones created by groin fields (**Brady et al., 2004; Stagonas and Müller, 2007; Weitbrecht et al., 2008**). Furthermore, Hauet et al. (**2008**) developed some advances to the LSPIV method for rivers application with two steps – geometric transformation and image reconstruction, capable of generating the field velocities and flow discharge in the section of study. Also another kind of characterization of flow depth and discharge was developed with laboratory experiments by Muste et al. (**2004**), for implementation in rivers and coastal areas.

LSPIV techniques is a robust alternative for taking measurements during extreme events such as floods, hurricanes or low flows in wetlands and small streams (**Muste et al., 2010**). LSPIV was implemented in rivers such as Iowa and Piano Key Weirs (**Creutin et al., 2003; Hauet et al., 2008; Jodeau et al., 2008; Kantoush et al., 2011; Muste et al., 2011; Sharma et al., 2014**), with comparison to experimental data and in some cases, numerical simulation as well. Furthermore, investigation was developed by Dobson et al. (**2014**) for the river surface velocity to increase the performance and the accuracy. In addition, river surface flow was measured by videotape from a helicopter with the applications to flood flow and a low flow in the Shin River in Japan (**Fujita and Hino, 2003**), as shown in **Figure 2:26**.

Figure 2:26 Surface field velocities on Shin river (**Fujita and Hino, 2003**)

LSPIV techniques were also applied to measure the flow inside sewers systems (**Jeanbourquin et al., 2011**), considering the complicated environment to conduct measurements and install equipment. Also LSPIV was applied using hydraulic kinematic model in order to generate three-dimensional flow fields for discharge approximation (**Bradley et al., 2002**).

2.3.5 Mobile large-scale particle image velocimetry (MLSPIV)

The technique of mobile large-scale particle image velocimetry (MLSPIV) was developed with the principle of the large-scale particle image velocimetry (LSPIV) techniques, with the evolution of the mobile device in the last decades. The technique captures real time visualization and estimates the instantaneous averaged flow characteristic of a free surface river with minimum equipment from the banks of the river (**Kim *et al.*, 2008**).

The instruments for the measurement include the imaging device (video or digital camera), the telescoping mast, and a truck with a control and data processing unit, capable for remote control and real time display of the characteristic of the river, as shown in **Figure 2:27**.

For this technique the authors developed two types of programs – the PTU program (**Trivedi, 2004**) which controls the camera and the LSPIV program Hauet et al. (**2009**) for the image processing and evaluation of the discharge in the river. The software is based on the algorithm developed by Fujita et al. (**1998**).

The procedure of MLSPIV has three steps including the first step related to the truck and peripherals, the second step of camera positioning and image acquisition and the final step of image processing to obtain the velocity fields and discharges. This technique was compared with the measurements of discharge by the U.S. Geological Survey (USGS) stream gauging station in Iowa, USA.

Furthermore, the last investigation was to use the MLSPIV techniques to measure flood discharge in the Arc river in France (**Dramais *et al.*, 2011**), because in flood events the velocity is one important parameter to measure, but is not easy to measure with high flow approximation in the river. The paper compares the results with conventional measurement and with numerical simulation.

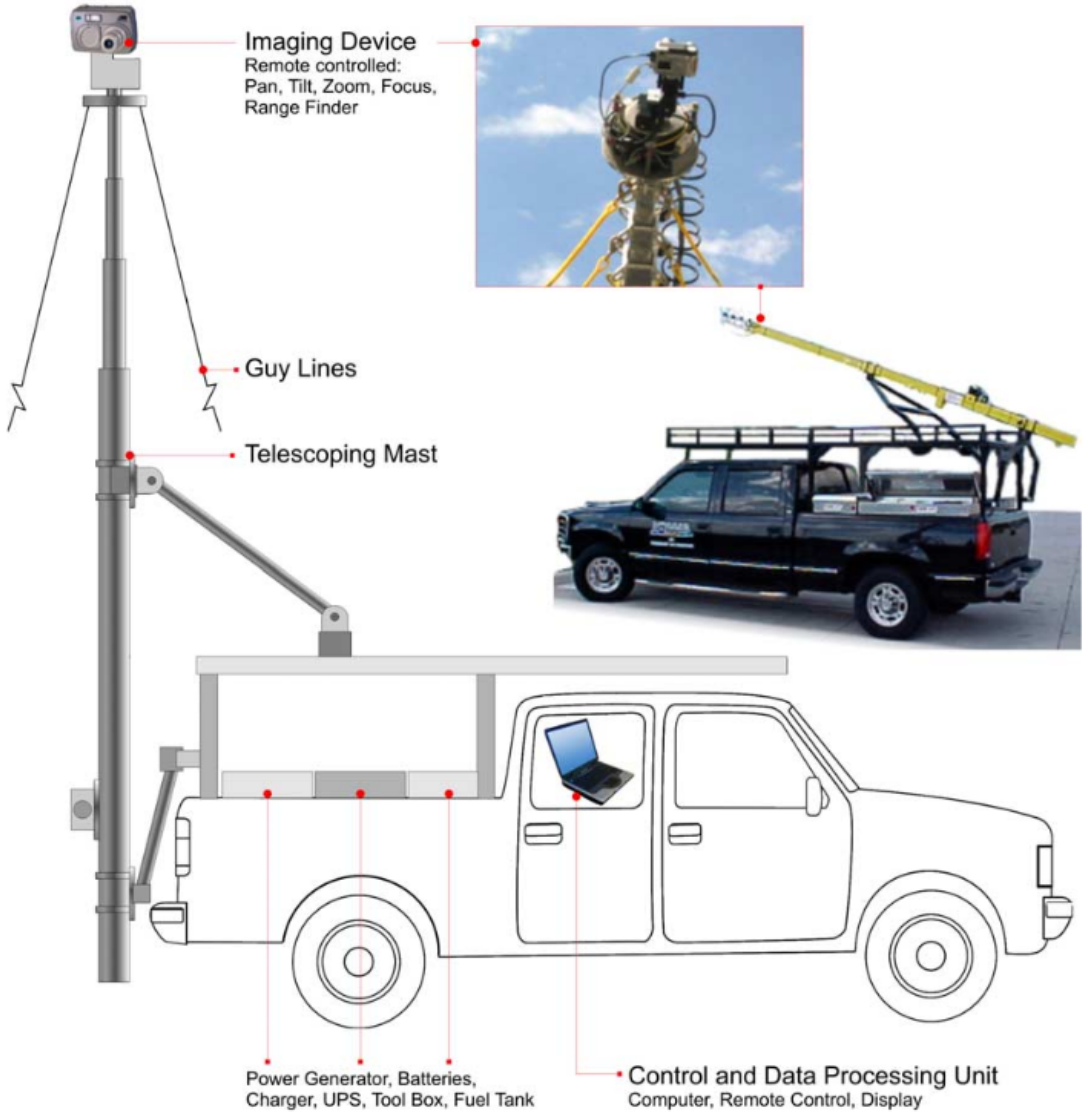

Figure 2:27 Sketch of measurements using MLSPIV (**Kim *et al.*, 2008**)

2.3.6 Direct Visual Measurement using digital video recording systems

This technique called Direct Visual Measurement was developed using closed-circuit television (CCTV) systems, and compared with two different methods – Large-Scale Particle Image Velocimetry (LSPIV) and Space-Time Image velocimetry (STIV). The technique was evaluated also with experimental measurements by standard equipment. The location of this study was in the Tempaku river located in the central part of Japan (**Tsubaki et al., 2011**). Also, the CCTV camera was located near to the Nomani bridge station as shown in **Figure 2:28**.

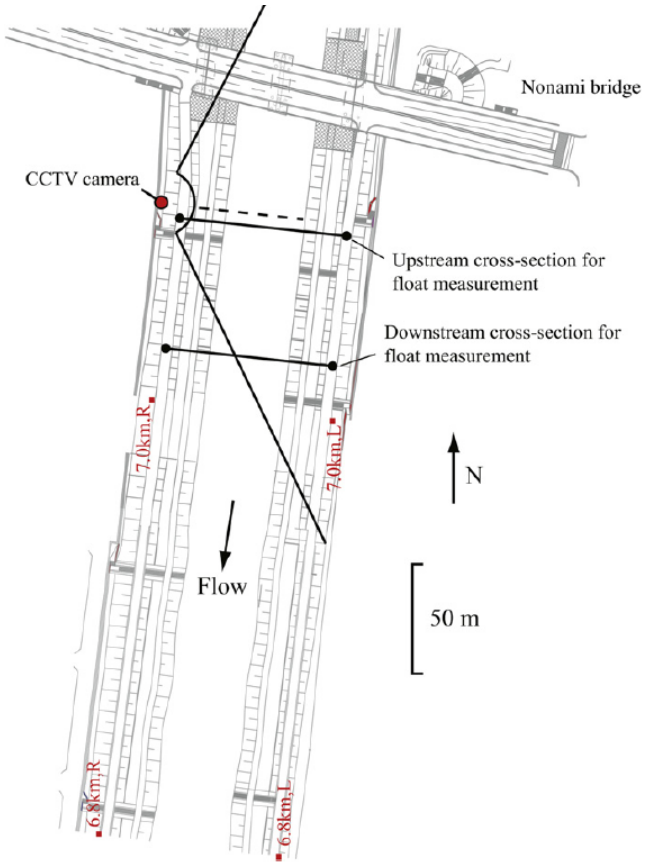

Figure 2:28 Sketch of measurements using digital video recording systems (CCTV) (**Tsubaki et al., 2011**)

This technique was created because, in some cases, deteriorated tracer image with a poor quality format in video recordings proved difficult to apply directly to the PTV technique or PIV technique. For example, when the image recorded was done in midnight. For this reason considerations were taken to correct the angle and generate the mean velocity using flooding debris or float as tracers, with the following **Equation *[2:46]***:

$$\vec{u} = \frac{\overrightarrow{p_2} - \overrightarrow{p_1}}{t_2 - t_1} \qquad \textit{[2:46]}$$

Where: $\vec{u}$: is the mean velocity vector of the target.

$\overrightarrow{p_1}$: is the position vector of the target at instant t_1.

$\overrightarrow{p_2}$: is the position vector of the target at instant t_2.

In conclusion, the surface flow velocity by direct visual measurement techniques compared with the conventional float measuring present a correlation coefficient of 0.76. Nevertheless, this is a useful tool for discharge measurement to establish a rating curve for hydraulics applications for rivers.

Furthermore, direct visual measurements compared with the LSPIV and STIV techniques show different magnitudes of flow rate, where the difference between experimental measurement versus LSPIV are 26% and with STIV techniques of 9%. These effects are because the LSPIV techniques are more sensitive to the details of the surface pattern than the STIV techniques (**Tsubaki et al., 2011**).

Chapter 3 Surface Flow Image Velocimetry (SFIV) Technique

3.1 Introduction

The aim of this chapter is to describe the application of the Surface Flow Image Velocimetry (SFIV) to develop a hydraulic analysis of the velocity fields in the vicinity of inlet grates and measurement of flows nearby, to improve the knowledge and the design of new inlets and their spacing. This visual technique allows the approximation of the surface flow velocity field where other techniques can fail. Especially in the case when the flow is supercritical near the inlet, with small depths, the introduction of other devices to measure velocity fields (ADV, etc.) strongly modifies the flow around the gage and it is useless the data collected. SFIV allows to get in a non-intrusive way an approach of the flow velocities in the area covered by the images.

This chapter defines the experimental methodology proposed and implemented in this doctoral thesis dissertation. It describes the experimental installation, the instrumentation used, the design of the experimental campaign and the testing phase of the implementation.

The design of the experiment is the step prior to the realization of the essays. This phase describes the experimental facilities and equipment chosen to perform the experiment, planning the assembly of the various elements and finally a calculation of the fields of velocities and distribution of flows through the processing of images.

The image processing allows to obtain approximated results according to the test parameters chosen and gives an idea of the viability of the experiments as well as of the experimental conditions to be imposed in order to minimize the errors.

The experimental facilities are located in the hydraulic laboratory of the Technical University of Catalonia. The physical model used for this work is a platform simulating a road lane where surface drainage inlets can be located. The experiments facilities can be divided in two groups: in the first there are included the hydraulic platform, light equipment (reflectors) and the grate located on the platform, while in the second group there are the high speed and resolution camera and a computer with enough storage and high computer processing units that will be described next section. Video cameras of high resolution and speed with commercial codes were used to characterize the flow patterns in some of the most common grate inlets used in Barcelona. Measurements of velocity fields using video techniques and image processing algorithms have been compared with the approaching velocity (1D flow) for 3 types of grates, and with the intercepted flow measured in the tests. Flow measured in the lab is the total intercepted flow, but no differences between frontal and lateral flow are made, so the only way to know this difference would be using the SFIV or other similar techniques, from the velocity distributions next to the inlet.

Another purpose of this chapter is to assess the viability of the implementation of Digiflow and PIVlab in specific experimental conditions as were tested in the experimental campaign of this thesis with specular reflection of light interacting with the small waves on the free surface, instead of conventional particle seeds to estimate the flow visualization, because in this case represents an option to get the flow patterns through SFIV methodology.

3.2 Description of the research line developed by the Institute Flumen

Few years ago, following a demand from the former sewerage management company of Barcelona, CLABSA (Clavegueram of Barcelona S. A), now BCASA, a series of tests about the hydraulic behavior of a set of the most common inlets in Barcelona was conducted in the hydraulic laboratory of the Technical University of Catalonia. This gave rise at the beginning to a line of specific work by the Research Institute Flumen that, with the passing of the years, has always attracted more interest in this topic.

Other recent campaign was developed to study the hydraulic behavior of continuous transverse grates (typical in squares and pedestrian zones) (**Russo and Gómez, 2014**) or clogging factor related to conventional grate inlets (**Gómez *et al*., 2013; Gómez *et al*., 2018**).

3.2.1 Conventional grates tested

In the first phase of the experimental campaign carried out by Russo (**Russo, 2009; Gómez and Russo, 2011**), the most common grates used in the city of Barcelona were tested to estimate their hydraulic performance under different geometric and circulating flow conditions. These grate inlets and their geometric characteristics are shown in the **Table 3:1**, as well as in the **Figure 3:1** and **Figure 3:2**. The results related to the grates types 1, 2, 3, 4, 5, 6, 7, 8 and 9 were used to develop the methodology explained below, while the grates types 10 and 11 were used to validate the methodology.

Moreover, it was called (Q) the flow rate approaching along the street (In this case our platform function as a street), in the essays was measured the depth at the edge of the platform, immediately upstream the grate and the flow captured or flow intercepted called (Q_{Int}) for a combination of values of slopes and flow rates as shown in the **Equation *[3:1]***.

$$E = \frac{Q_{int}}{Q} \qquad [\ 3{:}1\ ]$$

Where: Q : is the approaching discharge (l/s)

Q_{int} : is discharge intercepted by the grate inlet (l/s)

E : is the efficiency of the grate inlet between 0 and 1

The data of flow rate captured by the grate does not reflect too well the hydraulic behavior of the grate. An intercepted flow rate of 10 l/s is high if the approaching flow for street is 20 l/s, and is a small value in front of 150 l/s. Efficiency explains much better the performance of a grate in front of the circulating flow along the street. So, the comparison between grates efficiency should be done in terms of efficiency.

The capacity of intercepted flow for all types of grates was obtained for each flow rate and different combinations of platform slopes tested. 8 longitudinal slopes and 5 cross slopes were tested, and all the corresponding combinations (in total 40 combinations) were tested with 5 different flow rates and all the types of grate.

Figure 3:1 Grates tested during experimental campaign (types grates 1, 2, 3, 4, 5, 6, 7, 8, 9).

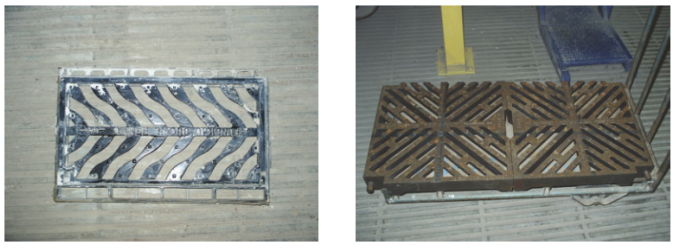

Figure 3:2 Two types of grates (Types 10 and 11) used to validate the methodology carried out.

Grate	Length (L) cm	Width (W) cm	Area including void area (A_g) m^2	Void area (A_H) m^2	Number of longitudinal bars (n_l) Units	Number of transversal bars (n_t) Units	Number of diagonal bars (n_d) Units
Type 1	78.0	36.4	0.2114	0.1214	5	1	0
Type 2	78.0	34.1	0.1850	0.0873	1	17	0
Type 3	64.0	30.0	0.1647	0.0693	1	0	12
Type 4	77.6	34.5	0.2250	0.1050	2	13	0
Type 5	97.5	47.5	0.3431	0.1400	3	7	0
Type 6	80.0	30.0	0.1622	0.0736	0	15	0
Type 7	60.2	31.5	0.1807	0.0881	2	1	10
Type 8	74.5	26.0	0.1540	0.0852	1	0	11
Type 9	100.0	50.0	0.5000	0.2012	1	3	21
Type 10	60.2	31.5	0.1807	0.0865	2	0	8
Type 11	99.9	50.0	0.4940	0.1760	1	3	28

Table 3:1 Geometric characteristics of the tested grates in the Laboratory of Hydraulics from UPC.

Different adjustments that allow easy application of the experimental results were attempted. Initially linear relations were proposed between hydraulic efficiency and flow depth on the platform. This allows to set a line for

each current circulating flow down the street. This adjustment is more clear for high flow rates and less evident for low flow rates.

Following experiences in other countries, an adjustment was made between the inlet hydraulic efficiency (E) and the ratio of flow rate and depth (Q/y). Previous studies by other authors as Spaliviero et al. (**2000**) suggested linear relationships of E vs Q/y. On the basis of the data from the tested results, a potential relation was proposed following the **Equation *[3:2]***:

$$E = A \cdot \left(\frac{Q}{y}\right)^{-B} \qquad [\ 3{:}2\ ]$$

Where: Q : is the approaching discharge (m^3/s)

y : is water depth (m)

$A\ and\ B$: are the parameters that depend on the geometry of the grate

The proposed adjustment **Equation *[3:2]*** describes quite well the behavior of the grates studied as shown in the **Table 3:2** and **Figure 3:3** (Gómez and Russo, 2011). Moreover, Spaliviero et al. (**2000**), did not reach high values of Q/y, with values close to 1, while for the tests carried out in the laboratory of the UPC, the flow conditions reached values up to 8 and more (**Russo, 2009; Gómez and Russo, 2011**).

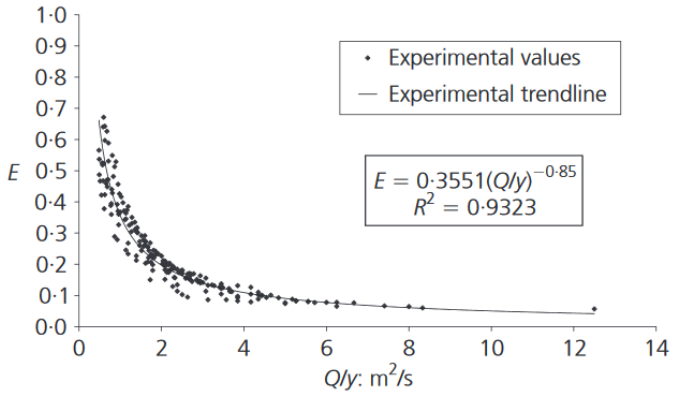

Figure 3:3 Potential adjustment from the experimental data.

Grate type	1	2	3	4	5	6	7	8	9	10	11
R^2 (%)	81.04	91.20	92.13	85.08	88.39	88.05	90.34	93.23	82.53	88.73	81.97

Table 3:2 Correlation coefficient for tested grates.

The values of the coefficients A and B for the tested grates are identified to fully characterize the grate. **Table 3:3** summarizes the parameter values of A and B found using the potential adjustment of **Equation *[3:2]*.**

Grate type	1	2	3	4	5	6	7	8	9	10	11
A	0.447	0.386	0.397	0.4301	0.536	0.3703	0.390	0.3551	0.556	0.3522	0.515
B	0.739	0.873	0.830	0.815	0.790	0.8645	0.079	0.8504	0.707	0.7175	0.688

Table 3:3 Values of coefficients A and B.

The adjustment (**Equation *[3:2]***) considers only the flow rate through a platform width of 3 meters. In the case that the width of mid road is different from 3 meters, the **Equation *[3:2]*** can be generalized to any type of geometric section considering flow rate circulating on the half of the street (Q_{Street}) and a uniform velocity distribution (**Gómez and Russo, 2005; Russo and Gómez, 2011**).

In order to extend the methodology for streets with several lanes presenting a half roadway width x different from 3 m it is possible to generalize the **Equation *[3:2]*** according to the flow depth (y) using the following expression in the **Equation *[3:3]***.

$$E' = A \cdot \left[k \cdot \frac{Q_{roadway}}{y}\right]^{-B} \qquad \textit{[3:3]}$$

Where: $Q_{roadway}$: is the flow approaching to an inlet related to half roadway (m^3/s)

E' : is the inlet efficiency related to a width of half roadway x=3 m

y : is water depth (m)

$A\ and\ B$: is the parameter that depend on the geometry of the grate

k : is a coefficient related to the street geometric conditions and to the flow depth (y)

For this reason, the **Table 3:4** shows the formulas that generalize the **Equation *[3:3]*** for any type of road.

Coefficient k for each type of street and geometric conditions and each flow depth	
Half roadway width x=3 m	
Any y	k =1
Half roadway width x < 3 m	
$y \leq x \cdot I_x$	k =1
$x \cdot I_x \leq y \leq 3 \cdot I_x$	$k = \frac{1}{1-\left(1-\frac{x \cdot I_x}{y}\right)^2}$
$y \geq 3 \cdot I_x$	$k = \frac{1-\left(1-\frac{3 \cdot I_x}{y}\right)^2}{1-\left(1-\frac{x \cdot I_x}{y}\right)^2}$
Half roadway width x > 3 m	
$y \leq 3 \cdot I_x$	k =1
$3 \cdot I_x \leq y \leq x \cdot I_x$	$k = 1-\left(1-\frac{3 \cdot I_x}{y}\right)^2$
$y \geq x \cdot I_x$	$k = \frac{1-\left(1-\frac{3 \cdot I_x}{y}\right)^2}{1-\left(1-\frac{x \cdot I_x}{y}\right)^2}$

Table 3:4 Equations for determine value of k.

Where $Q_{roadway}$ is defined as the circulating flow related to the real geometry of the street, while Q was the flow circulating on the UPC platform of 3 meters width. Flow hydraulic sections and flow depths vary depending on the street geometry and on the circulating discharge. Moreover, $Q_{roadway}$ and Q generate the same flow depth at the curb (y), but the difference is that the first corresponds to the real geometric characteristic of the street, while the second one is related to platform geometry. Also, the product ($k \cdot Q_{roadway}$) represents the discharge Q approaching

the inlet for a roadway width x=3m (corresponding to the platform width). Once E' was calculated, the intercepted flow Q_{int} can be determined by the **Equation *[3:4]***:

$$\boldsymbol{Q_{int} = E' \cdot Q = E' \cdot k \cdot Q_{roadway}} \qquad \textit{[3:4]}$$

While this methodology is easy to use, it would be desirable to extend this analysis to grates that have not been tested. Although the best results are obtained from the tests, it is evident that experimental data may not always be available. For all that, a correlation between the parameters A and B of the potential law and some important geometric characteristics of the tested grates was found. After several attempts the **Equation *[3:5]*** and **Equation *[3:6]*** to estimate A and B parameters were proposed (**Gómez and Russo, 2011**).

$$\boldsymbol{A = \frac{1.988 \cdot A_g^{0.403}}{p^{0.190} \cdot (n_t + 1)^{0.088} \cdot (n_l + 1)^{0.012} \cdot (n_d + 1)^{0.082}}} \qquad \textit{[3:5]}$$

Where: A_g : is the minimum area that includes all the voids in the grate inlet (m^2)

p : is ratio between the void area and A_g (%)

n_t : is the number of transversal bars (unit)

n_l : is the number of longitudinal bars (unit)

n_d : is the number of diagonal bars (unit)

$$\boldsymbol{B = 1.346 \cdot \frac{L^{0.179}}{W^{0.394}}} \qquad \textit{[3:6]}$$

Where: L : is the length of the grate inlet (in cm)

W : is the width of the grate inlet (in cm)

This setting reproduces the behavior of all types of grates with a range of values of their geometry characteristics similar to those tested. With these expressions, it is possible to approximate the equation to adjust the efficiency of a grate without having to perform any previous essay. The range of validity of the above equations is shown in **Figure 3:4**.

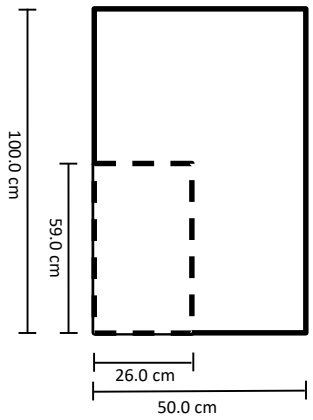

Figure 3:4 Range of validity for the **Equation *[3:2]***, **Equation *[3:3]*** and **Equation *[3:4]*.**

3.3 Description of experimental facilities to estimate inlet hydraulic efficiency

3.3.1 Main physical model facilities and characteristics

The hydraulic efficiency of the most common inlets used in Barcelona was analyzed through experimental tests in real scale (1:1) avoiding scale effects. In order to achieve this aim, the flow intercepted by the inlet was going to be measured from a known approximation flow. Thus the inlet's capture capacity for a given flow and transversal and longitudinal slopes in the street was obtained.

Figure 3:5 Sketch of physical model.

Test facilities consisted of a platform simulating a road lane where the grate inlet can be placed. The test zone dimensions on the fore-mentioned platform are 3 meters width and 5.50 meters length. These dimensions reproduce approximately the width of a circulation lane on an urban street, thus allowing the 1:1 scale of the study as shown in **Figure 3:5**. Water flows over the platform longitudinally. The platform slope can be altered both in the sense of the flow (longitudinally) as well as transversally. The range of the studied slopes goes from 0 to 4% of transversal slope, and between 0 and 10% of longitudinal slope. The experimental campaign was carried out in the Hydraulic Laboratory of the Technical University of Catalonia by Flumen Research Institute (**Figure 3:5**).

The laboratory has a pumping station able to discharge up to 250 l/s from a storage tank located at the basement of the building to another tank on the rooftop as shown in the **Figure 3:6**. Given the water's level oscillation in the tanks, energy losses, etc. the maximum flow is limited up to 200 l/s. The aim of the rooftop tank is to maintain a constant water level, and work as a regulation element for the laboratory's supply flow. It is located approximately 15 meters above the test zone.

Figure 3:6 Reservoir tank located at the roof of the building

A motorized multi stream valve regulates the supply flow. The valve is manually controlled. The flow measurement is done using a Fischer & Porter electromagnetic flow meter, with an estimated precision of 1 l/s. Thanks to this installation, the test flow can be regulated in an easy and reliable way, with the electronic control table for hydraulics pumps as shown in the **Figure 3:7**.

Figure 3:7 Electronic control of hydraulics pumps

3.3.2 Inlets test installation

Water enters into the platform through a small reservoir on the platform's head. This tank is responsible to dissipate entrance energy of the flow and to provide horizontality of the water level. So, one-dimensional movement condition in free surface for the water is favored: in a section (perpendicular to the flow direction) the water height is the same for the whole width, with a triangular cross section in case of positive transverse slope of the platform. This makes the flow easier to reach the approach conditions in steady and uniform flow.

In order to reproduce as faithfully as possible, the water approach (on the street) to the inlets in real conditions, the water enters into the test platform with a transversal distribution of water depths very similar to the one that takes place in a real city street. The head tank is 3.85 m wide (it includes all the useful platform), approximately 2 meters high (allowing water assume enough height on the platform) and one-meter width, which ensures a storage volume enough to guarantee a smooth entrance flow. The tank and the platform are connected by an elastic joint, that allows movements of the platform (mobile) with reference to the head tank (that is fixed) and guarantees the imperviousness and preventing water to escape **Figure 3:8**.

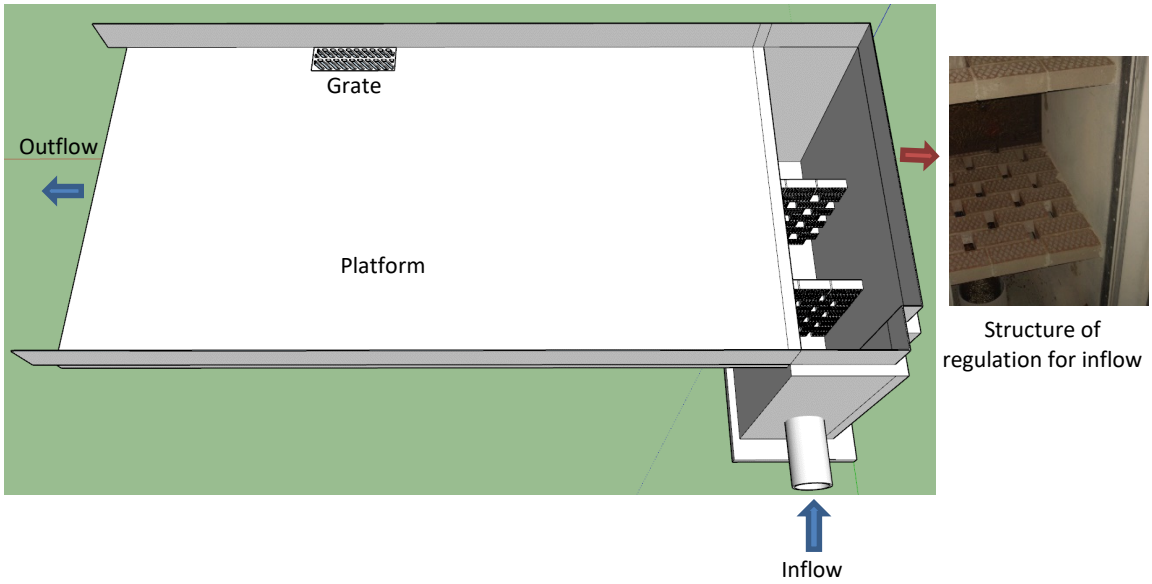

Figure 3:8 Sketch of the tank of regulation inflow

The platform has a total area of 3.20 x 6.70 m^2. The useful area for the circulation of water is 3.00 x 5.50 m and is limited by two PVC walls, approximately 30 cm high. The maximum water height during the tests will be 15 cm, equivalent to the curb height existing in most of the streets. The platform is based on three points: the two corners near the header tank and one point to the other end downstream of it. The first support is formed by a ball joint on a column with a height of 1.80 m that allows turns but no displacements, so it is the fixed point of the platform. It is located on the left upstream corner. The second support is located in the right upstream corner. It is formed by a supported kneecap in a threaded bar inside a column of 1.65 m. A flywheel on the threaded bar can vary the vertical displacement of the said support point, varying the cross slope of the platform to a maximum of 4%. The third support allows twists and scrolling vertically and horizontally. It is provided with an alternating current motor that allows the easy modification of the longitudinal slope. The maximum value allowed is 10% as shown in the **Figure 3:9**.

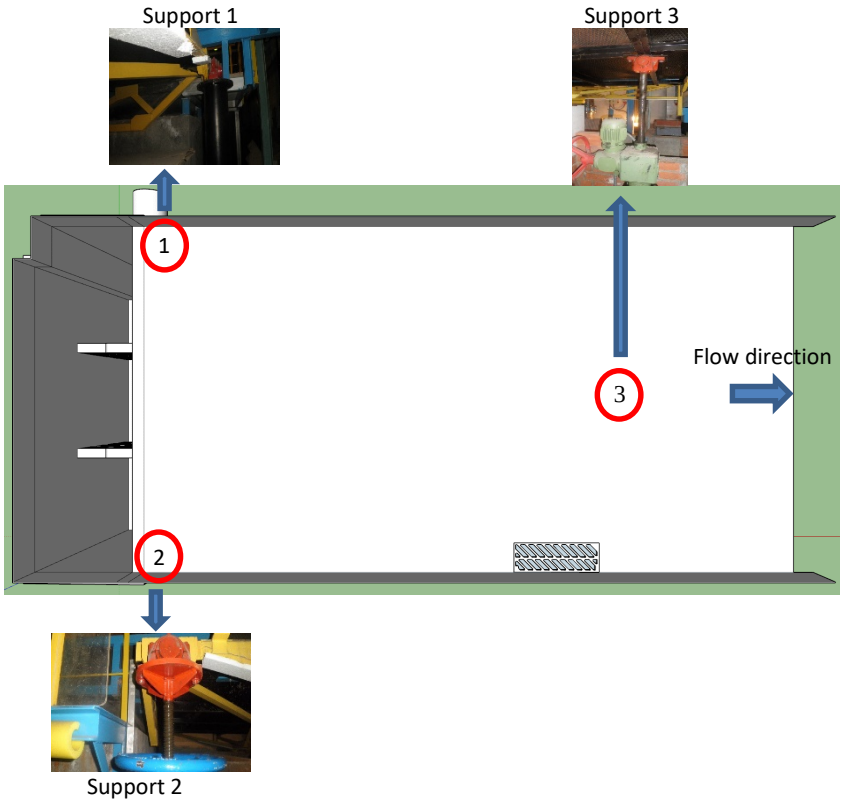

Figure 3:9 First point of based with ball for change the transversal slope.

Flow collected by the tested inlet falls down to a small pool, at the end of which is a V-notch weir where the discharge is measured by means of the use of a limnimeter which provides an accuracy of a tenth of millimetre for readings as shown in the **Figure 3:10**.

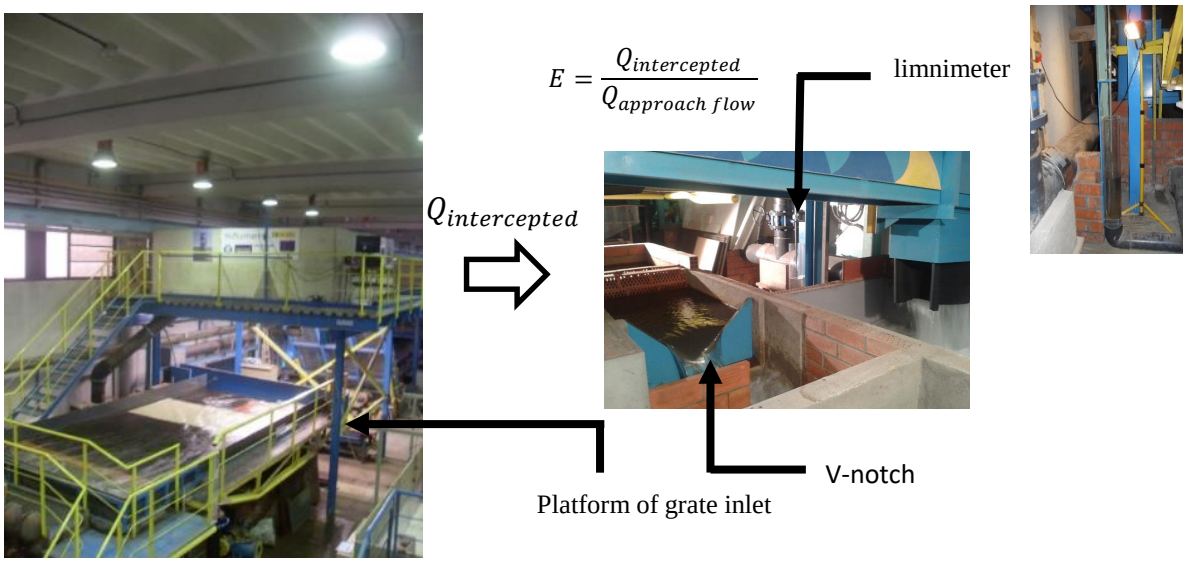

Figure 3:10 V-notch and limnimeter.

3.3.3 Test conditions

Flow range. **-** The study of the inlet efficiency was carried out according to a testing protocol considering 5 discharge values: 25, 50, 100, 150 and 200 l/s.

The upper limit is imposed by the pumping capacity of the laboratory. The limit value of 25 l/s was determined on the basis of previous tests, in which the measurements of the flow depth produced by lower discharges is very hard.

The range of studied discharges is greater than the usual values found in bibliography and close to the real discharges that can be generated during heavy storm events on urban streets.

Slope range. **-** Testing protocol considered the following slopes values:

Transversal Slopes:

I_x 0% 1% 2% 3% 4%

Longitudinal Slopes:

I_y 0% 0.5% 1% 2% 4% 6% 8% 10%

3.4 Methodology of SFIV Technique

3.4.1 Experimental and theoretical frameworks

This section defines the experimental methodology to estimate the flow velocity field in the nearness of a grate inlet. The methodology has been implemented in the hydraulic laboratory of the Technical University of Catalonia using the facilities described in the previous section and is proposed as one of the main achievement of this doctoral thesis. This section describes the preliminary studies on the installation, the design of the experimental campaign, the implementation of the experimental installation, the instrumentation used and the results obtained.

In this case, the proposed methodology can become a useful tool to understand the velocity fields of the flow approaching the inlet where the traditional measuring equipment's have serious problems and limitations (**Tellez et al. 2015**) with final objective to understand better the inlet hydraulic interception process (**Tellez et al. 2015; Tellez et al. 2016**).

To solve a problem of image processing for any experiments, the following 3 stages must be carried out as shown in **Figure 3:11**.

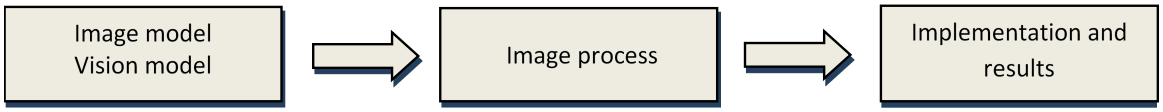

Figure 3:11 Three stages for the solution of an image processing problem (**Stucki, 1979**)

For the case of this campaign, an image model was developed through the use of experimental facilities and laboratory equipment's. Then an image process was defined and implemented using algorithms of flow pattern correlations by specific software and, finally, flow velocity field in the nearness of the grates was obtained.

Surface Flow Image Velocimetry (SFIV) allows to measure complex surface velocity fields in engineering. This may be particularly important when a single camera provides a 2D image of the real complex flow. Flow visualization is useful to understand the mechanics of a particular flow field and the provided information is invaluable for rapid feedback during experimental development (**Adrian and Westerweel, 2011**).

The practical application of SFIV for grate inlet efficiency estimation presented here, together with specific procedures to achieve these results, need enough contrast on the water surface to provide accurate measurement of the flows. The method that relies on several techniques of image processing evaluates the velocity field following the block diagram shown in **Figure 3:12**.

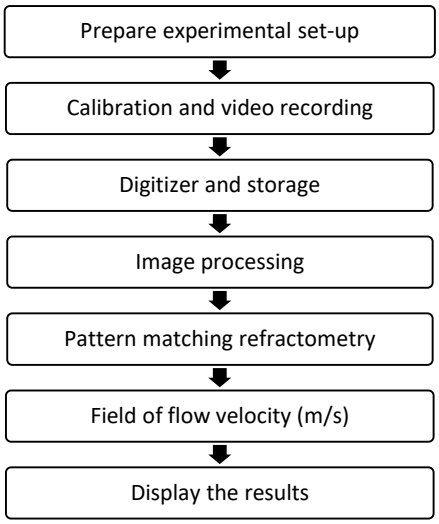

Figure 3:12 Diagram of general steps of the process based on SFIV technique

Images are obtained through a downward looking camera, located at a height of 4 meters above the platform, sustained vertically by a metal frame. The position of the light over the platform is located in the place that provides the best possible lighting in the study area, and it is able to achieve the best image resolution with the maximum velocity of the camera. The power of the two spotlights used was of 500 watt and 100 watt respectively. They were located at an angle of 45-degree respect to the platform when the lane is completely horizontal, to optimize reflection and minimize noise in the video image (**Figure 3:13**).

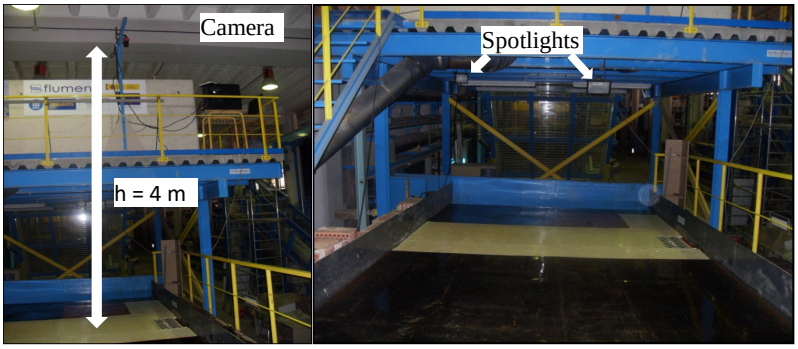

Figure 3:13 Location of camera and spotlights in the physical model

In addition, a strip of 1.35 x 3 m was also painted in light brown color with the objective of increasing the image contrast to have a better definition of the surface flow. In order to obtain several fiducial point references on the

video images, 21 points were plotted with a cross (+) using a simple marker on the area that can be best focused by the camera (0.94 m x 1.18 m) when it is completely flat on the platform (**Figure 3:14**).

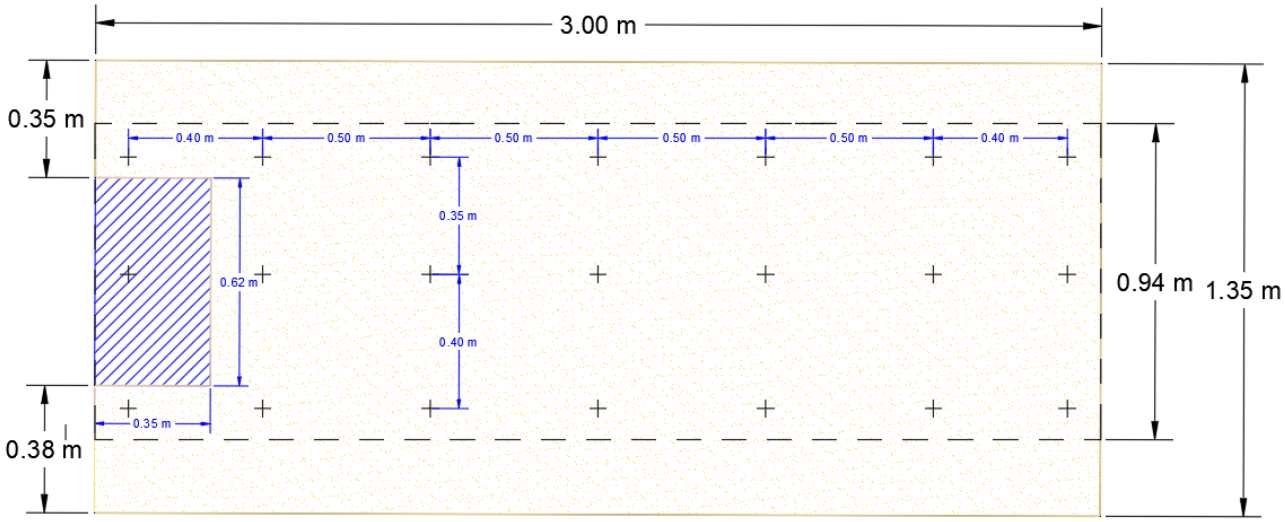

Figure 3:14 Painted section and marks on the platform used as reference points in the images

Next generation of laboratory experimental campaign, 3 different types of grate inlets (**Figure 3:15**) were tested to determine first the intercepted flow, it was same grate inlets used in the previous experimental campaign, proposing an images processing technique to get their detailed local velocity field for a large range of geometric conditions and different approaching discharges.

Grate Type 3 | Grate Type 5 | Grate Type 6

Figure 3:15 Type of grates used in the experimental campaign

For each of the grate inlets analyzed, the experiments were performed varying the flow rate and the longitudinal and transversal slopes. Flow captured measurements and video recordings were registered. Transversal slopes of 0%, 2% and 4% and longitudinal slopes of 0%, 0.5%, 1%, 2%, 4%, 6%, 8% and 10 were considered, with a total of 24 combinations. Moreover 5 different flow rates (25 l/s, 50 l/s, 100 l/s, 150 l/s and 200 l/s) for all the geometric combinations were considered reaching a total of 120 tests for each grate inlet.

3.4.2 High resolution and speed camera

The evolution of high-speed cameras makes possible the recording of video with excellent conditions for image processing, while the display of flow phenomena allows processes that are impossible to be captured by the human eye, or at conventional frequencies. It is of great interest to use a very high speed camera and also high spatial resolution to record the tests for flow velocity analysis. The selection of the type of camera depends on the flow but the main aspects, such as the sensitivity and speed of the camera, the capacity of memory recording and the resolution of the image, have to be considered. For the experiments presented here "Photonfocus" MV2-D1280-640 CMOS Area Scan Camera model was used (**Figure 3:16**). Technical specifications

of the camera are: resolution of 1280 x 1024 pixels, color format monochrome, frame rate of 488 fps, gray scale resolution output 8 bits, using also an optic Nikon 50 mm lens. Additionally, the camera needs a computer of large capacity with a data acquisition board to acquire and store the amount of information generated in the process of recording the video. Among the main features of the computer there are the Intel Core i7 processor and RAM of 12 GB. In addition, the computer has a video card that provides sufficient resources for the post-process images.

Figure 3:16 MV2 – D1280-640 CMOS Camera.

In addition, the software is provided to set camera parameters and stored within the camera. The camera has a digital Camera Link Full interface; image preprocessing is available as an option, the general specification and features of the camera are listed in the following **Table 3:5** (**User Manual Camera, 2008**) .

Parameter	Value
Technology	CMOS active pixel
Resolution	1280 x 1024 pixels
Pixel size	12.0 µm x 12.0 µm
Active optical area	12.36 mm x 12.29 mm
Color Format	Monochrome
Min. region of Interest (ROI) in 8 tap mode	1 row x 16 columns
Min. region of Interest (ROI) in 10 tap mode	1 row x 40 columns
Greyscale Resolution	10 bit (internal) / 8 bit (CameraLink output)
Digital Gain	X1 / x2 /4
Exposure Time	10 µs … 100 ms
Exposure Time Increment	2 µs
Frame Rate (T_{int} = 10 µm)	488 fps
Camera Taps	8 or 10
Readout mode	Sequential or simultaneous readout

Table 3:5 Specification of the MV2-D180-640 Camera

3.4.3 Video recording and preparation of video for image process

In order to prepare the sequence of the surface flow image, the open software VirtualDub (**www.virtualdub.org**) was used. It is a very powerful and free program, that allows modifications like cut or join videos or extract tracks from the long film. It also allows to change the resolution of videos, modify their quality, convert video from one format to another, etc. VirtualDub takes the video and prepares the sequence of images captured for 150 frames/second (for a time of 10 second, 1500 frame images were used). The images were processed in gray scale with an 8-bit palette of 256 colors, ranging from black (0) to white (255); a few thousand frames are enough to analyse the average flow during some seconds. The results presented here correspond to steady state flows, but this could be applied to transients too.

Moreover, for our case study, with the video captured in the area of location of the grate inlet (**Figure 3:17**), some parts of the image contain some black areas corresponding to the outside part of platform and the inlet holes. The part of area of visualization that was not necessary for the analysis and the areas outside of the platform were not considered. Taking into account that the area of field view change depending on the geometry of the platform (change in slopes), the area of video according to the geometry of platform was resized every time.

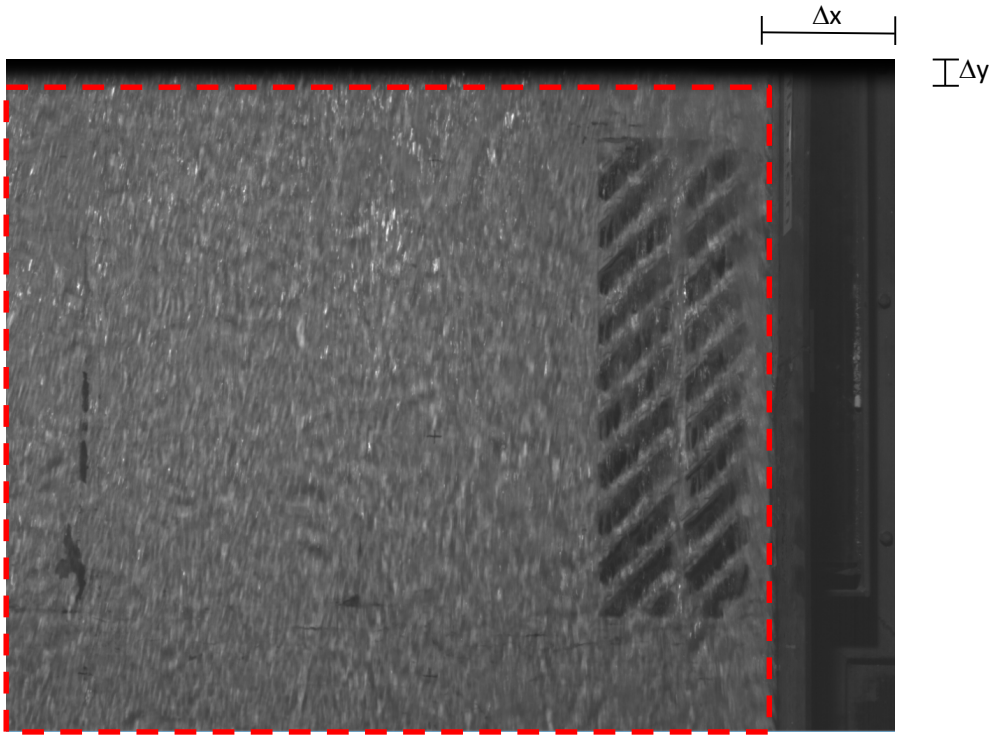

Figure 3:17 Cut the black area of visualization.

In order to calibrate the results of the velocities in the IS (m/s) it is useful to previously use the information of reference coordinate system obtained from the fiducial points and distances described in **Figure 3:18** and **Table 3:6**. Considering that the platform can change the slope in the transverse direction of 0% to 4% and in the longitudinal one from 0% to 10%, and with the purpose to correct its angle of incidence, the focus area on the platform was measured and it was noted that it had a variation of the area from 94.70 cm. x 118 cm. in case of it was fully flat and from 104.60 cm. x 130.10 cm. with a longitudinal slope of 10% and transversal slope of 4%, having an average ratio of 10 pixels/cm.

	Transversal slopes 0%		**Transversal slopes 2%**		**Transversal slopes 4%**	
	High (m)	**Width (m)**	**High (m)**	**Width (m)**	**High (m)**	**Width (m)**
Longitudinal slope 0%	0.947	1.180	0.964	1.201	0.977	1.218
Longitudinal slope 0.5%	0.947	1.183	0.964	1.201	0.977	1.220
Longitudinal slope 1%	0.953	1.186	0.970	1.209	0.985	1.227
Longitudinal slope 2%	0.963	1.197	0.978	1.221	0.986	1.236
Longitudinal slope 4%	0.978	1.218	0.995	1.239	1.008	1.256
Longitudinal slope 6%	0.992	1.239	1.005	1.257	1.021	1.278
Longitudinal slope 8%	1.005	1.254	1.026	1.278	1.038	1.293
Longitudinal slope 10%	1.018	1.267	1.033	1.287	1.046	1.301

Table 3:6 Dimension of focus area of the camera on the platform.

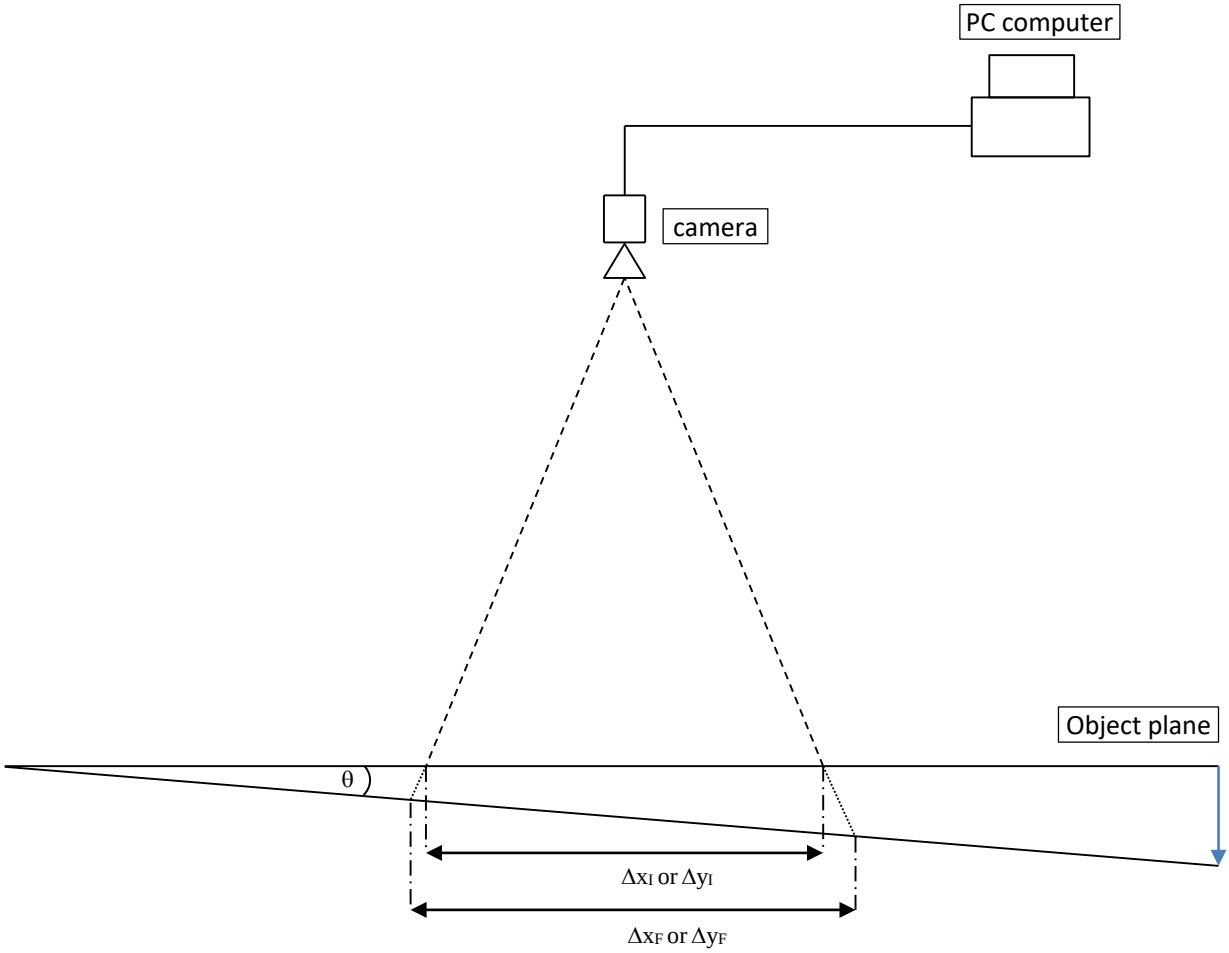

Figure 3:18 Correction of the inclination angle of the platform.

3.4.4 Image processing

Using the CCD camera around the grate inlet, sequence of images was registered and stored. Applying the image processing with a cross-correlation of a set of images recorded of surface waves, with a small size of interrogation box, 20 by 20 pixels, instantaneous velocity vector fields were obtained as shown in **Figure 3:20**.

The cross-correlation algorithm consists in to define the interrogation box that includes the marker (surface waves) in the area of the image (Frame1), and search the same marker in the second frame (Frame 2), with more probable displacement between two consecutive images (**Figure 3:19**). Velocity vector can be determined with the displacement of the centre of interrogation box (Δx or Δy), divided by time interval (Δt), following the **Equation *[3:7]***.

$$\boldsymbol{u(x.t) = \frac{\Delta x\,(x,t)}{\Delta t}\,;\, v(y.t) = \frac{\Delta y\,(y,t)}{\Delta t}} \qquad \textbf{[3:7]}$$

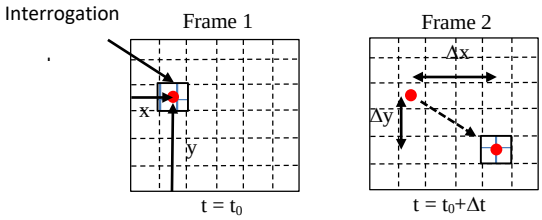

Figure 3:19 Scheme of SFIV cross-correlation.

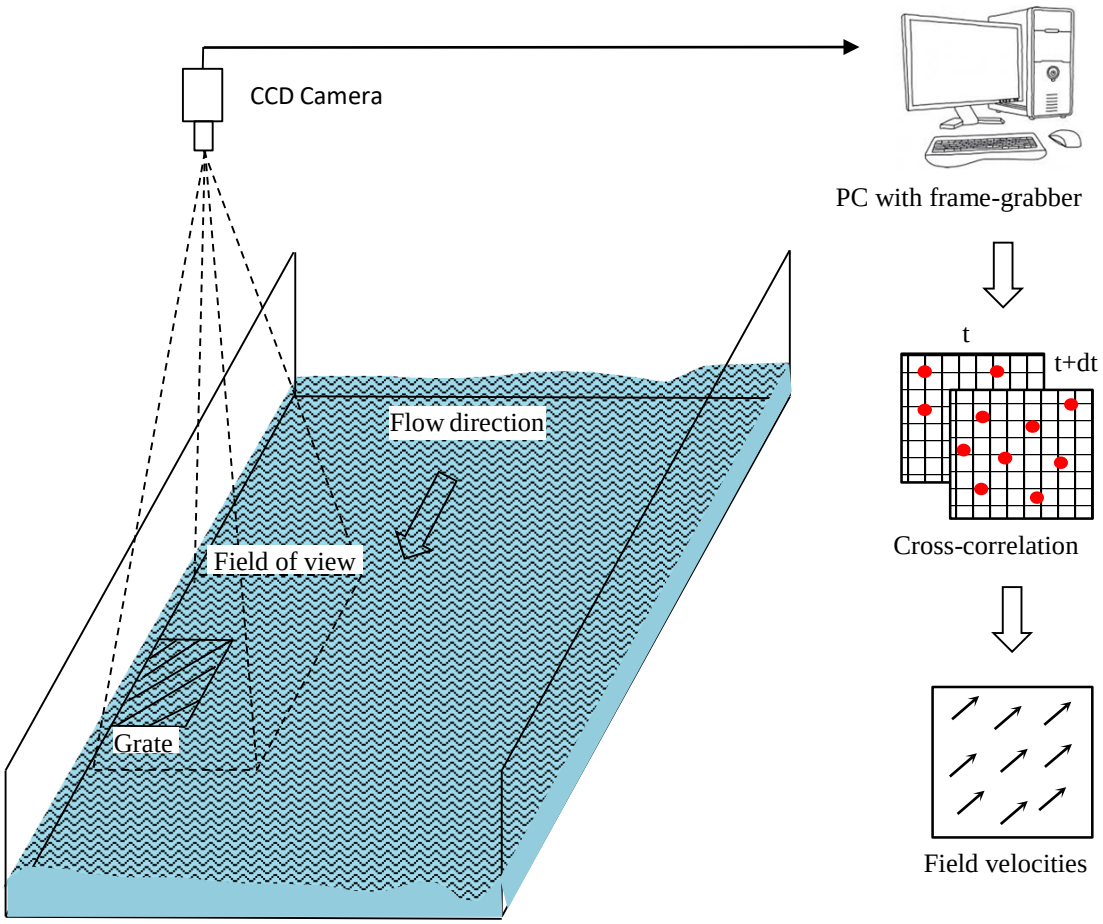

Figure 3:20 Layout of SFIV technique application (data collection and image processing).

3.4.5 Digital image processing using Digiflow

The image analysis is performed through the implementation of DigiFlow, advanced visualization software developed by S. Dalziel at the Department of Applied Mathematics and Theoretical Physics (DAMTP), at the University of Cambridge (**Dalziel, 2012**). Digiflow has an important component of correlation particle image velocimetry (CPIV) that uses a pattern matching synthetic schlieren. Many other systems of PIV also owe their development to synthetic schlieren described by (**Dalziel et al. 1998, Dalziel and Redondo, 2007**). In this thesis it was followed only the wave patterns on the water surface in order to convert this motion into a velocity field through a CPIV type algorithm, because it is faster and more simple (**Dalziel et al., 2000**).

Following the interrogation of the synthetic schlieren method in DigiFlow, the displacement data of the small surface waves or micro-vortices detected in the images are converted to field velocities, by dividing the displacement of the pixel per unit length and by the exposure time delay.

Although there are not particles there, it looks like the Froude number is high enough for the gravity-capillary waves to be treated as simple patterns that are advected by the mean flow. Consequently, getting a velocity field out of the experiment appears feasible.

3.4.6 Velocity field around the grate inlet

Some examples of the velocity pattern for the grates type 1, type 2 and type 3 are shown in the **Figure 3:21**. The figures show the average local velocity vectors at steady conditions. The images are the results of SFIV associated to the flow discharge approaching the inlets. The value of the velocity is in the range of 1 m/s to 2.02 m/s for this type of geometric configuration of the platform.

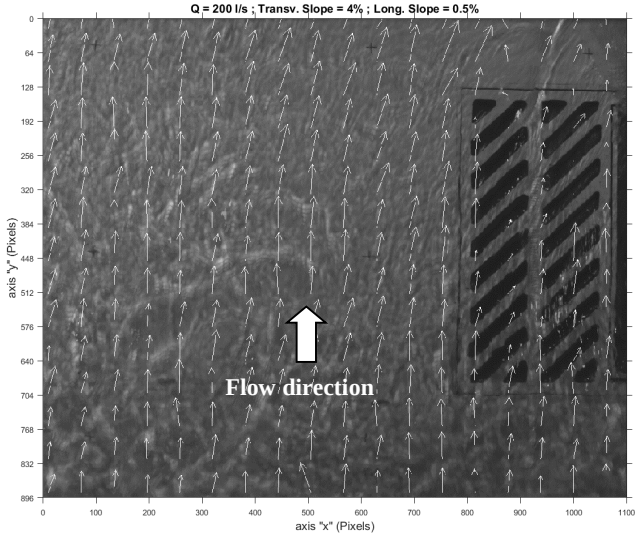

Type 3 grate, Q=200 l/s, Transv. Slope=4%, long. Slope=0.5%.

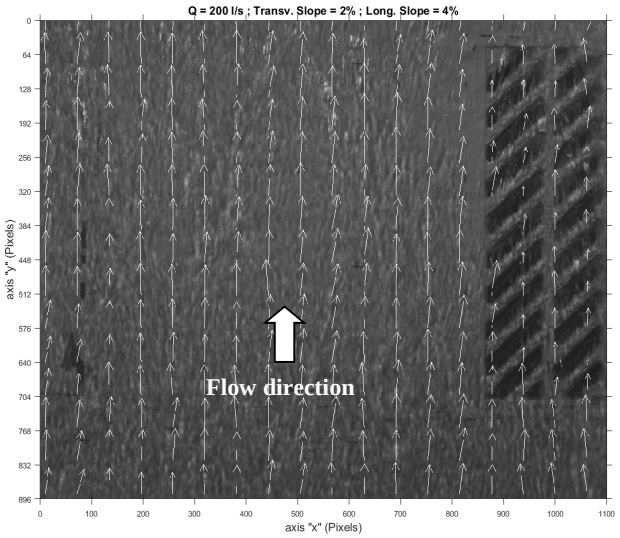

Type 5 grate, Q=200 l/s, Transv. Slope=2%, long. Slope=4%.

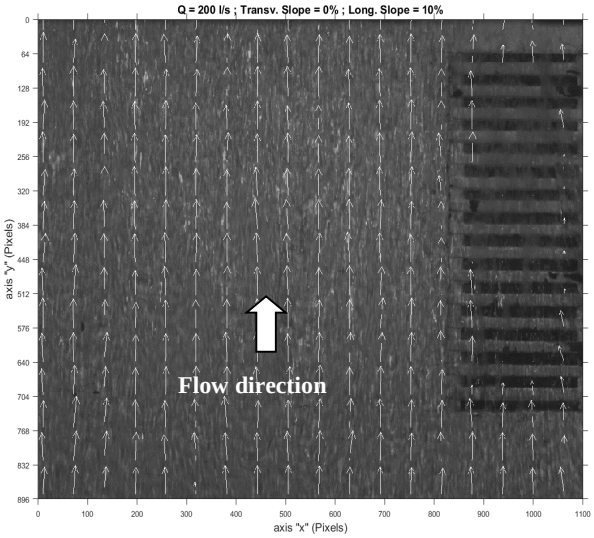

Type 6 grate, Q=200 l/s, Transv. Slope=0%, long. Slope=10%.

Figure 3:21 Field velocities of different grate inlet.

It is necessary to consider that the velocity field around the grate inlet with the technique SFIV gave a good approximation, but over the grate inlet, due to the strong vertical component of the three dimensional flow, the velocity is not accurate because the holes generate a discontinuity in the convergence region that affects the horizontal correlations. Moreover, the splash on the grate produce perturbation in the surface flow forcing a 3D behavior.

The vector field at the free surface not only generates the velocity in one direction, it may obtain the surface velocity in two components velocities on a surface (U_x and V_y), and for this reason it is possible to estimate the frontal and lateral flow rates approaching the grate. Moreover, in the example concerning the grate type 1 (**Figure 3:21**), it is possible to visualize the influence of the flow captured by the grate in the velocity field, where the vectors near the grate present a curvature towards the right side.

3.4.7 Approaching flow

The flow approaching the inlet is mainly basically one dimensional in the platform, in order to define as the circulating flow related to the real geometry for a wide of 3 meters. It presents different types of gutter section depending of the transverse slopes and the water level vary according the flow approaching, where a rectangular gutter section is when the transverse slope is null, triangular gutter section when the water level not exceed the spread of 3 m ($y < 3 \cdot Ix$) and the trapezoidal gutter section when the flow rate generate a high values of water level $y > 3 \cdot Ix$ as shown in the **Figure 3:22**¡Error! No se encuentra el origen de la referencia.. So knowing the flow and the water level measured in the platform is possible to calculate the average velocity for every test. This value can be compare this value with the average velocity obtained with the SFIV technique measured at the curb immediately upstream from the inlet (Point 1 of the **Figure 3:25**).

Furthermore, the motion of the flow on the street present a longitudinal slope I_y, with a wetted cross section according to the transverse slope I_x as shown in the **Figure 3:22**.

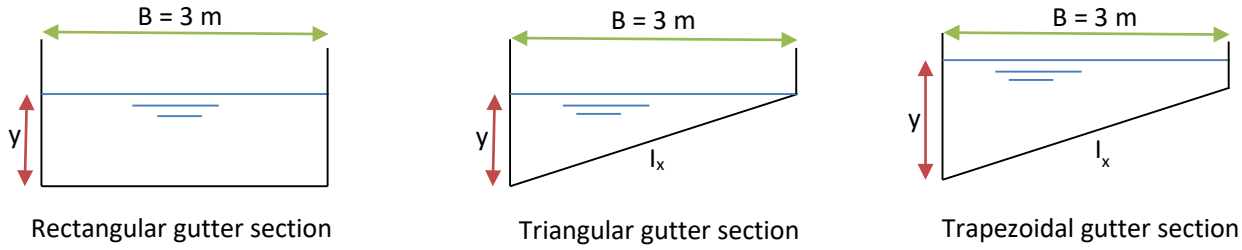

Figure 3:22 Gutter cross sections.

In order to validate the average velocity, the comparison between the velocity values upstream the grates calculated with Digiflow are represented versus the values considering average velocity and obtained through flow depth measurements (**Figure 3:23**). The correlation factors R^2 of the fits are between 0.83 and 0.86, so the comparison of results is quite satisfactory, so SFIV technique can be used to predict the velocity even in places where conventional measurements are not possible.

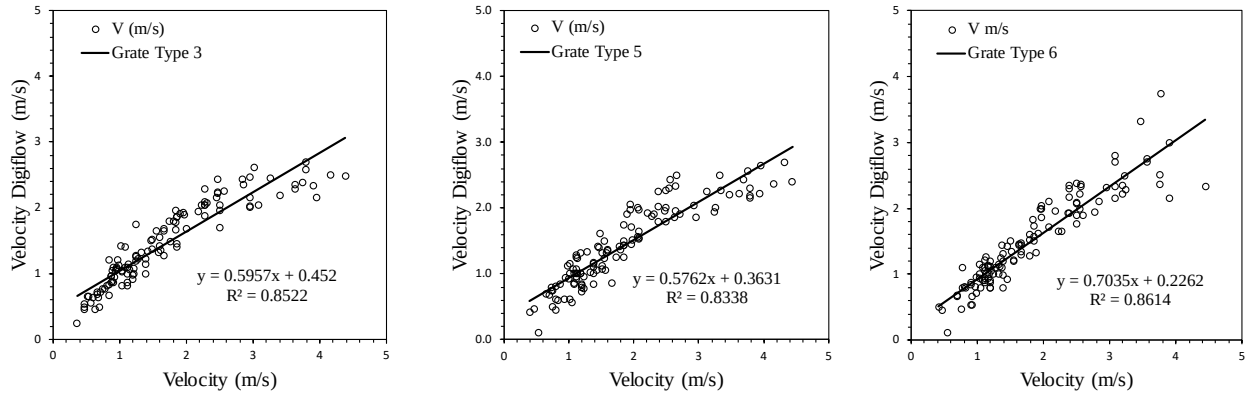

Figure 3:23 Comparison of the average velocity calculated and the velocity calculated by SFIV in Digiflow, for the approaching flow.

3.4.8 Distribution of flow rate around the grate inlet

Flow intercepted by an inlet can be considered as a combination of two flows: frontal and lateral flow. According to the **Figure 3:24**, it is possible to distinguish between frontal and lateral flow.

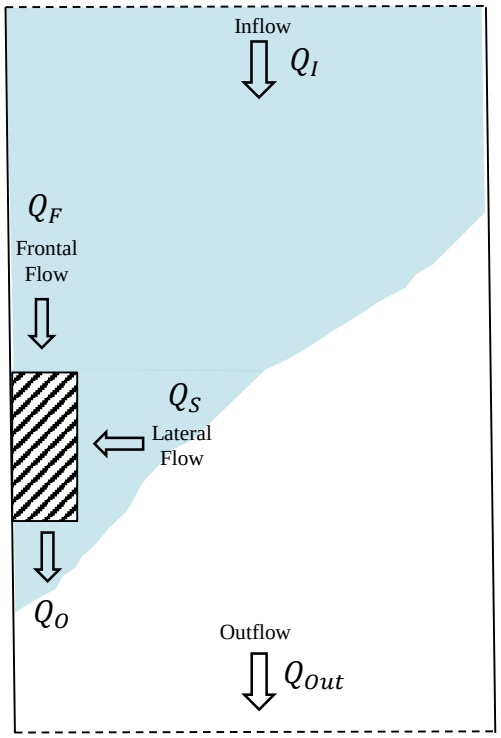

Figure 3:24 Sketch of distribution of flow rate intercepted by the grate inlet.

Considering a 1D approaching flow is maybe the simplest form to compare the experimental calculated velocities with SFIV results. 2D flow approach is more complicated and SFIV could be more useful in this case. From the 2D velocity field it is possible to estimate the flow captured by the grate, applying the mass balance over the grate. This possibility was implemented through the development of a code in MATLAB. For this practical case, the conceptual model of the distribution of flow rate on the grate is shown in **Figure 3:24**.

From the mass balance over the grate (**Equation *[3:8]***), the flow rate intercepted by the grate is equal to frontal flow rate plus the lateral flow rate minus the outflow / carryover of the grate:

$$\mathbf{Q_{Int} = Q_F + Q_S - Q_0} \qquad \textit{[3:8]}$$

Given that the image processing in Digiflow only provides results of field velocities, combined with the measure of some depths in the vicinity of the grate, it was calculated the flow at every line considered in grate perimeter. The depth at 10 points 2 cm around the grate was measured where the flow depth were assumed as shown in **Figure 3:25**. Velocity field obtained gives a value at every pixel, and from the water level previously assumed at this pixel, the flow was obtained as show in **Figure 3:25** and from the following equations:

$$\boldsymbol{Q_t = \int_A V_s dA} \qquad \textit{[3:9]}$$

$$\mathbf{\sum_{i=1}^{n} q_i = V_{S1} \cdot A_1 + V_{S2} \cdot A_2 \ldots\ldots\ldots\ldots\ldots + V_{mn} \cdot A_n} \qquad \textit{[3:10]}$$

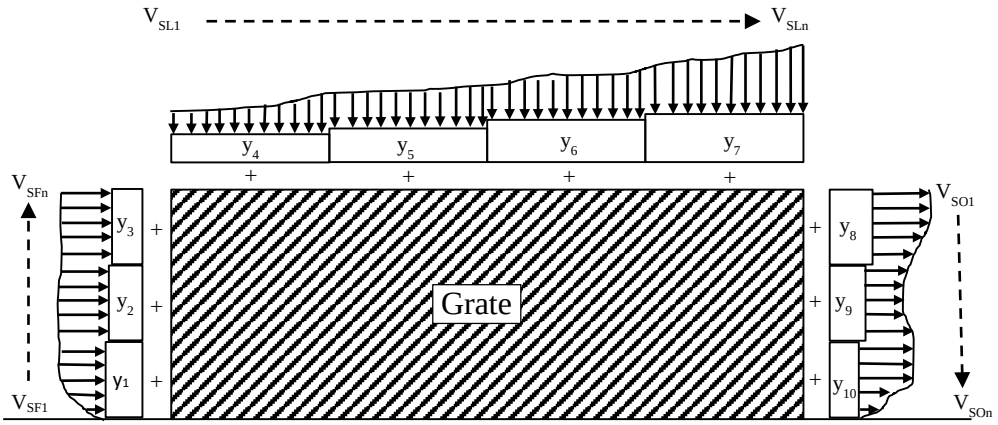

Figure 3:25 Measure of water depth (+) and discretization of the flow rate for each grate inlet.

Since values of flow captured by the grate through the test in the platform were available, the comparison of the intercepted flow measured versus the intercepted flow obtained using the image process by SFIV techniques with Digiflow was performed, following the methodology described in section **3.4**.

The results of the comparison on the grate inlet (Considering all the geometric configuration and the approaching flows) between intercepted flow measured and the intercepted flow obtained using SFIV process (**Figure 3:26**) are quite encouraging because these relations for the three types of grates show a coefficient of correlation between 0.89 to 0.95, indicating that the difference of the intercepted flows are quite small, although it is useful to say that the greatest differences were found with low longitudinal slopes of 0.5 and sometimes 1%, associated with very low velocities.

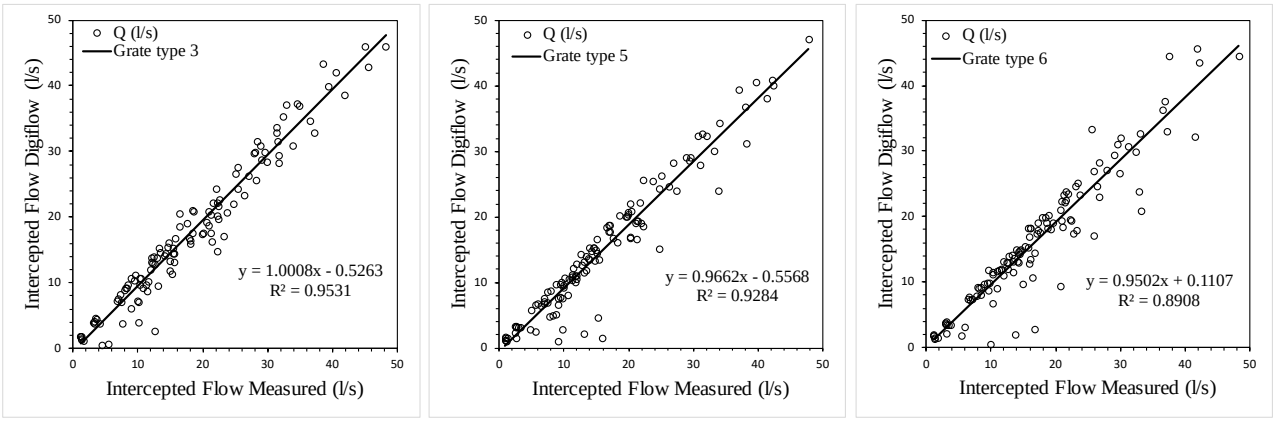

Figure 3:26 Comparison between Intercepted Flow Measured vs Intercepted Flow obtained by SFIV.

Another utility associated to the velocity fields obtained from this SFIV technique for each combination of slopes and flow rate provides is the evaluation of the flow rate captured by the grate inlet according to the **Equation *[3:8]***. Mass balance on the grate inlet provides the values of frontal and lateral flow rate on the grate that is important to understand how the flow is captured by the grate.

In order to analyse the distribution of flow rate around the grate inlet, **Figure 2:27**, **Figure 2:28** and **Figure 3:29** shows the results of percentage of frontal and lateral flow rate captured for the three different types of grates studied where the range of values in percentage are between 60% to 100% approximately of the frontal flow rate and between 0% to 40% for the lateral flow rate, confirming previous studies. In addition, the lateral flow for slopes of 2% and up, the percentage do not exceed the 30%, being the 40% for cases with less reliability of results.

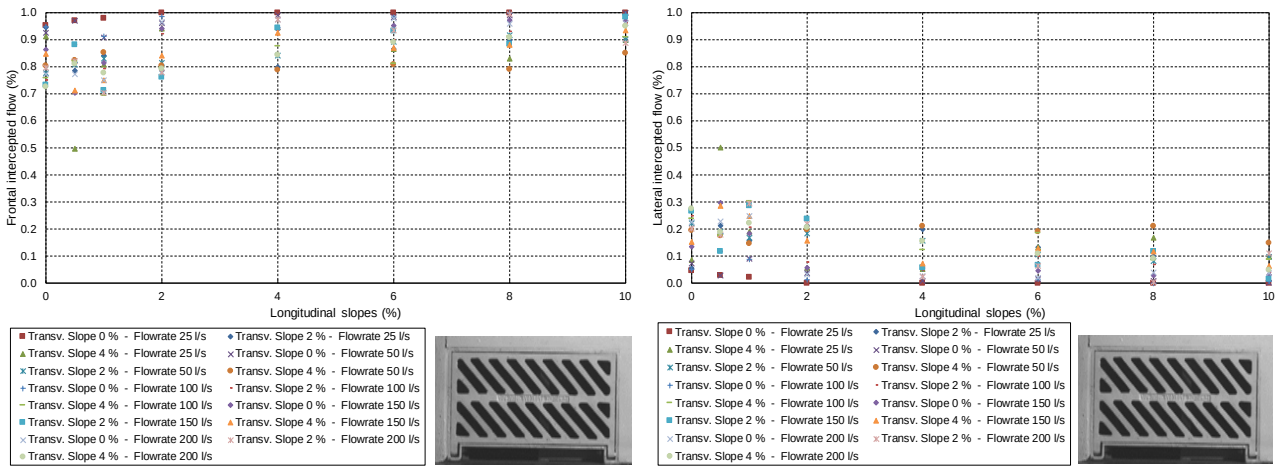

Figure 3:27 Left: Porcentage of frontal intercepted flow; Right: Porcentage of lateral intercepted flow. Grate Type 3.

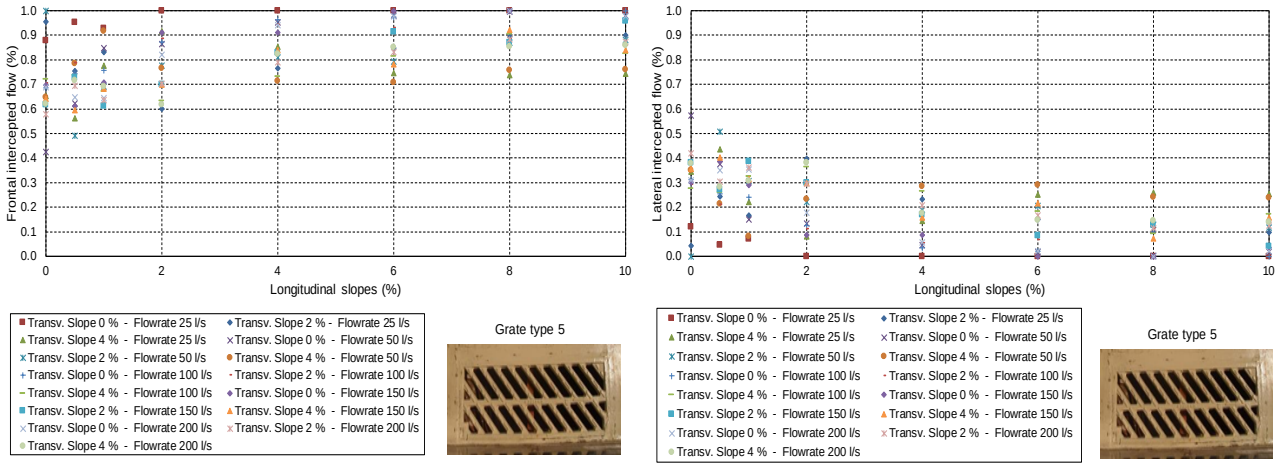

Figure 3:28 Left: Porcentage of frontal intercepted flow; Right: Porcentage of lateral intercepted flow. Grate Type 5.

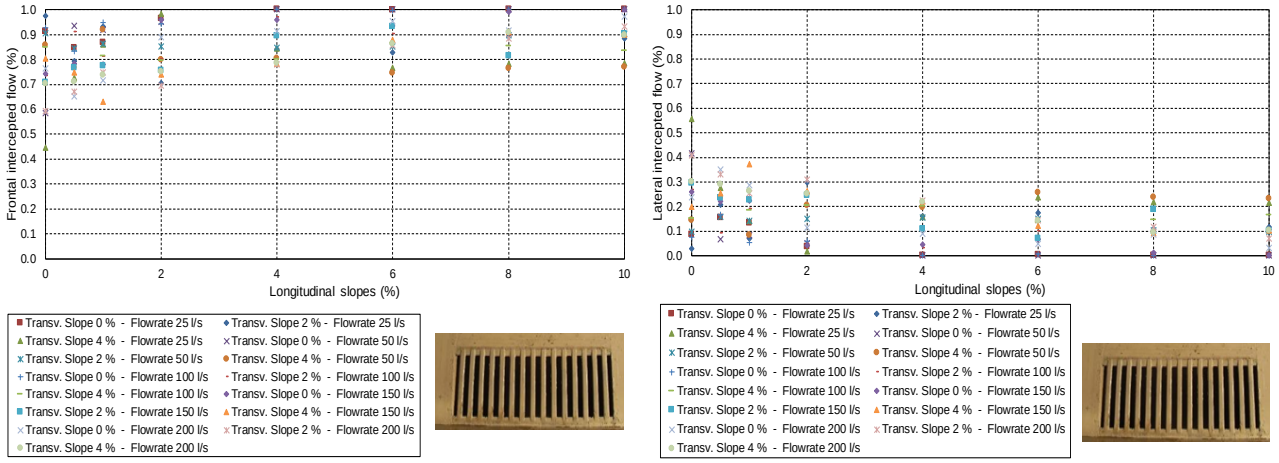

Figure 3:29 Left: Porcentage of frontal intercepted flow; Right: Porcentage of lateral intercepted flow. Grate Type 6.

Moreover, it is important to note that for low slopes when a recirculation of the flow at the end of the grate occurr, this effect changes the boundary condition of the mass balance because some times inflow in the last part of the grate can exist. On the other hand, for slopes more than 2%, it is possible to state that the flux is mainly 1D.

3.4.9 Validation of the SFIV techniques

The validation of SFIV techniques is an approach that combines the correlation analysis of a group of perturbations of flows or surfaces waves on the image. The validation of the SIFV techniques was based on the results of the laboratory tests. The flow rate captured by the grate inlet was compared to the obtained one using SFIV technique. **Figure 3:26** shows the comparison of the intercepted flow by the grate, with a correlation of more than 83 percent, which indicates that the methodology, accuracy and performance of the SFIV techniques are quite good.

3.4.10 Optimization parameters of the simulations

In order to optimize the SFIV techniques, not only good approximation of the results has been provided, but, also, the analysis of the combination of parameters that were introduced in the solver Digiflow with the aim to find the best setting to obtain the better recorded image sequence.

So, after some iterations of combining the parameters involved in the correlation, it was decided to fix the values of interrogation windows, quality, algorithm of correlation, while the parameter that it was decided to change for each combination of geometry and flow approximation was the values of Bias in the algorithm.

Biased search is the preferential displacement when the flow is more in one direction, used for a large domain with a less time of computation. The parameter of Bias in the correlation of the image depends on the density of tracers on the image, and the geometry of the street in this case the longitudinal and transversal slopes, and the flow rate of approximation. This type of combination of parameters is useful for small area of search domain with good accuracy and approximation with slopes more than 1%.

If the mean flow of velocity field has a significant bias in one direction, it is possible to specify nonzero "Bias". This allows a greater computational efficiency with smaller values for shift. The only slightly non-standard bit is setting the yBias. The units of "Bias" are pixel displacements and have an effect similar of shifting the second image by negative of the specific amount (**Dalziel, 2012**).

For this reason, when there is a previous "history", that "history" is used to set the bias and the max shift is reduced, with the precise amount of reduction determined by a more complex algorithm. This approximation is obtained from a correlation analysis over a larger domain.

Results of the comparison of intercepted flow and average velocity for the three different types of grates tested with the best values of bias provide good accuracy of the results as shows in **Figure 3:23** and **Figure 3:26**. To simplify the range of Bias values a statistical analysis was done in order to find a relation between the Bias values for different combinations of flow approaching and geometry of street.

The selection of values of bias was established plotting the values of Bias, building three groups for each trasnversal slopes, where the central point of the tredline was the medium values well-known as average bias values as show in the **Figure 3:30** and **Table 3:7**.

Transversal slope (%)	Longitudinal slope (%)	Flow rate (l/s)	Bias
0	0, 0.5, 1, 2, 4, 6, 8 and 10.	50 l/s, 100 l/s, 150 l/s and 200 l/s.	9
2	0, 0.5, 1, 2, 4, 6, 8 and 10.	50 l/s, 100 l/s, 150 l/s and 200 l/s.	10
4	0, 0.5, 1, 2, 4, 6, 8 and 10.	50 l/s, 100 l/s, 150 l/s and 200 l/s.	12
0 , 2 and 4	0, 0.5, 1, 2, 4, 6, 8 and 10.	25 l/s	8

Table 3:7 Values of Bias.

The first steps were to find the best relation for both parameters. The values of bias were divided into 3 different groups with flow rate of 50, 100, 150 and 200 l/s where the values of bias were equal to 9 for transversal slope of 0%, equal to 10 for transversal slopes 2% and equal to 12 for transversal slope of 4% (**Figure 3:30**). For flow rate of 25 l/s and all the geometric configuration, the value of bias is equal to 8.

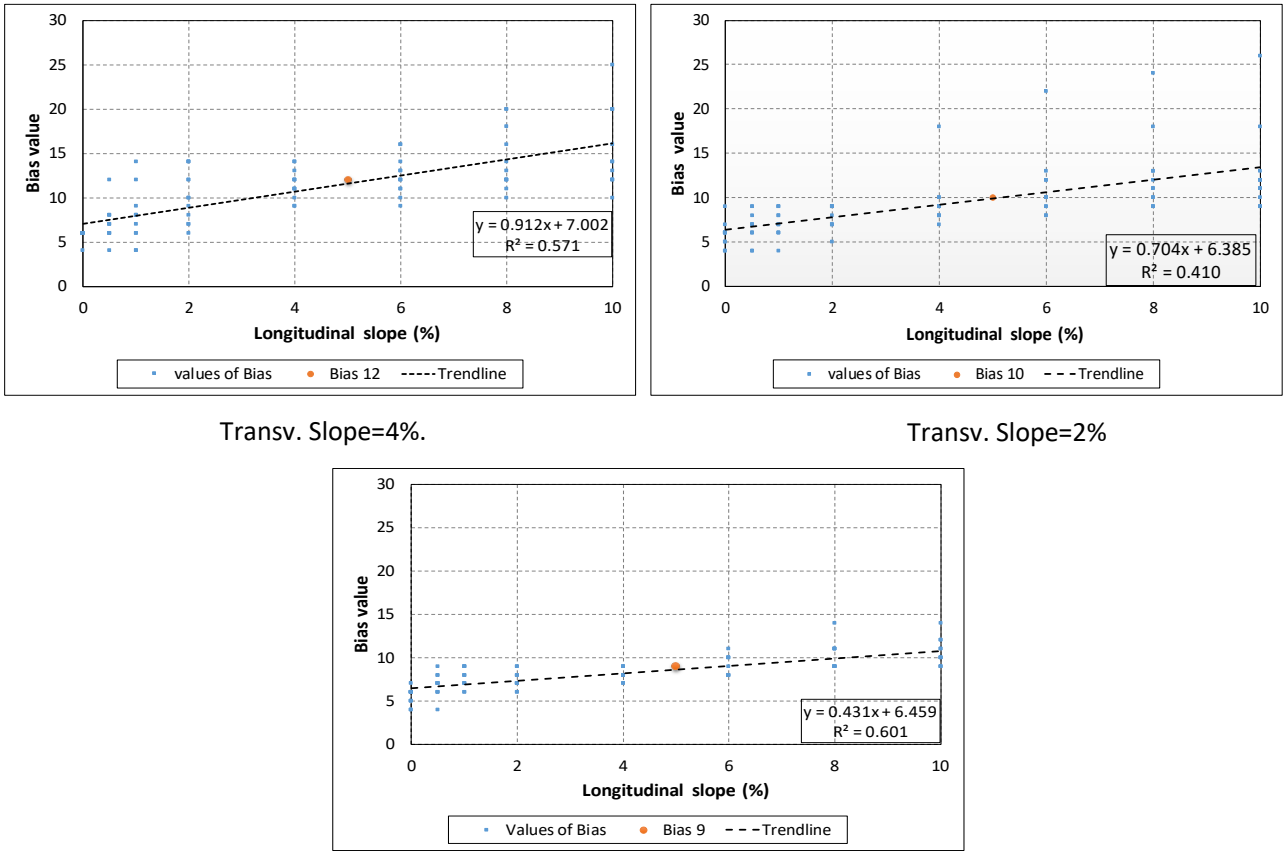

Figure 3:30 Correlation Bias factor for grates Type 3, 5 and 6 and approaching flow of 200 l/s, 150, l/s, 100 l/s and 50 l/s.

In summary, as the variation of the bias is too big, for the first aproximation of the results it is possible to evaluate it using an average value of bias equal to 10, and it further simplify the methodology of SFIV techniques. Furthermore, the analysis of the results show that the bias depends not only on the numbers of tracers, but also depends on the geometry of the gutter section.

3.5 SFIV techniques using another software

The main purpose of this section is to assess the viability of the implementation of PIVlab in specific experimental conditions as were tested in this thesis with the image analysis using the Digiflow using the same methodology of the SFIV techniques.

PIVlab has been selected for the following reasons: it is an open source code, which takes advantage of several features of Matlab and facilitates subsequent data processing by providing a close link to the popular Matlab user interface.

PIVlab is an open source developed by Prof. Dr. Eize J. Stamhuis and Dr. William Thielicke in the framework of his PhD research at the University of Groningen, Netherlands. Besides, the literature realised by Dr. William Thielicke and Prof. Dr. Eize J. Stamhuis (**2014**) constitutes the main reference of the PIVlab software that provides understanding of the mathematical background and the implementation of the functions of PIVlab.

PIVlab has a user-friendly interface, that is programmed in Matlab. The version 1.41 that was released in February 2016, has been used for this study. PIVlab was developed through digital particle image velocimetry (DPIV)

techniques. It was originally used in conventional measurement scenarios found in laboratory activity associated with fluid mechanics topics.

3.5.1 Description of the algorithm

PIVlab architecture (shown in **Figure 3:31**) is the tool menu, with simple and intuitive graphical user interface for image processing. The input needs to be a sequence of minimum two images. The next steps are pre-processing, image evaluation, post processing, data exploration and results exporting, where it is possible to choose the format of plotting.

Image pre-processing is optional that can significantly change the quality of the image captured. This filters implementation increases the readability of images or eliminate undesirable features that can affect the correlation processing. PIVlab presents three different filters in the pre-processing – contrast limited adaptive histogram equalisation (CLAHE), intensity high pass and intensity capping.

In the steps of Image evaluation, PIV lab incorporates two different methods of correlation as Direct Cross-correlation (DCC) and Fast Fourier Transform (FFT). DCC has a disadvantage in the analysis of complex flow patterns, whereas the second approach FFT is an extremely powerful tool that remarkably reduces computational effort and time in the cross-correlation process.

PIVlab was developed with some advanced interrogation strategies that include multipass interrogation and multigrid interrogation to obtain a result where multipass approach consists in two steps: first, analysis with conventional interrogation with interrogation windows proposed, and second displacement of the interrogation windows.

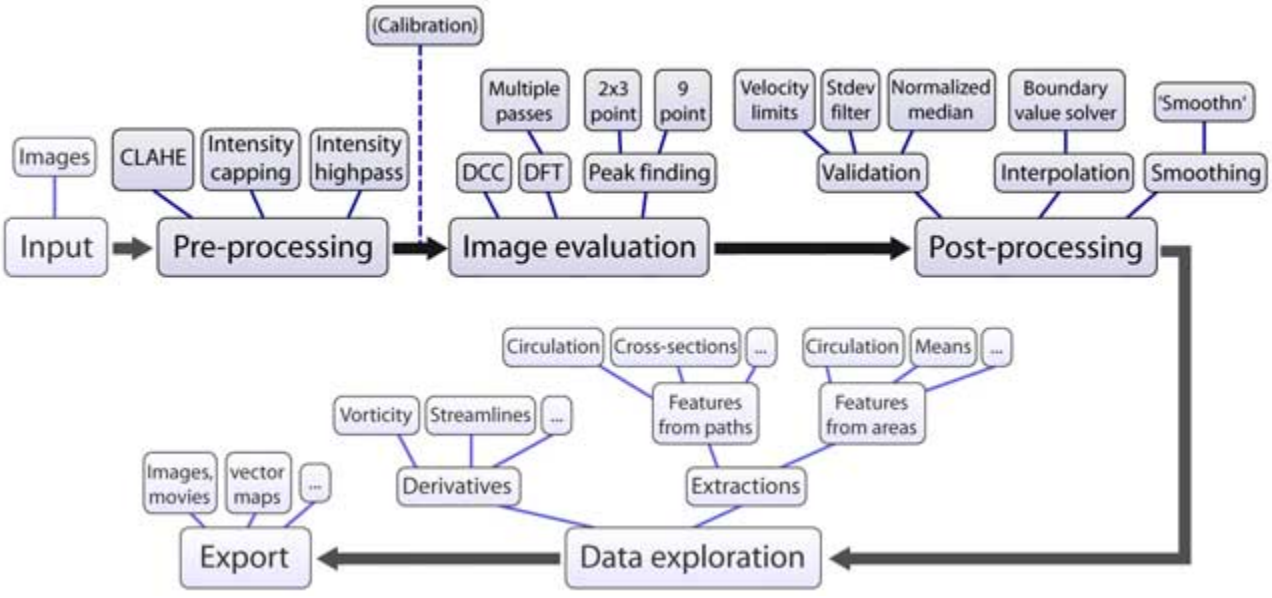

Figure 3:31 Scheme of PIVlab (**Thielicke and Stamhuis, 2014**).

Moreover, PIVlab includes a multi-frame interrogation in its algorithm using experiment where it is possible to combine a High-speed camera CMOS with laser equipment with a high frame resolution and high frame rate. Specification about the comparison between CCD and CMOS digital cameras was studied by Hain (**2007**) and some examples were published by Kähler (**2000; 2004**) about the method of multi-frame interrogation.

In addition, the PIVlab was developed from Digital Particle Image Velocimetry techniques in the field of visualisation of complex's flows using MATLAB code (**Thielicke and Stamhuis, 2014**). The idea was to use the same software PIVlab but with the methodology of Surface Flow Image Velocimetry techniques developed by Tellez et al. (**2016**).

3.5.2 Image processing through PIVlab

For the cross-correlation of the image sequence, it is possible to choose a single pass direct cross-correlation called DCC or discrete Fourier transform correlation with multiple passes and deforming windows called FFT. In order to estimate the value of framerate of camera according to the interrogation box to have a good approach for the experiments to be done, the proposed interrogation box value is 20 pixels (in both directions). For this reason, the **Equation *[3:11]*** is used in order to convert velocity in m/s into pixel/frame. The velocity in pixel by frame is useful to estimate a priori the minimum dimension of the interrogation area to set in PIVlab.

$$\mathbf{V}_{\left(\frac{\mathbf{Pixel}}{\mathbf{Frame}}\right)} = \mathbf{V}_{\mathbf{Mean\ velocity}} \cdot \frac{\frac{\Delta_{\mathbf{t\ camera}}}{\mathbf{Framerate}_{\mathbf{camera}}}}{\Delta_{\mathbf{size\ IA}}} \qquad \textit{[3:11]}$$

Where: $V_{\left(\frac{Pixel}{Frame}\right)}$: is the framerate of camera (Pixel/Frame)

$V_{Mean\ velocity}$: is the mean velocity (m/s).

$\Delta_{t\ camera}$: is the interval of time (seconds).

$Framerate_{camera}$: is the framerate of camera (frames/seconds)

$\Delta_{size\ IA}$: Size of interrogation area (IA) (m)

In this case, the value of interval of time was 1 second, the framerate of the camera used was of 150 fps and the size of interrogation area was 0.00094. In order to have the first approach, it was decided to take an example of 200 l/s with transversal slopes of 2% and longitudinal slopes of 2% where the value of mean velocity is about 1.5 m/s. Applying the **Equation *[3:11]***, the result indicates that the displacement is around 10 pixels, computed within an image pair.

Focusing on the process of PIV analysis to generate the field velocities with PIVlab, a four-pass PIV calculation was selected (**Figure 3:32**) , with a sequential interrogation area of sizes of 128 x 128, 64 x 64, 32 x 32 and 20 x 20 pixels considered as an optimal choice in this case study. Practically the first pass uses relatively large interrogation areas (128 x 128 pixels) to calculate the displacement of image data reliably. The larger the interrogation areas, the better the signal-to-noise ratio, and the more robust is the cross correlation.

Furthermore, on the right of the **Figure 3:32** it is possible to define the values of interrogation area, where for the first pass it is possible to insert the value of the step between interrogation areas indicating the areas overlap one another when performing the cross correlation procedure. The step is important because there is additional displacement information at the borders and corners of each interrogation area. This information is used to calculate displacement information at every pixel of the interrogation areas via bilinear interpolation. The second, third and fourth steps are set equal to 50% of the interrogation area.

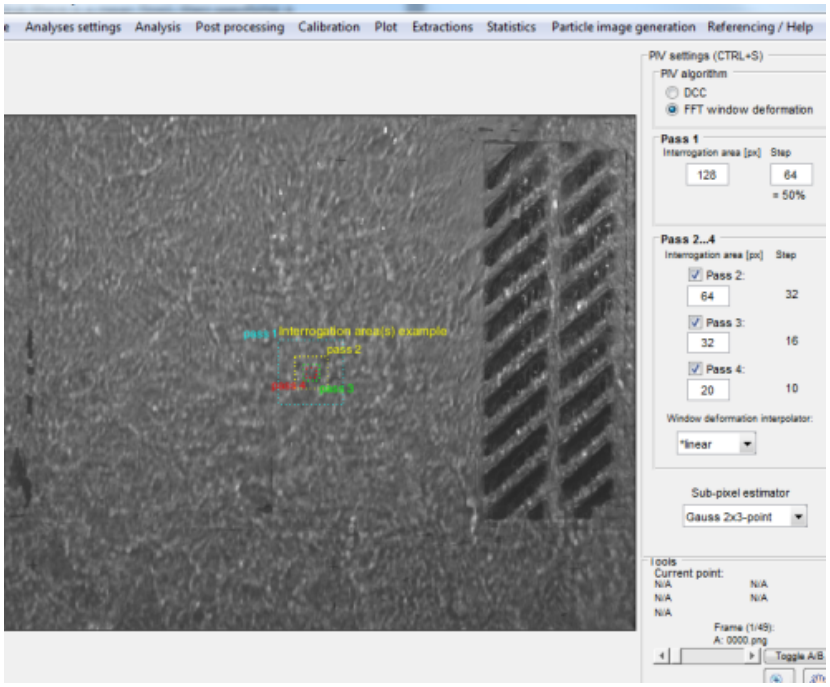

Figure 3:32 Set of controlling options for PIV analysis with PIVlab.

Velocity magnitude from PIVlab shows different setting to plotting colour maps to illustrate the velocity magnitude to represent the velocity field in good quality and approximation as shown in Figure 3:33. Moreover, to visualise and study more deeply the pattern structure of the flow is better to generate the streamline as derivative of the vector field in both direction axis “x” and axis “y”.

The velocity pattern for the grate type 5 is shown in the **Figure 3:33**. The image on the left shows the visualization of velocity map, the image in the right shows the streamline around grate inlet and the image on the left show the velocity magnitude. The range of longitudinal slopes are 0%, 0.5%, 1%, 2%, 4%, 6%, 8% and 10% with a range of transversal slopes of 0%, 2% and 4%, and flow rate of 50 l/s, 150 l/s and 200 l/s. The images are the results of SFIV associated to the flow discharge approaching the inlets.

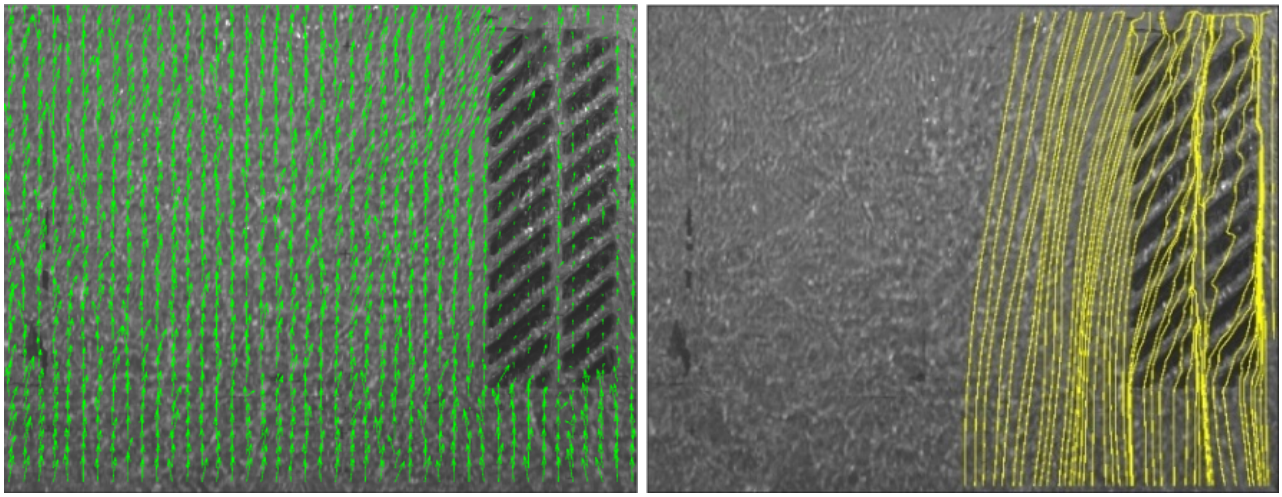

Figure 3:33 Vector field and corresponding velocity magnitude map. Transversal. Slope 2%, Long. Slope 2%, Flow rate 200 l/s and Grate type 5.

In PIVlab it is possible to plot the streamline from the two-dimensional velocity map in order to derive them; this kind of visualisation is capable of rendering detail on very complex vector fields releasing streamlines at every grid point of the vector field. Clicking on a point within the flow field it is possible to draw the corresponding streamlines; hence their spatial resolution is arbitrarily chosen. To guarantee an optimal readability, it is favourable to trace them directly on the images avoiding superimposed vector map as shown in **Figure 3:33**.

The result of the SFIV techniques using PIVlab code to develop a field velocities around the grate inlet show a good aproximation, but also have some problem to represent the velocity on the grate inlet. The next step for us is to evaluate the flow rate capture by the grate inlet. The analysis in the next section was following the same methodology that used with the Digiflow program in the chapter before.

In order to understand the theoretical background, a brief treatment of the gutter flow is presented. A commonly applied methodology for measuring and estimating the discharge of an open channel is based on a simplified form of the continuity equation. In physics it is an equation that derives from a simple mass balance, describing the transport of some conserved quantity. Following the section **3.4**, it is possible to find more details about the equation to quantify the distribution of the flow rate around the grate inlet for incompressible fluid, such as liquid water, where the flow rate is equal to the product of the cross-sectional area and its mean velocity in order to measure the flow rate capture by the grate inlet.

3.5.3 Comparison of velocities and flow rates between PIVlab and Digiflow

The results provided by the two software, in terms of velocity maps, are found to be quite similar even though their algorithms are substantially different. The agreement between Digiflow and PIVlab is encouraging, especially considering the challenging conditions that potentially may compromise a proper image pairing. Also this comparative approach provides insight for the selection of appropriate processing parameters.

Experimental analysis traditionally focuses on the assessment of the reliability and accuracy of the results obtained. Notably, this chapter is specifically aimed at determining the quality of the resulting velocity fields deriving from PIV technique implemented through PIVlab and Digiflow. Of particular concern are, in this framework, the conditions that optimize the measurements performance.

Practically this is achieved by means of three distinct steps: prior to the comparison between SFIV technique estimated velocities and theoretical predictions from simple formulas of hydraulics, instantaneous velocity field from both PIVlab and Digiflow are reported in order to study the mismatch existing between the spatial distribution of the documented velocity fields. In this way trueness and precision of different algorithms may be inferred, focusing on how pattern matching algorithms are reflected in the results.

In addition, the accuracy of the respective methods is discussed through a kind of validation procedure. Considering that the direct quantification of the error in the velocities delivered by the software is actually impossible. For this reason, was used the same method of the distribution of flow rate with a mass balance of the grate inlet order to have a good approximation of the velocities. Finally, some considerations are reported about the general image patterns of the water surface giving insight into the amount of water intercepted by the inlet frontally and laterally.

The methodology used to study the intercepted flow rate was similar that was used with the model based on water mass balance allows to correlate the experimental data of captured flow rate with discharges simulated through water depths and PIV estimated velocity. Finally, some considerations are reported about the general image patterns of the water surface giving insight into the amount of water intercepted by the inlet frontally and laterally.

Most important of all, discharge estimates obtained with PIV velocities show good agreement with discharge directly measured, whilst it has been ascertained that a rigorous uncertainty analysis of surface velocity fields is an extremely complicated task that is beyond the scope of this thesis.

In order to validate the results of PIVlab the first comparison was to compare the velocity between PIVlab and Digiflow versus the average velocity obtained as shown in the **Figure 3:34** (left), where we can see in the graphics that results show a good approximation using both software. Where the correlation coefficient for the comparison with Digiflow is 0.81 and with PIVlab is 0.77, for this reason it is possible to state that the Digiflow is a little bit more accurate than PIVlab. The comparison was for flow rates of 100 l/s, 150 l/s and 200 l/s.

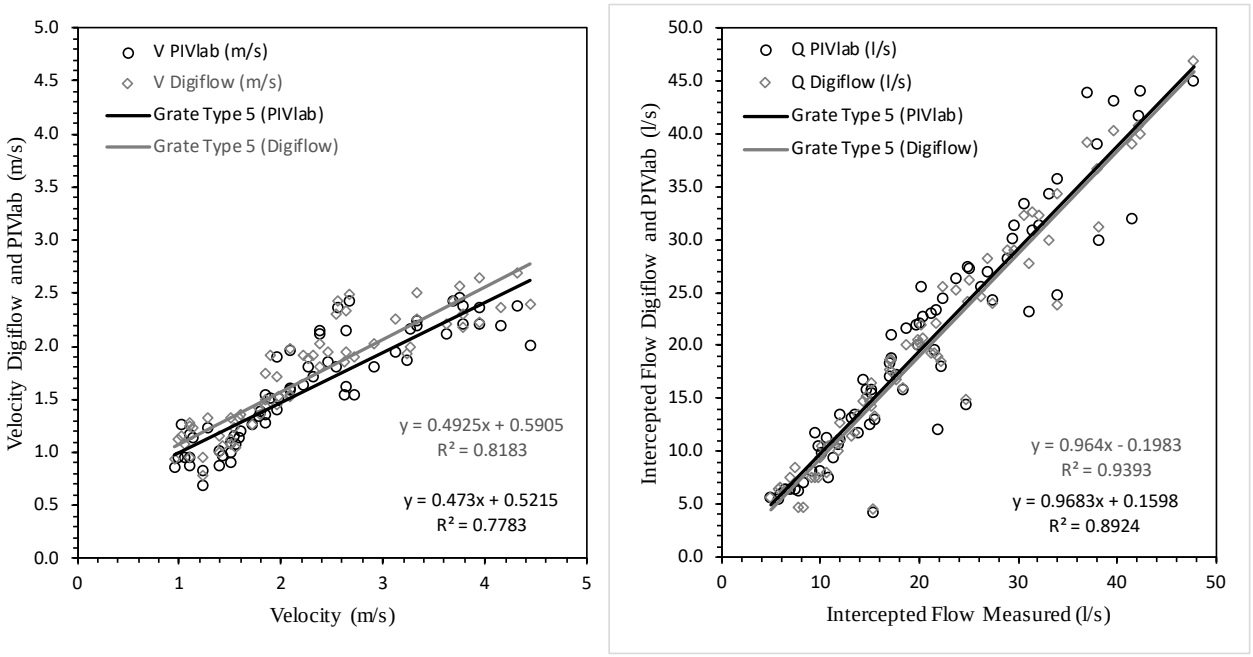

Figure 3:34 Comparison of velocty PIVlab and Digiflow versus Velocity Izzard. Flow rate 100 l/s, 150 l/s and 200 l/s.

Furthermore, the next steps was to compare the intercepted flow by the grate inlet (Type 5) with the experimental data as shown in the **Figure 3:34** (right), where the comparison showed a good approximation for both codes with correlation coefficient of 0.89 for PIVlab approximation versus experimental data, and 0.93 with Digiflow. The comparison was for flow rates of 100 l/s, 150 l/s and 200 l/s. Results of intercepted flow indicate that Digiflow show a little better approximation than PIVlab.

Moreover, with SFIV techniques using PIVlab code the distribution of flow rate around the grate inlet was obtained following the same methodology described in the section **3.4**. At the same time the distribution of frontal and side flow rates between PIVlab and Digiflow program was compared as shown in the **Figure 3:35**, **Figure 3:36**, **Figure 3:37** and **Figure 3:38**, for different geometries and three different flows of approximation (100 l/s, 150 l/s and 200 l/s).

Analyzing the frontal intercepted flow (**Figure 3:35** and **Figure 3:36**), it shows that the frontal flow decrease as the transversal slope increase, also the range of percentage of efficiency for low transversal slopes as 0% increase with the longitudinal slopes between 0.7 to 1, for different flow approach (100 l/s and 200 l/s). But for transversal slopes of 2% the profile of percentage is more homogenous along the longitudinal slopes of 2% to 10%, with range 0.85 to 0.95, with flow rate of 100 l/s. For the same condition but changing the flow rate to 200 l/s, the efficiency increase along the longitudinal slope between 0.7 to 0.88 approximately.

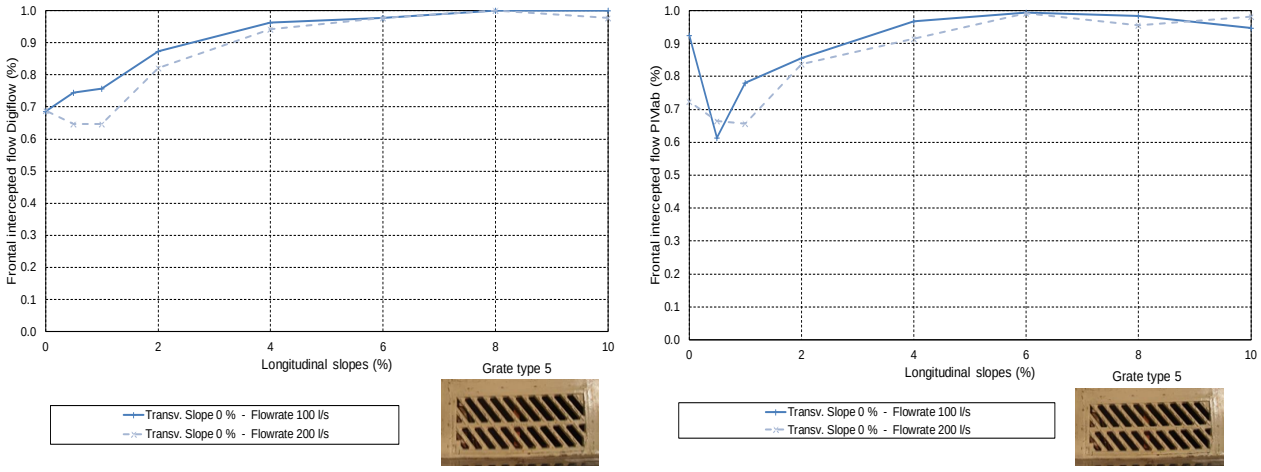

Figure 3:35 Comparison between Digiflow and PIVlab of Frontal intercepted flow by the grate type 5. Transversal slope 0%.

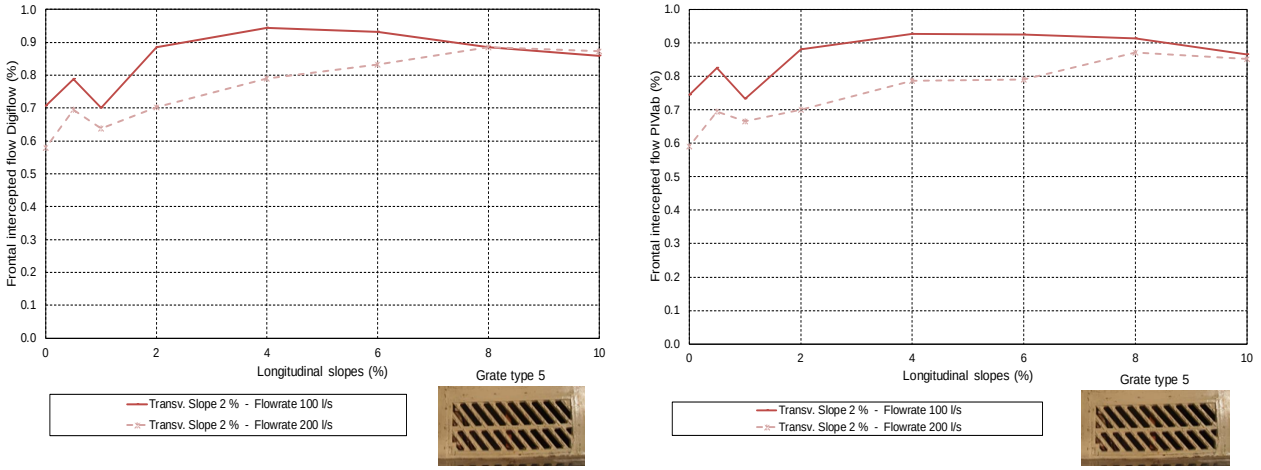

Figure 3:36 Comparison between Digiflow and PIVlab of Frontal intercepted flow by the grate type 5. Transversal slope 2%

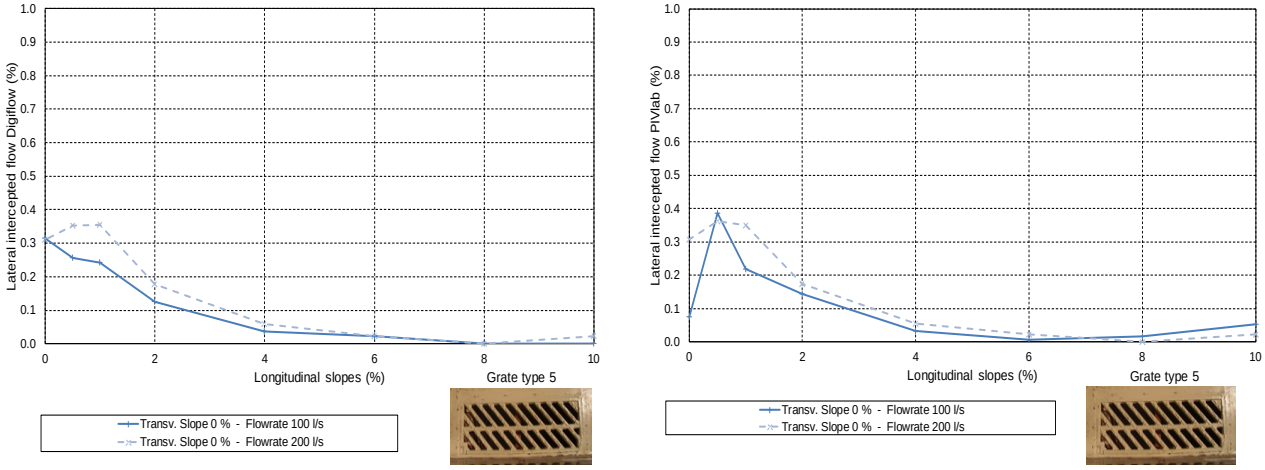

Figure 3:37 Comparison between Digiflow and PIVlab of Lateral intercepted flow by the grate type 5. Transversal slope 0%.

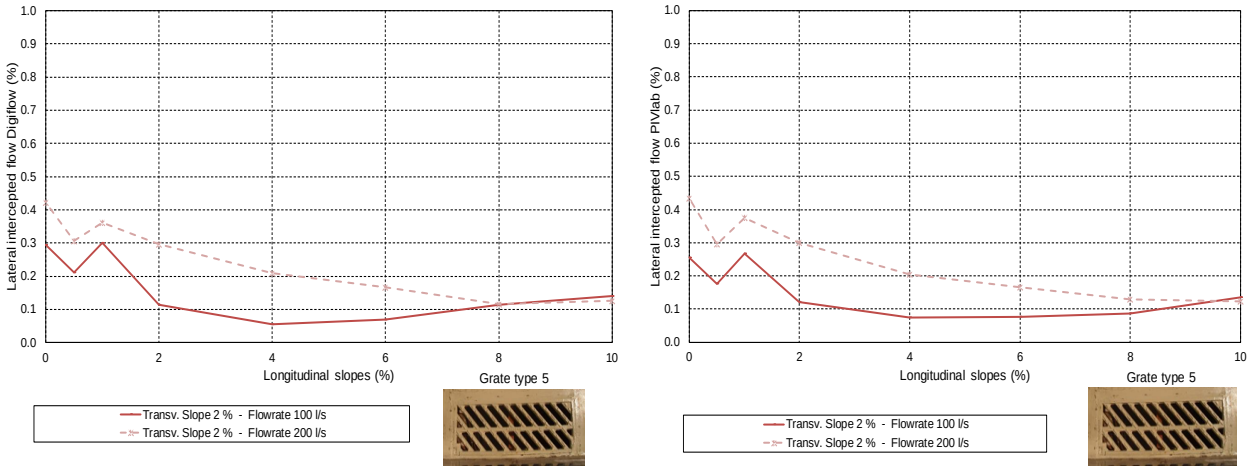

Figure 3:38 Comparison between Digiflow and PIVlab of Lateral intercepted flow by the grate type 5. Transversal slope 2%.

In addition, it is possible to see in **Figure 3:35** to **Figure 3:38**, that the efficiency threshold of the frontal and lateral intercepted flow is similar. This shows that with both software it is possible to reproduce the distribution of the flow around the grate inlet using the methodology of SFIV techniques.

In conclusion, PIVlab code developed in the platform of Matlab is another useful program capable to study the behavior of the flow around the grate inlet. It is an alternative to the SFIV techniques, considering that the Matlab code is one of the more common calculation codes used by the community of research.

Both program Digiflow and PIVlab demonstrate a good approximation in the results for this case study, but Digiflow show a little better approximation, because the code is specific for problems in fluids mechanics and PIVlab is a more general software with different applications. Also Digiflow presents more options for the users to evaluate the flow pattern. Finally, both codes are convenient to apply the methodology of the techniques Surface Flow Image Velocimetry (SFIV) for this case study, following the steps described in the section **3.4**. The major advantage of PIVlab is that it reproduces the streamline around the grate inlet.

3.5.4 Differences between PIVlab and Digiflow

This section has the aim to increase the sensitivity of the differences between the pattern matching algorithms encountered so far. In order to make the comparison between image flow fields, the user-adjustable parameters in PIV analysis have to be as much as possible equal in both codes. Naturally different correlation processing entail different internal workings for PIVlab and Digiflow; consequently, only a few controlling parameters in one code have their direct corresponding option in the other software. In this case, only the dimension of the interrogation area and its spacing (or step) is found explicitly in both codes. Thus they are fixed at 20 pixels for the IA size and 50% (i.e. 20 pixels) for the areas overlapping. On the other hand, the main differences in the processing algorithm lead to distinct features of the procedures.

Overall, analysing the processing schemes on a purely theoretical basis both Digiflow and PIVlab have advantages and drawbacks, considering the entire procedure performed in order to obtain the velocity field. The following points are some crucial considerations to bear in mind when discussing the result of flow fields:

- PIVlab and Digiflow results depends on the contribution of intensity of the images. For this reason, it is important to consider a good quality of videos with a high resolution and speed, capable to visualize and generate the field velocities.

- Digiflow is capable of introducing sequence of images or videos to study, but PIVlab only accept sequence of image, for this instant, is necessary to develop a code or use another program to decompose the video recorded during the experiments.
- Digiflow has more utilities according to analyse experiment on fluid mechanics as dye in the flow, particle tracking, PIV, etc., with also more possibilities to change the algorithm using parameters such as Bias, Max shift. PIVlab is more focused on PIV.
- Furthermore, Digiflow has the possibility to introduce the coordinate in both direction (x and Y), but in PIVlab, it is necessary to introduce the coordinate in one direction, and it takes for both directions.

3.5.5 Results and conclusions of the simulations based on the studied grates

SFIV technique is a non-invasive technique that does not disturb the flow as other methods do. It is also very important for this type of flow with very small depths because of the difficulties of using micro-sensors. The application of image processing techniques (SFIV) in the experimental investigation of the propagation of the flow rate in the model of urban drainage has been validated for use in a wide range of flows. Detailed velocity measurements are necessary, given that the situation requires a good understanding of different instruments of video recording and full knowledge of image processing techniques.

Another advantage of the SFIV technique is that it is possible to reproduce the field velocities in the surface flow depending on the characteristic of the test data, but the important parameters to consider in the laboratory condition or in the real case are the geometry of the section, resolution and quality of image, framerate, accuracy, algorithm of correlation and the illumination. These parameters are very important in experimental test and the image processing of complex flows. With the generation of the velocity field instantaneously and with the cross section, it is possible to monitor flow rate in some rivers, channels, streets and extend this technique to other engineering applications where surface patterns are identifiable.

Also this technique uses standard video equipment and cameras that are accessible nowadays because the technology of digital camera has had a huge development in the last decade. And if it continues, the advances in these type of tools, will become widespread both in laboratory and field hydraulics.

Since SFIV techniques have been shown to provide a good capacity to generate the surface velocity fields, important engineering application are open to new studies, such as floods, monitoring of rivers, laboratory applications in hydraulics and fluids mechanics, urban hydrology (streets and sediments), dam, debris flow, erosion of bank, ocean waves, etc.

For the specific problem presented here, flow patterns near the inlet, SFIV technique allow the estimation of flow patterns and the associated velocity field, and as a consequence the assessment of the frontal and lateral flow, as well as carryover flow. So it is possible to use these techniques to assess the hydraulic performance of the grate inlets and from the test results to improve or propose new designs. Comparison with 1D and 2D approach concerning circulating flow shows the good performance of this visual technique.

The application of image processing techniques in the experimental investigation presented in this paper has been validated in many different conditions of geometries (slopes) and flows.

Accuracy of results of velocity fields, depend on slopes values, because in case of flat surfaces and low velocities, the free surface does not have enough identifiable perturbations to do a significant correlation, as many of the wave patterns escape from the interrogation regions. For this reason, this technique is more useful to be used when there exists a supercritical flow.

A priory the application of SFIV technique was base in Digiflow, in this case of study Digiflow program present a little better accuracy than PIVlab following the same method of SFIV technique. Moreover, the Digiflow has more setting to change in the code to increase the quality of the results. The advantage of the PIVlab is more accessible to the community of research because is a package of MATLAB software.

Chapter 4 Interactions between surface flow and surcharged pipe flow

4.1 Introduction

This chapter presents results of the experimental campaign to study the interaction between surface flow and surcharged pipe flow carried out in the hydraulic laboratory of the Technical University of Catalonia through the same platform used for achieving the hydraulic performance of the grate inlet. The methods proposed to estimate the field velocities and distribution of flow rate are similar to those described in Chapter **3**, with some modifications in the experimental model.

Pressure flow conditions appear in sewer systems when flow exceeds the hydraulic capacity of the conduit, causing that some outflow is produced. Water exits through the inlets, in case they are directly connected with no flap gate. In this case, the flow leaving the sewer can be simulated assuming orifice flow conditions, but no references about the proper values of the discharge coefficient to be used are found in the literature.

An experimental approach is presented in this chapter, where, from real scale tests in a laboratory platform, different flows from 10 to 50 l/s are tested representing the outflow to the streets through one grate. In each test, water levels are measured manually over the grate and an orifice equation is used to calculate the discharge coefficient. Values show a dependence of the discharge, increasing the value with the outflow rate. A sensitivity analysis about the influence of longitudinal slope on this value demonstrated that discharge coefficients could be considered constant with the street longitudinal slope.

4.1.1 Previous research

Urban floods have been the object of interest of many researchers in last decades (**Hammond et al., 2018**). Moreover, the increase of imperviousness in the last decades, and potential effects of climate change, can increase these problems in a short and mid-term horizon (**Velasco et al., 2018**). During many years, the focus of the pluvial flooding in urban areas was basically oriented in the sewer network performance, assuming that all the runoff produced is introduced into the sewer. Traditionally drainage manuals imposed a security level of the sewer system based on specified return periods associated with the rain event used in the design (**Artina et al., 2001**), while no criteria were used to limit overland flow on the city surfaces during heavy storm events. The first references about manuals and procedures to limit street runoff can be found in USA (**DCG, 1969; CCRFCD, 1999; CDOH, 2000**) and United Kingdom (**BS 6367, 1983; Butler and David, 2004**). The behavior in a city during a rain event is a combination of the performance of the underground sewer network and the street network, and one of the key points is the flow transfer between surface level (streets) and underground level (sewer network). The proper way to analyse the behavior of the full drainage system is to consider the join effect of the sewer network and the overland flow.

The minor system provides a basic level of service by conveying runoff produced by the common (low rainfall intensity) rain events. So, the major system has to transport the runoff from the more extreme rain events (higher intensity and design return period) that are in excess of what the minor system can deal with this approach.

In the 70's, the city of Denver, Colorado, proposed the first design manual for this city (**DCG, 1969**), offering the first criteria that describe the connection between major and minor systems. Moreover, in 80's, the so called dual drainage approach, known as DDSWMM (Dual Drainage Storm Water Management Model) was included in many drainage codes of several cities of Canada (**Environment Canada and Ontario Ministry of the Environment, 1976**).

Notwithstanding these first experiences focused on real implementation of the dual drainage concept, the computational capacity of the computer codes made quite difficult complex 1D/2D simulations in urban areas (**Wisner and Kassem, 1983**). For this reason, 1D sewer models, assuming that all the runoff enters into the minor system were widely used in the following years (**Smith, 2006**). 1D models, simple to build up and with less complicated theory were well accepted as common engineering practice and supported by a wide range of software packages. In the 90's Djordjević et al. (**1991**) showed that the flows in the storm sewers are dependent on the excess volumes that are allowed to flow along the street network or if they are stored in a fictitious sub-basin above the surcharged manhole. Djordjević et al. (**1999**) identified some weak points of the existing models because they provide a "coarse surface descriptions" and a "lack of interaction between surface and underground flow components".

Nasello and Tucciarelli (**2005**) suggested this approach called Dual Urban Drainage Model as the best to describe what really happens in a city during rain events. The current approach is to consider a 1D model for the sewer network and a 2D model for the street flow networks (**Russo et al., 2015**) and can be used to analyse the urban flood problems in the sewer networks but, above all, the estimation of surface flood impacts like economic damages (**Velasco et al., 2015**), and business interruptions.

More recently, Chen et al., (**2016**) analyzed the flow transfers through the manholes neglecting the presence of the cover, although, before the manhole cover is moved during flooding produced by sewer surcharges, overflow occurs through the inlets existing in the urban area. **Chang et al. 2018** compared numerical simulations of urban flooding considering grate inlets and neglecting them and demonstrated that the effect of inclusion of inlets in dual drainage modelling improves the accuracy of flood modelling. As stated, the definitions of "major system" and "minor system" are referred, respectively, to the surface layer (streets and surface areas) and the ground level below (sewer network). For a reliable modelling a proper representation of the flow transferring between the surface and underground layer is essential. The surface flow must be intercepted by the inlets and introduced in the sewer system. Recent references about inlet efficiency can be found in the technical literature. In most cases, laboratory campaigns have been developed to test the hydraulic efficiency of grate inlets. For instance, tests were developed in United Kingdom, where Highways Agency (HA) commissioned HR Wallingford (HR) in association with the Transport Research Laboratory (TRL) to carry out a study on the hydraulic performance of gully grating used to collect surface water runoff from roads (**May and Todd, 1997**). Another scheme of facilities was developed to perform the British Standard in the University of Birmingham (**Russam, 1969**) and, more recently, the last physical model was done in the laboratory of the University of Sheffield (**Djordjević et al., 2013**). In Spain, in the hydraulic laboratory of the Technical University of Catalonia, a real scale platform was designed, built and used to test hydraulic efficiency of the most common grates used in Barcelona (**Russo, 2009; Gómez and Russo et al., 2011; Russo et al., 2013**).

Also in South Korea (**Ku and Jun, 2009**), and in the United States of America (specifically in the Colorado State University, Urban Drainage and Flood Control District (UDFCD) and Colorado Department of Transportation) other experimental facilities for testing hydraulic capacity of grate inlets were performed (**Comport and Thornton,**

2012). Another physical model to investigate the hydraulics of intake structures like grate inlets was developed in the University of Wuppertal in Germany by Kemper and Schlenkhoff (**2015**). In all of these cases, models objective was to estimated how much water can be intercepted by several types of grate inlets and the water that continues downstream.

Some authors have considered the hydraulics of this kind of process similar to an orifice or a weir process (**Rubinato et al., 2017**). This approach has the advantage that both are included in most of the commercial software available in the market for urban drainage modelling, making easier the application of this concept. If orifice option is adopted in the expression describing its hydraulics, the parameter to estimate the hydraulic of the orifice is the area of the holes, the energy immediately upstream the inlet and a discharge coefficient, different for every type of inlet, and also different for any hydraulic conditions.

Area of the holes is known for every considered inlet and the available energy "h" is a function of the flow along the street, depending, essentially, on rainfall and street geometry, while discharge coefficient C_d must be estimated by the user. Unfortunately, inlet providers and manufactures do not provide this information. Some companies like Neenah foundry give a set of abacus to assess the flow captured by the inlets depending on street and curb geometry, but not in the form of a specific discharge coefficient. In the last website version, Neenah foundry suggests to use a discharge coefficient equal to 0.6 (**NFCO, 2018**), thus it was used as a typical value for orifice coefficient in a tank outlet. So in case of estimating inlet captured flow, discharge coefficient must be estimated. In many cases, practitioners use similar values for inlets discharge coefficients proposed for orifices without considering that their discharge coefficient values depend on geometry and circulating flow. But it is not clear that this value could be used to reflect what really happens in the inlet. Some studies developed in last years (**Cárdenas-Quinteros et al., 2017**) have shown that discharge coefficients are far from the 0.6 value and, especially for supercritical flow conditions with high Froude numbers, C_d could be close to 0.1 or 0.2 for the flow entrance from the street to the sewer.

All these studies have been considered the entrance of water into the sewer, and not the opposite situation when the sewer is surcharged and flow exits from the sewer reaching the street level.

In the literature, it is possible to highlight studies about surcharged manholes that are located in the centre of the street while the grate inlets are generally located in the lateral curbs. **Martins et al. 2014** and **Lopes et. al. 2015** studied the surcharge of a gully box through experimental and numerical analysis. In a more recent experimental and numerical study carried out by Beg et al. (**2017; 2018**) in the Sheffield University, the effects on the surface of surcharge flow on sewer manholes were analyzed. In the same University, Rubinato et al. (**2018a and 2018b**) studied the flow leaving the sewer through manholes, assuming the cover has been removed by the outflow and estimated discharge coefficient considering orifice and weir approaches.

Moreover, concerning lateral grate inlets, Bazin et al. (**2014**) modelled a flow exchange between a street and drainage pipe in comparison with the experimental results obtained in the Ujigawa Open Laboratory in Tokyo, Japan. Finally, the effect of surcharged flow in urban areas was studied by Lee et al. (**2015**) and Bermudez et al. (**2018**).

In the work described in this chapter, an experimental study where an outflow is produced through the grate inlet is presented, reproducing the effect of pressurized sewer for different flows leaving the sewer and longitudinal slopes of the platform. The experiments consider just one grate inlet but the methodology can be extended to any type of inlet.

4.2 Methodology

This section presents the description of the experimental facility, hydraulic conditions for the tests and methodology to determine the field velocities and discharge coefficient.

4.2.1 Experimental set-up

An existing platform reproducing a street lane in the hydraulic laboratory of the Technical University of Catalonia (Barcelona) has been used for this experimental campaign. This platform (**Figure 4:1**) was also used for previous studies to determine inlets efficiency and their captured flow (**Gómez and Russo, 2005; Gómez and Russo, 2009; Russo et al., 2013**). Platform is 5.5 m long and 3 m width, and longitudinal and transverse slopes can be modified until a maximum of 10% for longitudinal slope and 4% for the transverse slope. The inlet considered is the so called Barcelona1, the most common grate inlet in Barcelona. Tests were done in real scale to avoid scale effects.

In the **Figure 4:1** a scheme of the laboratory installation is shown. In all the tests no flow on the surface layer was assumed, so the only exchange is from the sewer to the surface represented by the platform. Tests were done in steady flow conditions in all cases. Transverse slope was constant and equal to 2% for the different tests, as required in most of urban guidelines for pavement design and currently in Barcelona.

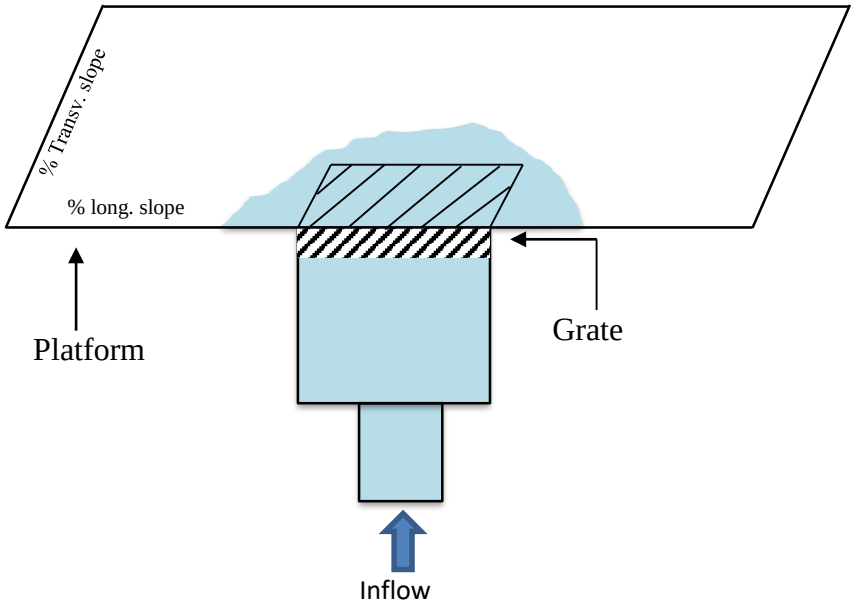

Figure 4:1 Scheme of the laboratory installation.

Figure 4:2 Inlet box below the grate.

Flow reaches the inlet through a 200 mm circular pipe. An inlet box of 90 x 30 cm and 50 cm height is located below the grate inlet (**Figure 4:2**). Also, the box hold the grate and has the inflow in the centre of its bottom.

The platform was modified in such a way flow through the inlet could be reproduced with the aim of representing the pressurized flow in the sewer and an outflow leaving the conduit. Flows considered through the grate were from 10 to 50 l/s. The water level over the grate inlet was measured manually, with a limnimeter of 1 mm accuracy. 23 points over the grate were taken into account and an average value of the 23 measures was considered as representative of the water level over the grate. In order to simulate the surcharged overflow by the grate, the experimental facilities present some modifications with additional pipes and valves electronically installed as shown in **Figure 4:3.**

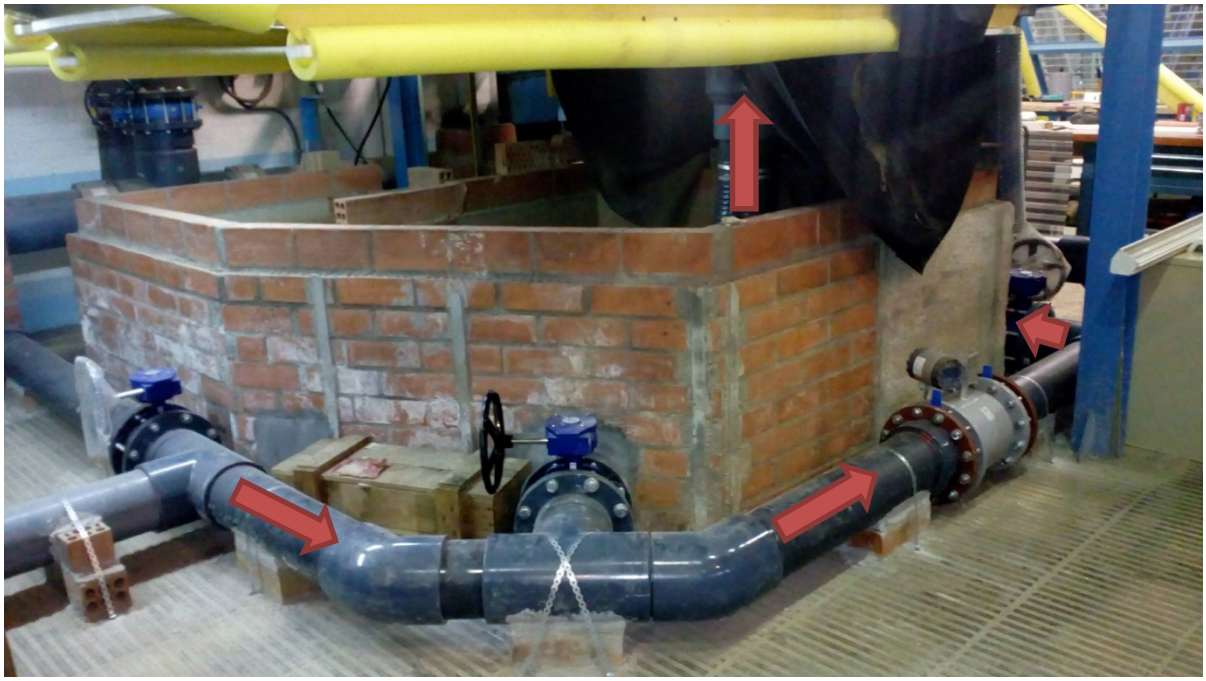

Figure 4:3 Hydraulic pipes system.

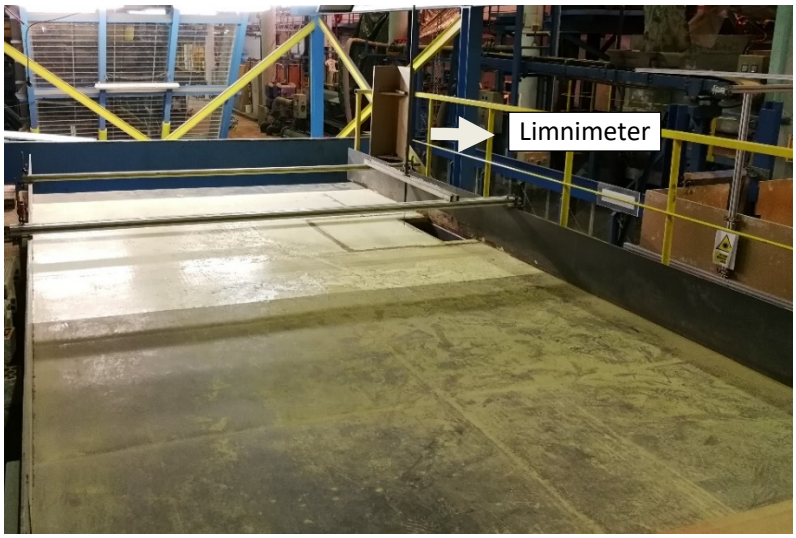

Figure 4:4 Graphics with the structure to support limnimeter.

In the previous chapter, the experimental set-up and the instrumentation necessary for the application of SFIV techniques were described. Through this equipment, it is possible to obtain a velocity field with a set of experiments with camera speed of 150 fps for all combinations of transversal slopes (0%, 2%, 4%) and longitudinal slopes (0%, 2%, 4%, 6%, 8%, 10%) considering the surcharged overflows of 10, 20, 30, 40 and 50 l/s. In total, 18 combinations for each flow rate and 90 cases of processed images for this type of grate were considered (**Figure 4:5**).

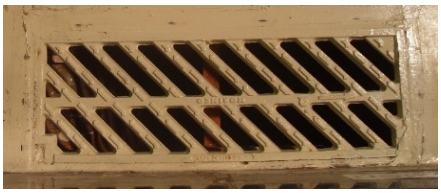

Grate Type 5

Figure 4:5 Type of grate used in the experimental campaign.

4.3 Discharge coefficient

Taking in account that the objective of this chapter is to study the surcharged overflow by grate inlet (**Figure 4:6**), which can be defined from the expression of the discharge coefficient for nozzles and orifices, the output flow is governed by the following **Equation [4. 1]** to calculate the discharge coefficient C_d:

$$C_d = \frac{Q_o}{A_h\sqrt{2g\Delta h}} \qquad \textbf{[4. 1]}$$

Where: $Q_{outflow}$: is the surcharged overflow by grate inlet (m^3/s)

C_d : is the discharge coefficient including all the effects of energy losses through the grate, effect of approaching velocity, etc.

g : is the gravitational acceleration (9.81 m/s^2)

A_h : is the area of holes of the grate (m^2)

Δh : is the water level above the grate (m)

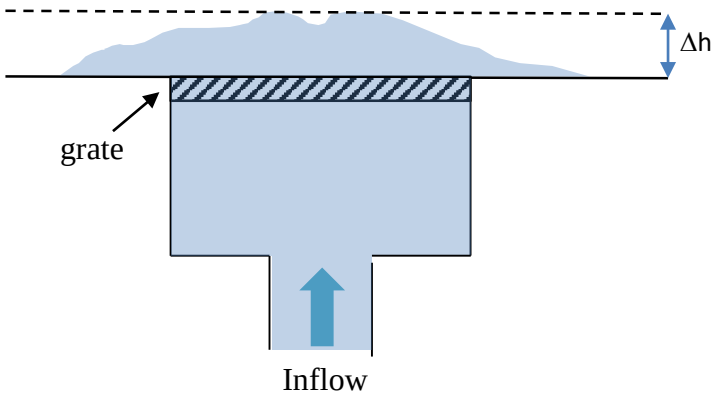

Figure 4:6 Sketch of exit surcharge flow of the grate inlet.

In the **Figure 4:7**, it is possible to observe the differences of water levels over the grate during the tests. Moreover, some oscillations of several millimetres (10 mm as maximum) were observed during the tests, so water level measure takes the average value with time of the water depths.

Figure 4:7 Outflow between 10 and 50 l/s for a geometric configuration of the platform with 2% of longitudinal and transverse slopes.

Although the grate inlet is designed to capture the surface flow, sometimes high flow rate or bad design of the sewer produce surcharged conditions. For this reason, it is important to analyse the behavior of the surcharged grate inlet and the interaction with the surface flow.

In order to understand the behavior of surcharged grate inlet, an experimental campaign was developed considering several surcharged overflows exiting by the grates (10 l/s, 20 l/s, 30 l/s, 40 l/s and 50 l/s), several longitudinal slope (0%, 2%, 4%, 6%, 8% and 10%) and a fixed transversal slope of 2%. Test were carried out without circulating flow on the platform, although the physical model is able to take into account this effect as descried before.

In order to estimate the discharge coefficient (C_d) for the tested grate, **Equation [4. 1]** was considered and for each surcharged overflow water levels were measured over the grate inlet in 23 points in order to achieve the average flow depth.

Imposing the outflows, for 10, 20, 30, 40 and 50 l/s, the values of mean water level over the inlet were obtained, for the case of 0% of longitudinal slope and 2% of transverse slope (**Table 4:1**).

Flow rate (l/s)	H_{grate} (mm)
10	39
20	56
30	74
40	92
50	105

Table 4:1 Average water level above the inlet grate.

In all the cases, the inlet is covered by water, even with the lowest flow. Reynolds values of the experiments ranged from 63662 to 318310, (lower value for 10 l/s and greater value for 50 l/s) were estimated in the pipe. From the water levels over the grate, it was possible to calculate the following discharge coefficient from the **Equation [4. 1]** (**Table 4:2**).

Flow rate (l/s)	Discharge Coefficient (C_d)
10	0.14
20	0.22
30	0.29
40	0.36
50	0.41

Table 4:2 Discharge coefficient for the Barcelona grate inlet (longitudinal slope 0% to 10%, transverse slope 2%).

So it is possible to observe that discharge coefficients are not the same as used for other orifice types of flow. **Figure 4:8** shows an evolution with the flow of the discharge coefficients, with an increasing value with the outflow, multiplying for more than 3 the minimum discharge coefficients. For the minimum flow tested, 10 l/s, value of 0.13 was found, while for the maximum flow, 50 l/s, a discharge coefficient of 0.41 was obtained.

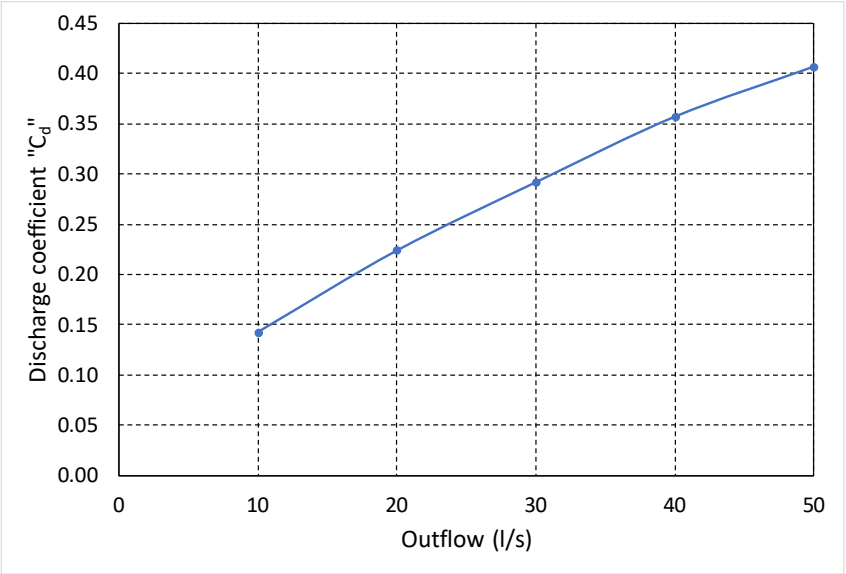

Figure 4:8 Discharge coefficient evolution with the outflow through the grate. Longitudinal Slope 0%, 2%, 4%, 6%, 8% and 10%, and Transversal slope 2%.

As said, these results were obtained with 0% longitudinal slope and 2% of transverse slope and the absence of flow approaching the inlet.

In order to carry out a sensitivity analysis regarding longitudibnal slope, the same tests were repeated fixing transverse slope to 2% and modifying longitudinal slopes. Specifically values of 2, 4, 6, 8 and 10% were tested. In all cases the same approach was used, considering an average value of the water level over the grate and measuring the water level in 23 points. In this case, for some combinations of flow and slope, especially for high slopes, not all the grate holes were covered by water, and the outflow was associated to a smaller area. Anyway, for those values with no water level above grate, 0 value was considered and they were included too in the average value. In all cases, although steady state was imposed, the effect of the flow through the grate produced oscillations around the water level, so an average value for the measured water level was defined in every case. Results are presented in the **Figure 4:9**.

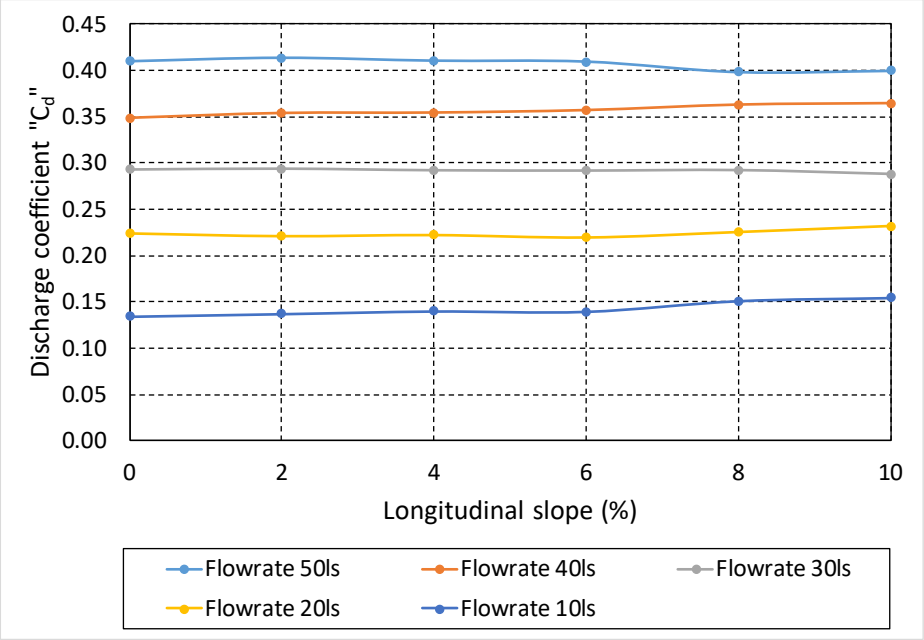

Figure 4:9 Values of Discharge coefficient "C_d".

It is possible to observe that the influence of the longitudinal slope is quite limited, so there is not a serious error to consider constant values, equal to those found for 0% of longitudinal slope. So for any grate inlet, it is possible to define the discharge coefficients and they are practically constant for any longitudinal slope.

4.4 Energy loss coefficient

The energy loss occurs when the motion of fluid pass around a section and the energy of the fluid changes. The energy loss depends on two conditions as the type of fluid and the motion of the fluid. Two different type of energy loss exists:

1. The friction losses
2. The local losses

where the friction losses depend on the viscosity of the fluid and if it is laminar or turbulent. Normally this loss occurs along the pipes. The local losses occur with a disturbance of flow due to a local change of geometry with a formation of eddies by the obstacle or structure (for instances, a grate can be considered as an element producing a local loss).

In **Table 4:3**, it is possible to see the typical values of energy loss coefficient "K".

Type	Classification	Values "K"
Elbows	Regular 90º, flanged	0.3
	Regular 90º, threaded	1.5
	Long radius 90º, flanged	0.2
	Long radius 90º, threaded	0.7
	Long radius 45º, flanged	0.2
	Regular 45º, threaded	0.4
	180º return bend, flanged	0.2

180º return bend	180º return bend, threaded	1.5
Tees	Line flow, flanged	0.2
	Line flow, threaded	0.9
	Branch flow, flanged	1.0
	Branch flow, threaded	2.0
Union, Threaded		0.08
Valves	Glove, fully open	10
	Angle, fully open	2
	Gate, fully open	0.15
	Gate, ¼ closed	0.26
	Gate, ½ closed	2.1
	Gate, ¾ closed	17
	Swing check, forward flow	2
	Swing check, backward flow	∞
	Ball valve, fully open	0.05
	Ball valve, 1/3 closed	5.5
	Ball valve, 2/3 closed	210

Table 4:3 Typical local loss coefficient "K" (**https://vanoengineering.wordpress.com/2012/12/30/head-loss-coefficients/**).

The estimation of energy loss coefficient in surcharged sewer overflow by grates depends on the inlet geometry. On the other hand, it is important to know the pressure losses that the water undergoes in its circulation through the grate. For the case of a reduced hydraulic section, the loss of energy can be calculated by **Equation [4. 2]** and consequently the energy loss coefficient "K" could be calculated by **Equation [4. 3]**:

$$\Delta h_k = K \frac{v_{outflow}^2}{2g} \qquad \textbf{[4. 2]}$$

$$K = \Delta h_k \frac{2g}{v_{outflow}^2} \qquad \textbf{[4. 3]}$$

Where: Δh_k : is the difference of water level above the grate (m)

K : is the Energy loss coefficient

g : is the gravitational acceleration (9.81 m/s^2)

A_h : is the grate hole's area (m^2)

$v_{outflow}$: is the velocity of surcharge flow through the grate inlet (m/s) ($v_{outflow} = \frac{Q_{outflow}}{A_h}$)

In addition, in order to calculate the values of energy loss coefficient "K", it was necessary to carry out other experimental tests avoiding the presence of the grate in the physical model and maintaing all the other features (same distribution of the measure points of water depth, the same surcharged overflow and longitdinal slopes).

In this case, flow velocity was calculated considering the section of the whole hole withouth following the **Equation [4. 3]**.

Results shown in **Figure 4:10** demonstrate that the parameter of water depth is very sensitive in the **Equation [4. 3]**, considering that the surface level is unstable and, due to the effect of turbulence, the values of "k" are not easy to evaluate. Also, the values for the 10 l/s present an added uncertainty because sometimes the area of the hole does not cover all the grate and the difference of water depth is very difficult to estimate. For this reason **Figure 4:10** does not show these cases.

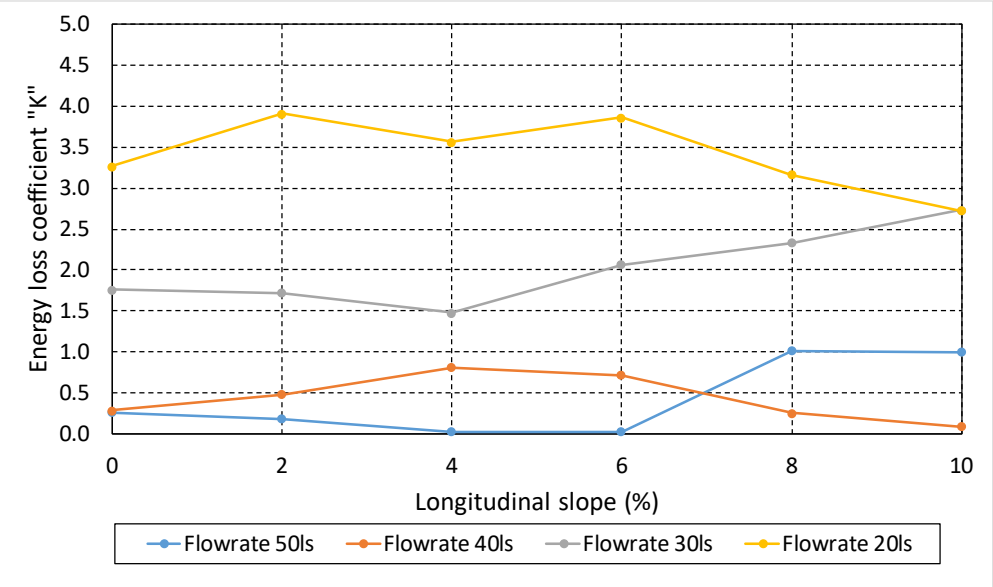

Figure 4:10 Graph of Energy loss coefficient "K".

After results analysis, a value of energy loss coefficient was proposed for each exit surcharged flow of the grate inlet that involves all the combinations of geometry (longitudinal and transversal slope) for each surcharged overflow studied as shown in **Table 4:4** and **Figure 4:11**, taking into account, as said, that the inflow 10 l/s was removed because its results do not present a good accuracy.

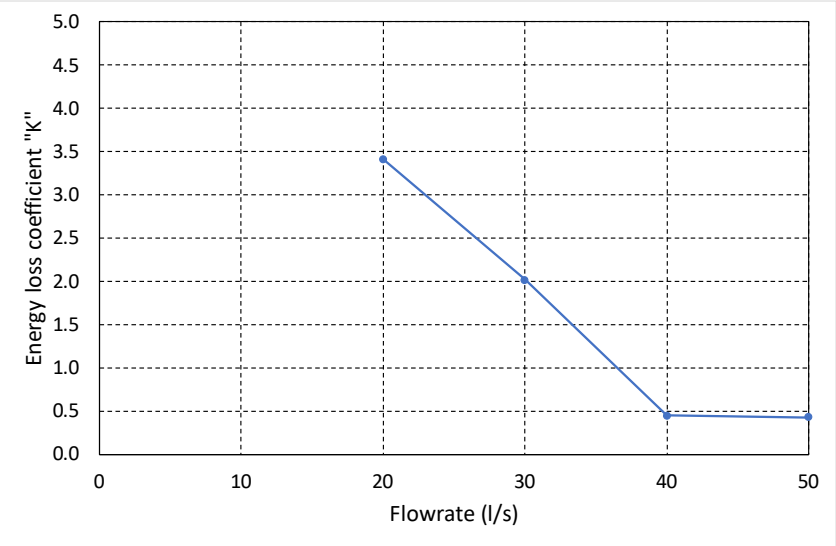

Figure 4:11 Graph of proposing an Energy loss coefficient "K".

Flow rate (l/s)	Energy loss Coefficient (K)
20	3.41
30	2.02
40	0.44
50	0.42

Table 4:4 Resume of Energy loss coefficient "K".

4.5 Image processing

Also for these tests, image processing technique was used to reproduce the flow pattern produced by sewer surcharged overflows. Again a video editor (VirtualDub) was useful to prepare the videos for the image processing. It removed and resized the captured image as show in **Figure 3:17** according to the geometry of the platform. In this case, the video was cut in one side (Δx) as shown in **Table 4:5**. Then, through the program VirtualDub the sequence of image in a resolution of 1280 x 1024 px and speed of 150 frames/second was saved.

Transversal slope (%)	Longitudinal slopes (%)	Δx (Px)
2	0	68
2	2	76
2	4	82
2	6	91
2	8	96
2	10	99

Table 4:5 Area of trim of image.

A changing parameter on this experiment was the angle of the platform (θ) (**Figure 3:18**). Considering a different value of pixels/meters for a resolution of 1280 x 1024 pixels for each combination of slopes, the first step is to measure the focus area of the image on the platform changing the angle of the platform (θ) as shown in the **Table 4:6**. In this case, the distance between the platform and the camera was 4.4 meters.

Furthermore, the image process was done through the code Digiflow, using an interrogation windows of 20 by 20 pixels. Also, the coordinate systems were generated between focus view of the lens camera and the focusing area on the platform. Once these parameters are defined, it is possible to generate the cross-correlation of the surface flow perturbations in Digiflow and generate the field velocities.

	Transversal slopes 2%		
	High (m)	Width (m)	Angle (θ)
Longitudinal slope 0%	0.961	0.986	6.232 ^{0}
Longitudinal slope 2%	0.946	0.972	6.159 ^{0}
Longitudinal slope 4%	0.925	0.957	6.022 ^{0}
Longitudinal slope 6%	0.910	0.947	5.904 ^{0}
Longitudinal slope 8%	0.890	0.930	5.775 ^{0}
Longitudinal slope 10%	0.894	0.928	5.800 ^{0}

Table 4:6 Dimension of focus area of the camera on the platform.

4.5.1 Velocity field and distribution of the flow

Using the tool Digiflow through the cross-correlation of the images, it is possible to view the maps of field velocities expressed in m/s, where the vector of velocity pattern is associated to the exit surcharged flow through the grate inlet. The values of field velocities are in the range of 0.15 m/s to 0.90 m/s for this type of combination (**Figure 4:12**).

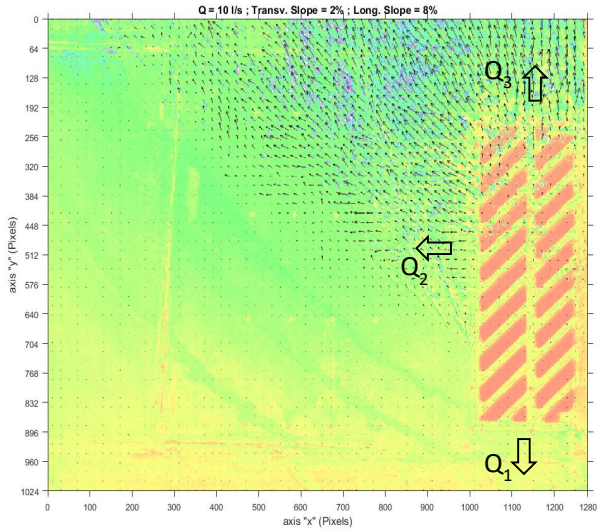

Outflow 10 l/s, Long. Slope 8%.

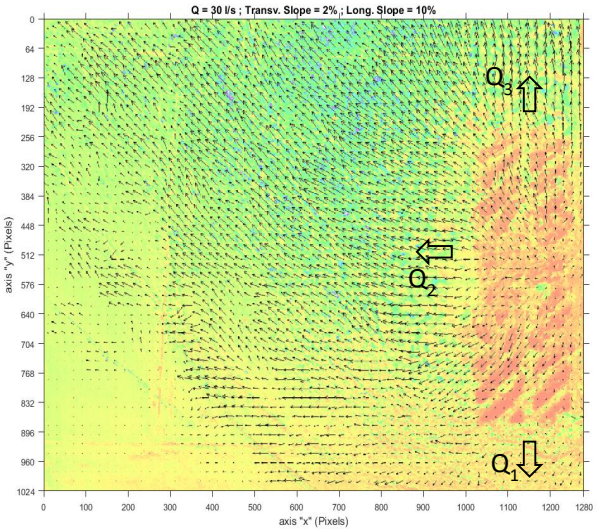

Outflow 30 l/s, Long. Slope 10%.

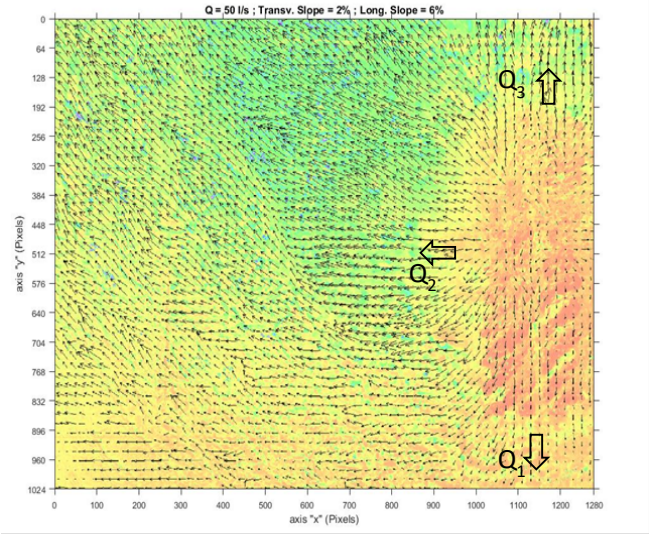

Outflow 50 l/s, Long. Slope 6%.

Figure 4:12 Field velocities around the grate inlet, Transv. Slope 2%.

4.5.2 Distribution of flow around the grate inlet

Following the scheme of the mass balance of the grate inlet (**Figure 4:13**), it is possible to determine the distribution of the flow rate around the grate, using the map of the velocity field, the flow depth measurements, the Matlab code and following the methodology of SFIV technique described in chapter **3**. With the mass balance on the grate, the total outflow by the grate is equal to outflow (1) plus outflow (2) plus outflow (3) of the grate following the **Equation [4. 4]**:

$$\boldsymbol{Q_{outflow} = Q_1 + Q_2 + Q_3} \qquad \textbf{[4. 4]}$$

Where: $Q_{outflow}$: is the outflow discharge from surcharge flow through the grate inlet (m^3/s).

Q_1 : is the outflow (1) (m^3/s).

Q_2 : is the outflow (2) (m^3/s).

Q_3 : is the outflow (3) (m^3/s).

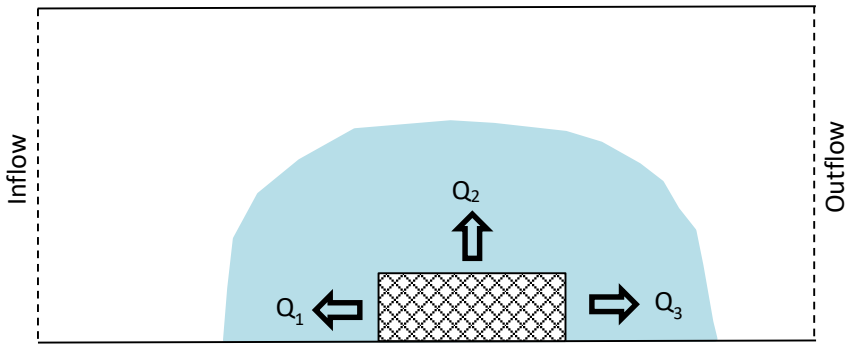

Figure 4:13 Scheme of the mass balance of the grate inlet.

Following the **Equation *[3:9]*** and **Equation *[3:10]***, it was described the discretization of the domain for different sides of the grate to obtain the mass balance in the grate inlet domain (**Figure 3:25**) as described in Chapter **3**. For these tests, 10 point of water level were taken around the grate inlet and the velocity was generated with cross-correlation of sequence of image, for an area of 0.5 m of width and 1 m of long.

Moreover, the generation of mass balance on the grate was obtained through a code in MATLAB and programmable excel sheet. The results of the comparison between experimental and measured exit surcharged overflow through the grate inlet and the flow rate obtained by the equation of mass balance using the velocities of Digiflow are shown in **Figure 4:14**. All the results are calculated for different platform geometries with a range of longitudinal slope 0%, 2%, 4% 6%, 8% and 10% and a fixed transversal slope of 2%, and several overflows (10 l/s, 20 l/s, 30 l/s, 40 l/s and 50 l/s). The greatest differences were found with low longitudinal slopes of 0% and 0.5%, flow rate of 10 l/s, associated with low velocities.

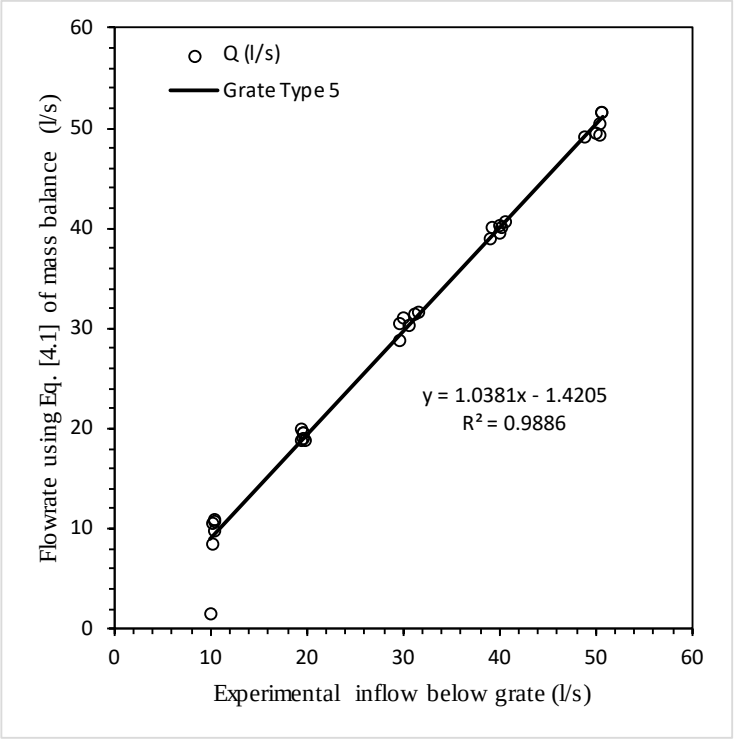

Figure 4:14 Comparison between measured exit surcharge flow of the grate inlet vs flow rate obtained by SFIV technique.

In order to further analyse the distribution of flow rate around the grate inlet, **Figure 4:15** shows the results in a percentage of flow rate where the 100% is the total flow rate introduced under the grate inlet. The distribution of flow rate in the grate inlet is divided according to the mass balance in 3 parts as Q_1, Q_2 and Q_3 (**Figure 4:13**); with the same combination of slopes and flow rate.

The results concerning the distribution of flow rate depend on the exit surcharged overflow and the longitudinal slopes as shown in **Table 4:7**. Summarizing, the range of the outflow "Q_1" is between 0-21%, the outflow "Q_2" is around 37-49% and the outflow "Q_3" is between 30-63% approximately, for all the combination of geometry described before and overflow between 20 and 50 l/s. The case of flow rate of 10 l/s is more difficult to analyse because it is not easy to generate a good velocity field for low velocities, but the maximum flow is governing by outflow "Q_3" between 49% to 78% and 13% to 50% for the outflow "Q_2" as show in **Figure 4:15**.

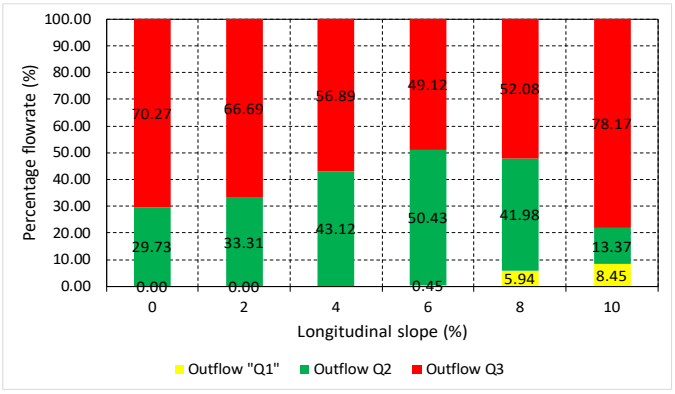

Outflow 10 l/s.

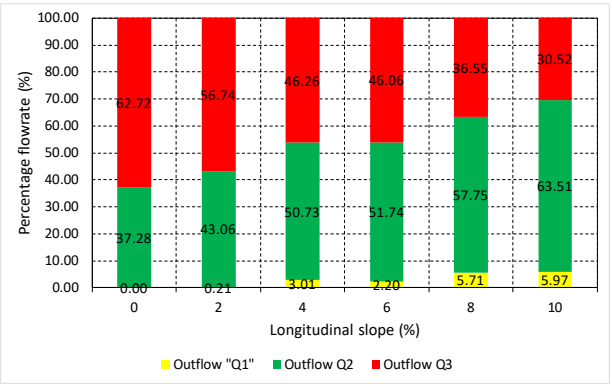

Outflow 20 ls.

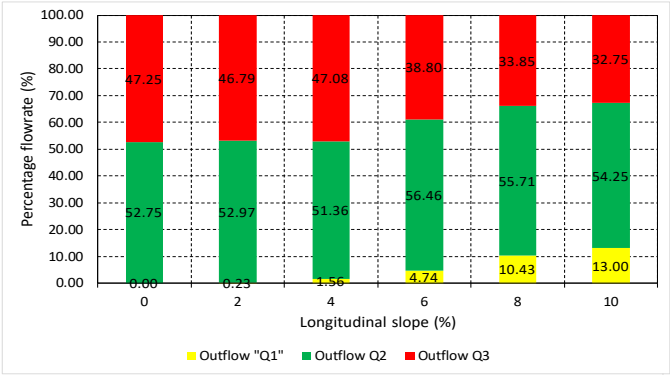

Outflow 30 l/s.

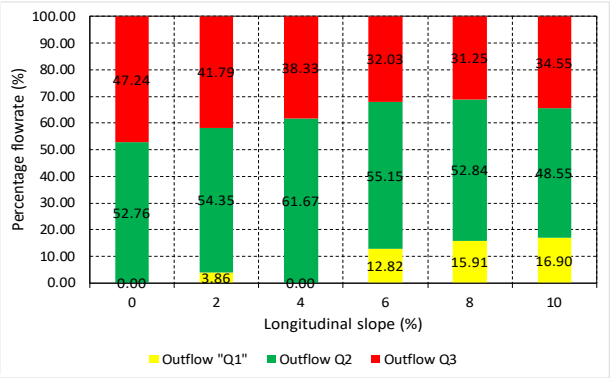

Outflow 40 l/s.

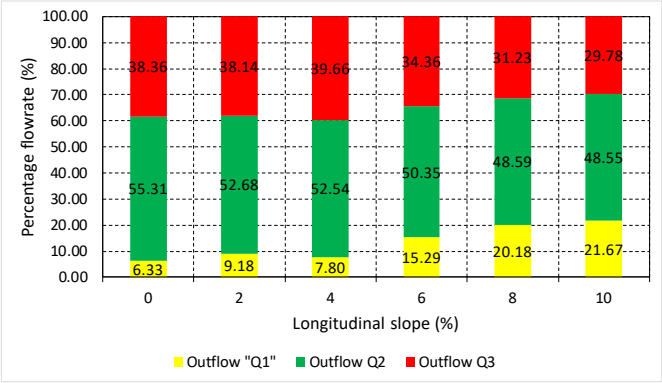

Outflow 50 l/s.

Figure 4:15 Graph of distribution of outflow, transversal slope 2%.

Inflow (l/s)	Outflow "Q_3" (%)	Outflow "Q_2" (%)	Outflow "Q_1" (%)
20	63 – 31	37 – 63	0 - 6
30	47 – 33	53 – 54	0 - 13
40	47 – 35	53 – 49	0 – 16
50	38 – 30	55 – 49	7 - 21

Table 4:7 Range of distribution of flow rate around grate inlet.

4.6 Conclusions

An experimental study representing the outflow from surcharged sewer systems through grate inlet has been presented. Full scale 1:1 tests were carried out considering different rates of overflows through grate inlet produced by surcharged pipes and different longitudinal slopes of the platform. The discharge coefficient calculated using the orifice expression show an evident variation with the outflow discharge. Values of these coefficients can increase three times depending on the overflow rate. Another interesting result is that the discharge coefficient is not sensitive with longitudinal slopes.

Moreover, through the SFIV technique and using the software Digiflow, it was possible to evaluate the distribution of the surcharged overflow through a grate inlet.

Results of the experimental campaign show a range of values of discharge between 0.13 to 0.41 for a flow rate surcharge between 10 to 50 l/s. Furthermore, is important that the values of C_d estimated were approximately constant for each outflow through the tested grate inlet, whereby the effect of transversal and longitudinal slopes has very poor influence. Tests considered the absence of surface flow approaching the grate inlet. Further analysis could be carried out to analyse the influence of the presence of runoff on the discharge coefficients values of the grate.

The flow transfer between the major and minor drainage systems and viceversa become one of the key elements for a good quality of the results. computer codes available now in the market allow this dual drainage modelling, so, in case of this approach the accuracy of the results rely on the good estimation of these flow transferring and the right choice of discharge coefficients, in case an orifice type approach is used to describe the flows through the grate.

Discharge coefficients are far from the values used in many cases by practitioners or suggested by some inlet manufacturers. The typical value suggested of 0.6 is too optimistic, and real values could be one third or one fourth. The differences can produce significant errors in the flooding simulations produced by 1D/2D coupled models. Most of the commercial software allows the orifice type to describe the flow transfer between sewer and surface. Grate inlet manufacturers could provide for every grate the specific discharge coefficients so the application to consider dual drainage can be done in a very easy way.

In addition, values of energy loss coefficient "K" was calculated for the same grate. In this case, it is possible to say that the values "K" is between 0.42 to 3.41 for the overflows between 20 and 50 l/s.

Chapter 5 Final remarks

5.1 Conclusions

The safe traffic and the general condition of the urban environment during rain events are given by the correct design of urban drainage systems and the right size of the drainage network. The function of the drainage systems is to collect and transport stormwater produced in urban area and the inlets system has to capture runoff generated on roads, sidewalks, and other pervious and paved areas no directly connected to the sewer system. Flooding in urban areas can be caused by the excess of runoff on the street, where the grate inlet has the principal objectives to capture the flow that circulates uncontrolled on the surface and introduce it in the sewer network. For this reason, the study of the hydraulic efficiency of grate inlets is important to locate them in the correct positions and to know how many inlets are necessary along the street.

This PhD dissertation is focused on engineering application concerning the hydraulic behavior of the grate inlet and the use of visual techniques to measure flow velocities. Specifically, one of its main objective is to develop a visualization technique to study the hydraulic efficiency, field velocities and distribution of flows around the grate. The second main issue of the thesis is to study the surcharged flow through a grate inlet in urban areas when the sewer systems gets pressurized. This PhD dissertation continues the research line concerning inlet hydraulics started approximately 20 years ago by the Flumen Institute of the Technical University of Catalonia.

This thesis contents results of two different experimental campaign from 2013 to 2017 on the platform for grate inlets testing located in the laboratory of hydraulics of UPC. The first campaign concerned the analysis of the flow distribution and the velocity field around the most common three grate inlets in the city of Barcelona, while the second campaign was to study the discharge coefficient and the behavior of the flow leaving the sewer through a grate (Barcelona1) when the sewer gets pressurized.

The methodology carried out to apply a new technique called Surface Flow Image Velocimetry (SFIV) relies on visualization techniques in engineering applications using the software of advanced image processing for fluid mechanics called Digiflow developed by Dalziel Research Partners at the Department of Applied Mathematics and Theoretical Physics (DAMTP) of the University of Cambridge.

The experimental campaign about the achievement of grate inlet discharge coefficient of surcharged sewer system was developed to fill an important gap in literature, where this topic has been not treated and default values proposed by engine software's are totally inadequate.

The document of this dissertation is divided into six chapters, where the scope of the thesis is described in chapter 1 with the principal objectives and introduction of visualization techniques for hydraulic application. The state of the art (Chapter 2) contents the theory of different experimental hydraulic measurement techniques and the description of different image processing techniques in the field of hydraulics. The scope of chapter 3 describes the methodology developed to generate the field velocities and the distribution of the flow around the grate inlet through visualization technique, applying a technique as SFIV. Chapter 4 is focused on the analysis of the hydraulic behavior of pipe surcharged flow through the grate inlet.

The first case studied in this thesis deals with the generation of field velocities and distribution of flow rate around the grate inlet. The tests were carried out for three different types of grates (the most common ones in Barcelona), on the hydraulic platform in scale 1:1 for grates testing developed at the Hydraulic Laboratory of the UPC. Results provided the field velocities around the grates for five different approaching flows with a range between 25 l/s to 200 l/s, changing the longitudinal (0, 0.5, 1, 2, 4, 6, 8, 10%) and transversal (0, 2, 4%) slopes and having in total 24 combinations for each approaching flow.

Following the same methodology of SFIV technique described in chapter 3, the next step was to do a comparison of field velocities and distribution of the flow around grate (Barcelona1) using the PIVlab tools of MATLAB package. The results presented a very good accuracy in comparison with experimental data and previous results through Digiflow.

SFIV technique is a good tool as visualization technique that can be used for another engineering application following the method developed in this dissertation such as floods, experimental application in hydraulics and fluids mechanics, streets, channels, tunnel, dam, debris flows, ocean waves, etc.

The first conclusion of the SFIV technique with the application in the nearness of a sewer grate is that the precision of the velocity field shows good accuracy special for supercritical flow. However, this technique has a dependency of slopes and approaching flow of the street, where results confirm that in a flat surface and low velocities is difficult to generate enough recognizable perturbations on the surface flow to reproduce the field velocities.

The second innovative experimental campaign was developed in the same experimental set-up with some changes to study the behavior of pipe surcharged overflow through the grate inlet. The originality to study the grate under pressure is that nobody has studied in deepness this problem yet in literature.

The new experimental methodology carried out allowed to study the values of discharge coefficient and the loss energy of the grate inlet and, at the same time, it was possible to study the distribution of the exit flow and the field velocities using the methodology of SFIV technique developed in this thesis and described in chapter 3. For this experiments, the transversal slope was fixed at 2% and the longitudinal slopes were 0, 2, 4, 6, 8 and 10%, for a range of exit flow between 10 l/s to 50 l/s.

5.2 Achieved results

The main contribution of this dissertation is the development of a Surface Flow Image Velocimetry technique to determine the filed velocities and the distribution of the approaching flow in the nearness of sewer grates developed in the Laboratory of hydraulics of UPC. The same technique can be extrapolated for other engineering applications following the methodology studied in this dissertation.

SFIV is a non-invasive technique that does not disturb the flow during the measure, convenient for small water level and high velocities where is more difficult to use other types of sensors. SFIV technique was validated for many combinations of slopes and approaching flow. It can be used for other engineering applications as river engineering, channels, waves in the coastal area, etc.

In this thesis, the methodology of the technique SFIV has been applied in urban drainage and, specifically, in the study of the behavior of the flow in the nearness of grate inlet, where it is possible to know the field velocities and the distribution of the flow around it.

After the tests of three different grates, the conclusion was that the distribution of the flow around the grate inlet is divided in 70% for frontal flow rate and 30% of lateral flow rate approximately. Furthermore, the SFIV technique provides a map of the field velocities around the grate inlet.

Another contribution is related to the discharge coefficient (C_d) for the grate inlets in case the flow exits from the sewer to the street (surcharged sewers conditions). The range of values for discharge coefficients proposed in this thesis for a sewer grate is between 0.13 to 0.40, for a range of surcharged outflows through the grate inlet between 10 and 50 l/s, showing significant difference respect to a usual values suggested in the technical literature for the discharge coefficient of orifice.

Results of discharge coefficient represent an important contribution especially for dual drainage systems where, in some case, the engineers use values of discharge coefficient of the orifice far from reality with significant errors considering that the relation of values of discharge coefficient between grate and orifice are too big.

Another issues treated in this research was the estimation of the values of energy loss coefficient "K", where the range of values obtained through the tests was between 0.42 and 3.41 with a range of exit flow from 20 l/s to 50 l/s.

5.3 Future work

This PhD dissertation opens the door to promising further researches:

- To extend the application of SFIV techniques for other engineering applications and also, to implement the methodology with another method of image capturing, because of it could be more adequate the study of big domains with drones or planes in rivers, coastal and oceans.

- To extend the experimental campaign of surcharge flow through the grate inlet to other different types of grate inlet in order to validate the methodology, and try to propose a correlation function for the discharge coefficient with the geometry of the grate.

- Moreover, to perform a new experimental campaign to study the interaction of exit surcharged flow with the surface flow along the street.

- To compare the results of experiments with the tridimensional numerical simulation results. The comparison could be interesting to confirm the values of discharge coefficient and energy loss coefficient values. In this case, 3D simulations could represent another useful tool to analyse the behavior of the interaction between the exit flow with the surface flow.

5.4 Publications derived from the thesis

Publications in Journals:

Tellez-Alvarez, J., Gómez, M., Russo, B., Redondo, J.M. (2018). *Application of SFIV Surface Flow Image Velocimetry techniques for the analysis of flow near grated inlets.* Proceedings of the Institution of Civil Engineers, Journal Water Management. (Minor revision)

Cosco, C., Gómez, M., Russo, B., **Tellez-Alvarez, J**., Macchione, F., Costabile, P., Costanzo C. (2018). *Proposal for grated inlet discharge coefficients using Froude number in case of orifice and weir approach.* Journal of Hydraulic Research (under review)

Gómez, M., Russo, B., **Tellez-Alvarez, J**. (2018). *Outflow from sewers in pressure flow conditions: discharg*e coefficients in case of orifice approach representing the grate hydraulics. Urban Water Journal (Minor revision)

Russo, B., Gómez, M., & **Tellez, J.** (2013). Methodology to Estimate the Hydraulic Efficiency of Nontested Continuous Transverse Grates. Journal of Irrigation and Drainage Engineering, 139(10), 864–871. doi:10.1061/(ASCE)IR.1943-4774.0000625.

Other publications

Proceedings of national and international conferences:

Oral Presentation

Tellez-Alvarez, J., Gómez, M., Russo, B. "Image processing technique for hydraulic application", Proceedings of ISP RAS, 29:6 (2017), 289–298. doiI: 10.15514/ISPRAS-2017-29(6)-18.

Tellez, J., Gómez, M., Russo, B., Zanon, F. *Comparación de métodos de análisis de imágenes para determinar el campo de velocidades en las cercanías de las rejas de alcantarillado*. Jornadas de Ingeniería del Agua, JIA 2017. Coruña, 2017, p. 1-12.

Tellez, J., Gómez, M., Russo B. and Redondo, J.M. (2016). *Metodología para la obtención del campo de velocidad en la proximidad de las rejas de alcantarillado.* XXVII Congreso Latinoamericano de Hidráulica. 2016, Lima, Perú.

Tellez, J., Gómez M., B. Russo and J.M. Redondo. (2016). *Surface Flow Image Velocimetry (SFIV) for hydraulics applications.* 18th International Symposium on the Application of Laser and Imaging Techniques to Fluid Mechanics, Lisbon, Portugal.

Tellez, J., Gómez, M. and Russo, B. (2015). *Metodología para determinar el campo de velocidades en los imbornales de captación.* VIII Seminario Red de Laboratorios de Hidráulica de España.

Poster presentation

Tellez, J., Gómez, M., Russo, B. and Redondo, J.M. (2016). *Characterize the hydraulic behaviour of grate inlet in urban drainage to prevent the urban's flooding.* EGU General Assembly Conference Abstracts.

Tellez, J., Gómez, M. and Russo, B. (2015). *Técnica para la obtención del campo de velocidad del flujo superficial en proximidad de rejas de alcantarillado.* Jornadas de Ingeniería del Agua (JIA 2015): la precipitación y los procesos erosivos, Córdoba, Spain.

Tellez, J., Gómez, M., Russo, B. and Redondo, J.M. (2015). *A simple measuring technique of surface flow velocity to analyse the behaviour of velocity fields in hydraulic engineering applications.* EGU General Assembly Conference Abstracts.

References

Admiraal, D. M., Stansbury, J. S. and Haberman, C. J. (2004) 'Case Study: Particle Velocimetry in a Model of Lake Ogallala', *Journal of Hydraulic Engineering*, 130, pp. 599–607. doi: 10.1061/(ASCE)0733-9429(2004)130:7(599).

Adrian, R. J. (1986) 'Image shifting technique to resolve directional ambiguity in double-pulsed velocimetry', *Applied optics,* Optical Society of America, 25 (21), pp. 3855–3858. https://doi.org/10.1364/AO.25.003855.

Adrian, R. J. (1991) 'Particle-Imaging Techniques for Experimental Fluid Mechanics', *Annual Review of Fluid Mechanics*, 23 (1), pp. 261–304. https://doi.org/10.1146/annurev.fl.23.010191.001401.

Adrian, R. J. (1996) *'Bibliography of particle image velocimetry using imaging methods: 1917-1995'*, *DLR-Mitteilung. DLR-Mitt--2011-01, 176 S*, pp. 1917–1995.

Adrian, R. J. (1997) 'Dynamic ranges of velocity and spatial resolution of particle image velocimetry', *Measurement Science and Technilogy*, 8 (12) 1393.

Adrian, R. J. (2004) 'Twenty years of Particle Image Velocimetry', in *12th International Symposium on Applications of Laser Techniques to Fluid Mechanics*, Lisbon, Portugal.

Adrian, R. J. (2005) 'Twenty years of particle image velocimetry', *Experiments in Fluids*, 39 (2), pp. 159–169. doi: 10.1007/s00348-005-0991-7.

Adrian, R. J., Christensen, K. T. and Liu, Z. C. (2000) 'Analysis and interpretation of instantaneous turbulent velocity fields', *Experiments in Fluids*, 29 (3), pp. 275–290. doi: 10.1007/s003489900087.

Adrian, R. J. and Westerweel, J. (2011) 'Particle Image Velocimetry', *Cambridge University Press*, pages 558.

Allamano, P., Croci, A. and Laio, F. (2015) 'Toward the camera rain gauge', *Water Resources Research AN AGU JOURNAL*, 51 (3), pp. 1744–1757. doi: 10.1002/2014WR016298.

Artina, S., Calenda, G., Calomino, F., Cao, C., La Loggia, G., Modica, C., Paoletti, A., Papiri, S., Rasulo, G., Veltri, P. (2001). 'Sistemi di fognature, Manuale di progettazione', *Hoepli editore*. Milano, Italy.

Barker, D. B. and Fourney, M. E. (1977) 'Measuring fluid velocities with speckle patterns', *Optics Letters*, *Optical Society of America*, 1 (4), p. 135. doi: 10.1364/OL.1.000135.

Bay, H., Ess, A., Tuytelaars, T. and Van Gool, L. (2008) 'Speeded-Up Robust Features (SURF)', *Computer Vision and Image Understanding*, 110 (3), pp. 346–359. doi: 10.1016/j.cviu.2007.09.014.

Bazin, P-H., Nakagawa, H., Kawaike, K., Paquier, A. and Mignot, E. (2014) 'Modeling Flow Exchanges between a Street and an Underground Drainage Pipe during Urban Floods', *Journal of Hydraulic Engineering*, 140 (10), p. 04014051. doi: 10.1061/(ASCE)HY.1943-7900.0000917.

Beg, M. N. A., Carvalho, R. F., Tait, S., Brevis, W., Rubinato, M., Schellart, A. and Leandro, J. (2018) 'A comparative study of manhole hydraulics using stereoscopic PIV and different RANS models', *Water Sciecne & Technology*, pp. 87-98. doi: 10.2166/wst.2018.089.

Beg, M. N. A., Carvalho, R., Leandro, J. (2017) 'Effect of surcharge on gully-manhole flow', *Journal of Hydro-environment Research*, 19, 224-236. doi: https://doi.org/10.1016/j.jher.2017.08.003.

Bermúdez, M., Ntegeka, V., Wolfs, V. and Willems, P. (2018) 'Development and Comparison of Two Fast Surrogate Models for Urban Pluvial Flood Simulations', *Water Resources Management*. 32 (8), pp 2801-2815. doi: 10.1007/s11269-018-1959-8.

Blois, G., Best, J. L., Christensen, K. T., Cichella, V., Donahue, A., Hovakimyan, N., Kennedy, A. and Pakrasi, I. (2016) 'UAV-based PIV for quantifying water-flow processes in large-scale natural environments' in 1*8th International Symposium on the Application of Laser and Imaging Techniques to Fluid Mechanics*, Lisbon, Portugal.

Bolognesi, M., Farina, G., Alvisi, S., Franchini, M., Pellegrinelli, A. and Russo, P. (2016) 'Measurement of surface velocity in open channels using a lightweight remotely piloted aircraft system measurement of surface velocity in open channels using a lightweight remotely piloted aircraft system', *Geomatics, Natural Hazards and risk*, 8 (1), pp 73-86. doi: 10.1080/19475705.2016.1184717.

Bradley, A., Kruger, A., Meselhe, E. A. and Muste, M. (2002) 'Flow measurements in streams using video imagery', *Water Resources Research*, 38 (12), p. 1315. doi: 10.1029/2002WR001317.

Brady, P. D. M., Boutounet, M. and Beecham, S. (2004) 'Free surface monitoring using image processing', in *15 th Australian Fluids Mechanics conference*, Sydney, Australia.

Butler, D. and Davies, J. W. (2004). 'Urban Drainage Book', *2nd Edition, Spon Press*, Simultaneously published in London, USA and Canada.

BS 6367. (1983). 'Drainage of roofs and paved area', *British Standards Institute*, London, United Kingdom.

Cárdenas-Quintero, M. and Carvajal-Serna, L. F. and Marbello-Pérez, R. (2017) 'Evaluación numérica tridimensional de un sumidero de reja de fondo (Three-Dimensional Numerical Assessment of Grate Inlet)', in *Ibero-American Seminar on Water and Drainage Networks (SEREA 2017)*, Bogota, Colombia.

Chang, T.J., Wang, C.H., Chen, A. and Djordjevic, S. (2018) 'The effect of inclusion of inlets in dual drainage modelling', *Journal of Hydrology,* 559. pp. 541 – 555. doi: 10.1016/j.jhydrol.2018.01.066.

Chen, A.S. Leandro, J. Djordjević, S. (2016) 'Modelling sewer discharge via displacement of manhole covers during flood events using 1D/2D SIPSON/P-DWave dual drainage simulations', *Urban Water journal*, 13 (8), pp. 830-840.

Clark County Regional Flood Control District (CCRFCD). (1999) 'Hydrological criteria and drainage design manual', Clark County, USA.

Colorado Department of Transportation (CDOH). (2000) 'Hydraulic Design criteria for highways', *Hydraulic Division Center*, Denver, USA.

Comport, B. C. and Thornton, C. I. (2012) 'Hydraulic Efficiency of Grate and Curb Inlets for Urban Storm Drainage', *Journal of Hydraulic Engineering*, 138 (10). doi: https://doi.org/10.1061/(ASCE)HY.1943-7900.0000552.

Creutin, J. D., Muste, M., Bradley, A. A., Kim, S. C. and Kruger, A. (2003) 'River gauging using PIV techniques: a proof of concept experiment on the Iowa River', *Journal of Hydrology*, 277 (3–4), pp. 182–194. doi: 10.1016/S0022-1694(03)00081-7.

Dabiri, D. (2006) 'Cross-Correlation Digital Particle Image Velocimetry-A Review', *Lecture notes of Department of Aeronautics & Astronautics, University of Washington*. Seattle, United States.

Dalziel, R. P. (2012) '*DigiFlow User Guide*', Department of Applied Mathematics and Theoretical Physics (DAMTP) - University of Cambridge, Cambridge, United Kingdom.

Dalziel, S. B. (1992) 'Decay of rotating turbulence: some particle tracking experiments', *Applied Scientific Research*, 49 (3), pp. 217–244. doi: 10.1007/BF00384624.

Dalziel, S. B., Hughes, G. O. and Sutherland, B. R. (1998) 'Synthetic Schlieren', in 8th International Symposium on Flow Visualization, 2 (1), pp. 1–6, Sorrento, Italy. doi: 10.1007/BF03182557.

Dalziel, S. B., Hughes, G. O. and Sutherland, B. R. (2000) 'Whole-field density measurements by 'synthetic schlieren'', *Experiments in Fluids*, 28 (4), pp. 322-335. doi: 10.1007/s003480050391

Dalziel, S.B. & Redondo, J.M. (2007) 'New visualization methods and self-similar analysis in experimental turbulence studies', *In Models, experiments and computation in turbulence. Ed. R. Castilla, E. Oñate & J.M. Redondo*, CIMNE, Barcelona, Spain.

Denver Council of Governments (DCG), Anon. (1969) 'Urban Storm Drainage Criteria Manual', *Wright-McLaughlin Engineers 1969*, United States.

Detert, M. and Weitbrecht, V. (2015) 'A low-cost airborne velocimetry system: proof of concept', *Journal of Hydraulic Research*, 53 (4), pp. 532–539. doi: 10.1080/00221686.2015.1054322.

Di Cristo C. (2011) 'Particle Imaging Velocimetry and Its Applications in Hydraulics: A State-of-the-Art Review', *In: Experimental Methods in Hydraulic Research. Geoplanet: Earth and Planetary Sciences*, Books series, Springer, Heidelberg, Berlin. doi: 10.1007/978-3-642-17475-9_3.

Dill, A. J. and Garcia, M. H., Valocchi, A. J. (1995) 'Video-Based Particle Trancking velocimetry technique for Measuring flow velocity in porous media', *Technical Report, Hydraulic Engineering Series no. 48,* University of Illinois at Urbana-Champaign, Illinois, United States of America.

Djordjević, S., Saul, A. J., Tabor, G. R., Blanksby, J., Galambos, I., Sabtu, I. and Sailor, G. (2013) 'Experimental and numerical investigation of interactions between above and below ground drainage systems', *Water Sciecne & Technology*, 67 (3), pp. 535-542. doi: 10.2166/wst.2012.570.

Djordjević, S., Ivetic, M., Maksimović, C. and Rajcevic, A. (1991) 'An approach to the simulation of street flooding in the modeling of surcharged flow in storm sewers', *Proceedings: New Technologies in Urban Drainage* UDT 91:101–8.

Djordjević, S., Prodanović, D. and Maksimović, Č. (1999) 'An approach to simulation of dual drainage', *Water Science and Technology,* 39 (9): 95–103. doi: 10.1016/S0273-1223(99)00221-8.

Dobson, D. W., Todd Holland, K. and Calantoni, J. (2014) 'Fast, large-scale, particle image velocimetry-based estimations of river surface velocity', *Computers and Geosciences*. Elsevier, 70, pp. 35–43. doi: 10.1016/j.cageo.2014.05.007.

Doppler, C. (1842) 'Über das farbige Licht der Doppelsterne und einiger anderer Gestirne des Himmels', *Proceedings of the Bohemian Society of Sciences, Praga, Chech Republic.*

Dramais, G., Le Coz, J., Camenen, B. and Hauet, A. (2011) 'Advantages of a mobile LSPIV method for measuring flood discharges and improving stage–discharge curves', *Journal of Hydro-environment Research*, 5 (4), pp. 301–312. doi: 10.1016/j.jher.2010.12.005.

Dudderar, T. D. and Simpkins, P. G. (1977) 'Laser speckle photography in a fluid medium', *Nature*, 270, pp. 45–47. doi: 10.1038/270045a0.

Gad-el-Hak, M., Pollard, A. and Bonnet, J.-P. (1998) '*Flow control : fundamentals and practices',* Book of Springer-Verlag.

Environment Canada and Ontario Ministry of the Environment, Anon. (1976) 'Manual of Practice on Urban Drainage, Research Report No. 10', Project 76-B-3B 1976, Canada.

Ettema, R., Fujita, I., Muste, M. and Kruger, A. (1997) 'Particle-image velocimetry for whole-field measurement of ice velocities', *Cold Regions Science and Technology*, 26(2), pp. 97–112. doi: 10.1016/S0165-232X(97)00011-6.

Fischler, M. a. and Bolles, R. C. (1981) 'Random sample consensus: a paradigm for model fitting with applications to image analysis and automated cartography', *Communications of the ACM*, 24 (6), pp. 381–395. doi: 10.1145/358669.358692.

Flór, J. B. and Van Heijst, G. J. F. (1996) 'Stable and unstable monopolar vortices in a stratified fluid', *Journal of Fluid Mechanics*. Cambridge University Press, 311 (1), p. 257. doi: 10.1017/S0022112096002595.

Fomin, N. A. (1998) *'Speckle Photography for Fluid Mechanics Measurements', Book of Springer Berlin Heidelberg*, Berlin, Heidelberg:. doi: 10.1007/978-3-662-03707-2.

Foucaut, J. M. and Stanislas, M. (2002) 'Some considerations on the accuracy and frequency response of some derivative filters applied to particle image velocimetry vector fields', *Measurement Science and Technology*, 13 (7), pp. 1058–1071. doi: 10.1088/0957-0233/13/7/313.

Fouras, a and Soria, J. (1998) 'Accuracy of out-of-plane vorticity measurements derived from in-plane velocity field data', *Experiments in Fluids*, 25 (5), pp. 409–430. doi: 10.1007/s003480050248.

Fujita, I., Muste, M., Kruger, A. (1998) 'Large-scale particle image velocimetry for flow analysis in hydraulic engineering

applications', *Journal of hydraulic research*, 36 (3), pp. 397–414. doi: 10.1080/00221689809498626.

Fujita, I. and Hino, T. (2003) 'Unseeded and seeded PIV measurements of river flows videotaped from a helicopter', *Journal of Visualization*, 6 (3), pp. 245–252. doi: 10.1007/BF03181465.

Fujita, I., Kosaka, Y., Honda, M. and Yorozuya, A. (2012) 'Tracking of river surface features by space time imageing', in *15th International Symposium on Flow Visualization*, Minsk, Belarus.

Fujita, I., Notoya, Y. and Shimono, M. (2015) 'Development of aerial STIV to videotated movie from multicopter based on high-accurate image stabilization', *Annual Journal of Hydraulic Engineering, JSCE*, 71 (4), pp. I_829-I_834. doi: 10.2208/jscejhe.71.I_829

Fujita, I. and Tsubaki, R. (2002) 'A Novel Free-Surface Velocity Measurement Method Using Spatio-Temporal Images', *Hydraulic Measurements and Experimental Methods Specialty Conference (HNEM), Estes Park, Colorado, United States of America*. doi: 10.1061/40655(2002)85

Fujita, I., Watanabe, H. and Tsubaki, R. (2007) 'Development of a non-intrusive and efficient flow monitoring technique: The space-time image velocimetry (STIV)', *International Journal of River Basin Management*, 5 (2), pp. 105–114. doi: 10.1080/15715124.2007.9635310.

Fujita, I. and Komura, S. (1994) 'Application of Video Image Analysis for Emasurements of Rivert-Surface Flows', *Proceedings of hydraulic engineering*, 38, pp. 733-738 doi: 10.2208/prohe.38.733.

Fujita, I., Aya, S. and Deguchi, T. (1997) 'Surface Velocity Measurement of River Flow Using Video Images of An Oblique Angle', in *Proceedings of the 27th Congress of IAHR, Theme B*, 1, pp.227-232, San Francisco, California, United States of America.

Gómez, M., Hidalgo, G., Russo, B. (2013) 'Experimental campaign to determine grated inlet clogging factors in an urban catchment of Barcelon', *Urban Water Journal*, 10 (1), pp. 50-61. doi: 10.1080/1573062X.2012.690435

Gómez, M., Paréas, J., Russo, B., Martinez-Gomariz, E. (2018) 'Methodology to quantify clogging coefficients for grated inlets. Application to SANT MARTI catchment (Barcelona)', *Journal of Flood Risk Management*. doi: 10.1111/jfr3.12479

Gómez, M. and Russo, B. (2005) 'Comparative study among different methodologies to determine storm sewer inlet efficiency from test data: HEC-12 methodology vs UPC method', *Water Resources Management III*, p. 623.

Gómez, M. and Russo, B. (2009) 'Hydraulic Efficiency of Continuous Transverse Grates for Paved Areas', *Journal of Irrigation and Drainage Engineering*, 135 (2), pp. 225–230. doi: 10.1061/(ASCE)0733-9437(2009)135:2(225).

Gómez, M. and Russo, B. (2011) 'Methodology to estimate hydraulic efficiencyu of drain inlets', *Proceedings of the Institution of Civil Engineers - Water Management*, 164 (2), pp. 81-90. doi: 10.1680/wama.900070

González, R. C. and Woods, R. E. (2002) 'Digital image processing', Book of *Prentice-Hall,* New jersey, United States of America. doi: 10.2307/1574313.

Grousson, R. and Mallick, S. (1977) 'Study of flow pattern in a fluid by scattered laser light', *Applied Optics*. Optical Society of America, 16 (9), pp. 2334–2336. doi: 10.1364/AO.16.002334.

Hain, R., Kähler, C. J and Tropea, C. (2007) 'Comparison of CCD, CMOS and intensified cameras', *Experiments in Fluids*, 42 (3), pp. 403–411. doi: 10.1007/s00348-006-0247-1.

Hammond, M. J., Chen, A. S., Djordjevic, S., Butler, D., Mark, O. (2013) 'Urban flood impact assessment: A state of the art review', *Urban Water Journal*, 12, (1), 14-29. Taylor & Francis. doi.org/10.1080/1573062X.2013.857421.

Hast, A., Nysjö, J. and Marchetti, A. (2013) 'Optimal RANSAC - Towards a repeatable algorithm for finding the optimal set', *Journal of WSCG*, 21 (1), pp. 21–30.

Hauet, A., Creutin, J.-D. and Belleudy, P. (2008) 'Sensitivity study of large-scale particle image velocimetry measurement of river discharge using numerical simulation', *Journal of Hydrology*, 349 (1-2), pp. 178–190. doi: 10.1016/j.jhydrol.2007.10.062.

Hauet, A., Kruger, A., Krajewski, W. F., Bradley, A., Muste, M., Creutin, J.-D. and Wilson, M. (2008) 'Experimental System for Real-Time Discharge Estimation Using an Image-Based Method', *Journal of Hydrologic Engineering*, 13 (2), pp. 105–110. doi: 10.1061/(ASCE)1084-0699(2008)13:2(105).

Hauet, A., Muste, M. and Ho, H.-C. (2009) 'Digital mapping of riverine waterway hydrodynamic and geomorphic features', *Earth Surface Processes and Landforms*, 34 (2), pp. 242-252. doi: 10.1002/esp.1709

Hesselink, L. (1988) 'Digital Image Processing in Flow Visualization', *Annual Review of Fluid Mechanics*,20 (1), pp. 421–486. doi: 10.1146/annurev.fl.20.010188.002225.

Hornung, H. G., Willert, C., Turner, S. (1995) 'The flow field downstream of a hydraulic jump', *Journal of Fluid Mechanics*. Cambridge University Press, 287 (1), pp. 299-316. doi: 10.1017/S0022112095000966.

https://vanoengineering.wordpress.com/2012/12/30/head-loss-coefficients/

Ian Grant (1994) 'Selected papers on particle image velocimetry', *Edited by The international society of optics and phoonics*, SPIE PRESS BOOK.

Ismail, A. and Ulrich, L. (2007) 'Large scale PIV-measurements on the water surface of turbulent open-channel flow', *18thCongrès Français de Mécanique,* Grenoble, France.

Iwata, K., Hakoshima, T., Nagata, R. (1978) 'Measurement of flow velocity distribution by multiple-exposure speckle photography', *Optics Communications*, 25 (3), pp. 311-314. doi: 10.1016/0030-4018(78)90135-9

Jeanbourquin, D., Sage, D., Nguyen, L., Schaeli, B., Kayal, S., Barry, D. A. and Rossi, L. (2011) 'Flow measurements in sewers based on image analysis: automatic flow velocity algorithm', *Water Science and Technology*, 64 (5), pp. 1108–1114. doi: 10.2166/wst.2011.176.

Jodeau, M., Hauet, a., Paquier, a., Le Coz, J. and Dramais, G. (2008) 'Application and evaluation of LS-PIV technique for the monitoring of river surface velocities in high flow conditions', *Flow Measurement and Instrumentation*, 19, pp. 117–127. doi: 10.1016/j.flowmeasinst.2007.11.004.

Kähler, C. J. (2004) 'The significance of coherent flow structures for the turbulent mixing in wall-bounded flow', *PhD. Thesis, University of Göttingen - Georg-August-Universität Göttingen*, Germany.

Kähler, C. J. and Kompenhans, J. (2000) 'Fundamentals of multiple plane stereo particle image velocimetry', *Experiments in Fluids*, 29 (7), pp. S070–S077. doi: 10.1007/s003480070009.

Kantoush, S. A., Schleiss, A. J., Sumi, T. and Murasaki, M. (2011) 'LSPIV implementation for environmental flow in various laboratory and field cases', *Journal of Hydro-environment Research*, 5 (4), pp. 263–276. doi: 10.1016/j.jher.2011.07.002.

Keane, R. D. and Adrian, R. J. (1992) 'Theory of cross-correlation analysis of PIV images', *Applied Scientific Research*, 49 (3), pp. 191–215. doi: 10.1007/BF00384623.

Keane, R. D. and Adrian, R. J. (1998) 'Optimization of particle image velocimeters: I. Double Pulsed systems', *Measurement Science and Technology*, 2 (10), pp. 963–974. doi: 10.1088/0957-0233/2/10/013.

Kemper, S. and Schlenkhoff, A. (2015) 'Determination of the hydraulic efficiency of intake structures like grate inlets and screens in supercritical flow', *E-proceedings of the 36th IAHR World Congress*, The Hague, The Netherlands.

Kim, Y., Muste, M., Hauet, A., Krajewski, W. F., Kruger, A. and Bradley, A. (2008) 'Stream discharge using mobile large-scale particle image velocimetry: A proof of concept', *Water Resources Research*, 44 (9). doi: 10.1029/2006WR005441.

Kloosterzielt, R. C. and Heijst, N. (1991) 'An experimental study of unstable barotropic vortices in a rotating fluid', *Journal of Fluids Mechanics,* 223, pp. 1–24. doi: 10.1017/S0022112091001301.

Ku, H. and Jun, K. (2009) 'Design of Road Surface Drainage Facilities Based on Varied Flow Analysis', *In: Advances in Water Resources and Hydraulic Engineering*, 2410–245. doi: https://doi.org/10.1007/978-3-540-89465-0_45.

Lecuona, a, Nogueira, J., Rodríguez, P. and Santana, D. (2002) 'Accuracy and time performance of different schemes of

the local field correction PIV technique', *Experiments in fluids*, 33 (6), pp. 743–751. doi: 10.1007/s00348-002-0498-4.

Lee, S., Nakagawa, H., Kawaike, K. and Zhang, H. (2015) 'Urban inundation simulation considering road network and building configurations', Journal of Flood Risk Management, 9 (32), pp. 224–233. doi: 10.1111/jfr3.12165.

Lennon, J. M. and Hill, D. F. (2006) 'Particle Image Velocity Measurements of Undular and Hydraulic Jumps', *Journal of Hydraulic Engineering*, 132 (12), pp. 1283–1294. doi: 10.1061/(ASCE)0733-9429(2006)132:12(1283).

Li, D. X., Zhong, Q., Yu, M. Z. and Wang, X. K. (2013) 'Large-scale particle tracking velocimetry with multi-channel CCD cameras', *International Journal of Sediment Research*, 28 (1), pp. 103–110. doi: 10.1016/S1001-6279(13)60022-0.

Lindken, R. and Merzkirch, W. (2001) 'A novel PIV technique for measurements in multi-phase flows and its application to two-phase bubbly flows', *DLR-Mitteilung*, 33 (3), pp. 991–1003. doi: 10.1007/s00348-002-0500-1.

Liu, Z. C., Landreth, C. C., Adrian, R. J., Hanratty, T. J. (1991) 'High resolution measurement of turbulent structure in a channel with particle image velocimetry', *Experiments in Fluids*, 10 (6), pp. 301–312. doi: 10.1007/BF00190246.

Lloyd, P. M., Stansby, P. K. and Ball, D. J. (1995) 'Unsteady surface-velocity field measurement using particle tracking velocimetry', *Journal of Hydraulic Research*, 33 (4), pp. 519–534. doi: 10.1080/00221689509498658.

Lopes, P., Leandro, J., Carvalho, R. F., Páscoa, P., Martins, R. (2015) 'Numerical and experimental investigation of a gully under surcharge conditions', *Urban Water Journal*, 12 (6), 468–476. doi: https://doi.org/10.1080/1573062X.2013.831916.

Lowe, D. G. (2004) 'Distinctive Image Features from', *International Journal of Computer Vision*, 60 (2), pp. 91–110. doi: 10.1023/B:VISI.0000029664.99615.94.

Malik, N., Dracos, Th., Papantoniou, D.A. (1993) 'Particle tracking velocimetry in three-dimensional flows. Part II: Particle tracking', *Experiments in fluids*, 15 (4), 279-294. doi: 10.1007/BF00223406.

McKenna, S. P., McGillis, W. R. (2002) 'Performance of digital image velocimetry processing techniques ', *Experiments in Fluids*, 32(1), pp. 106–115. doi: 10.1007/s003480100348.

Martins, R., Leandro, J., Carvalho, R. F. (2014) 'Characterization of the hydraulic performance of a gully under drainage conditions', *Water Science and Technology*, 69 (12), 2423–2430. doi: 10.2166/wst.2014.168.

May, R. W. and Todd, A. P. (1997). 'Spacing of road gullies: Initial report, HR Report SR 505', *Prepared by HR Wallingford in association with the Transport Research Laboratory*, London, United Kingdom.

Meynart, R. (1980a) 'Equal velocity fringes in a Rayleigh-Benard flow by a speckle method', Applied Optics, OSA Publishing, 19 (9), pp. 1385–1386. doi: https://doi.org/10.1364/AO.19.001385.

Meynart, R. (1980b) 'Flow Velocity Measurement By A Speckle Method', *in Proceeding of 2nd European Congress on Optics Applied to Metrolog,* Strasbourg, France. doi: 10.1117/12.958310.

Meynart, R. (1982a) 'Convective flow field measurement by speckle velocimetry', *Revue de Physique Appliquée*, 17 (5), pp. 301–305. doi: 10.1051/rphysap:01982001705030100.

Meynart, R. (1982b) 'Digital image processing for speckle flow velocimetry', *Review of Scientific Instruments*. AIP Publishing, 53 (1), pp. 110–111. doi: 10.1063/1.1136808.

Meynart, R. (1983a) 'Instantaneous velocity field measurements in unsteady gas flow by speckle velocimetry', *Applied Optics*. Optical Society of America, 22 (4), p. 535. doi: 10.1364/AO.22.000535.

Meynart, R. (1983b) 'Speckle velocimetry study of vortex pairing in a low-Re unexcited jet', *Physics of Fluids*. AIP Publishing, 26 (8), p. 2074. doi: 10.1063/1.864411.

Muja, M. and Lowe, D. G. (2009) 'Fast Approximate Nearest Neighbors with Automatic Algorithm Configuration', *International Conference on Computer Vision Theory and Applications (VISAPP '09)*, pp. 1–10. doi: 10.1.1.160.1721.

Muja, M. and Lowe, D. G. (2014) 'Scalable nearest neighbor algorithms for high dimensional data', *IEEE Transactions on Pattern Analysis and Machine Intelligence*, 36 (11), pp. 2227–2240. doi: 10.1109/TPAMI.2014.2321376.

Muller, G.U., Kauppert, K. and Bruce, T. (2002) 'Particle image velocimetry: a simple technique for complex surface flows', in *Proceedings of International Conference on River of Fluvial Hydraulics, Riverflow 2002,* pp. 1227–1234, Lisse, Netherlands.

Muste, M., Fujita, I. and Hauet, a. (2010) 'Large-scale particle image velocimetry for measurements in riverine environments', *Water Resources Research*, 46 (4), pp. 1–14. doi: 10.1029/2008WR006950.

Muste, M., Ho, H.-C. and Kim, D. (2011) 'Considerations on direct stream flow measurements using video imagery: Outlook and research needs', *Journal of Hydro-environment Research*, 5 (4), pp. 289–300. doi: 10.1016/j.jher.2010.11.002.

Muste, M., Xiong, Z., Schöne, J. and Li, Z. (2004) 'Validation and Extension of Image Velocimetry Capabilities for Flow Diagnostics in Hydraulic Modeling', *Journal of Hydraulic Engineering*, 130 (3), pp. 175–185. doi: 10.1061/(ASCE)0733-9429(2004)130:3(175).

Nasello, C. and Tucciarelli, T. (2005) 'Dual Multilevel urban Drainage Model', *Journal of Hydraulic Engineering*, 130 (9), pp. 748. doi: 10.1061/(ASCE)0733-9429(2005)131:9(748).

Neenah Foundry Company (NFCO). (2018) 'Drainage grates', *Neenah Construction Castings*, 15th. Edition Catalog.

Nogueira, J., Lecuona, A., Rodriguez, P. A. (1999) 'Local field correction PIV: on the increase of accuracy of digital PIV systems', *Experiments in Fluids*, 27 (2), pp. 107–116. doi: 10.1007/s003480050335.

Nogueira, J., Lecuona, a and Rodríguez, P. a (2001) 'Local field correction PIV, implemented by means of simple algorithms, and multigrid versions', *Measurement Science and Technology*, 12 (11), pp. 1911–1921. doi: 10.1088/0957-0233/12/11/321.

Nogueira, J., Lecuona, A., Rodríguez, P. A., Alfaro, J. A. and Acosta, A. (2005) 'Limits on the resolution of correlation PIV iterative methods. Practical implementation and design of weighting functions', *Experiments in Fluids*, 39 (2), pp. 314–321. doi: 10.1007/s00348-005-1017-1.

Nortek AS (2004) '*User Guide: Vectrino Velocimeter*', *Nortek company*, Norway.

Oertel, H. (ed.) (2010) *'Prandtl's Essentials of Fluid Mechanics'*. *Applied Mathematical Sciences*, Springer, New York, United States. doi: 10.1007/978-1-4419-1564-1.

Oertel, H. (ed.) (2004) 'Prandtl's Essentials of Fluid Mechanics'. *Applied Mathematical Sciences*, Springer, New York, United States. doi: 10.1007/978-1-4419-7055-8.

Offutt, P. W. (1995) 'Development of experimental techniques and studies of spatial structure in turbulent thermal convection', *PhD. Dissetation,* University of Illinois at Urbana-Champaign, Illinois, United States of America.

Osorio-Cano, J. D., Osorio, A. F. and Medina, R. (2013) 'A method for extracting surface flow velocities and discharge volumes from video images in laboratory', *Flow Measurement and Instrumentation*, 33, pp. 188–196. doi: 10.1016/j.flowmeasinst.2013.07.009.

Prandtl L. and Tierjens, O.G. (1957) 'Fundamentals of Hydro-and Aeromechanics', *Book edition of Dover publication inc.*, New York, United States of America.

Prasad, A. K., Adrian, R. J., Landreth, C. C. and Offutt, P. W. (1992) 'Effect of resolution on the speed and accuracy of particle image velocimetry interrogation', *Experiments in Fluids*, 13 (2–3), pp. 105–116. doi: 10.1007/BF00218156.

Raffel, M., Willert, C.E., Wereley, S., Kompenhans, J. (2007) 'Particle Image Velocimetry: A Practical Guide', *Book edited by Springer Berlin Heidelberg,* New York, United States of America.

Raffel, M., Willert, C.E., Wereley, S., Kompenhans, J. (1998) 'Particle Image Velocimetry: A Practical Guide', *Book edited by Springer Berlin Heidelberg,* New York, United States of America.

Rubinato, M., Martins, R. and Shucksmith, J. D. (2018a) 'Quantification of energy losses at a surcharging manhole', *Urban Water Journal*, 15 (3), pp. 234-241. doi: 10.1080/1573062X.2018.1424217.

Rubinato, M., Seungsoo, L., Martins, R. & Shucksmith, J. D. (2018b) 'Surface to sewer flow exchange through circular inlets during urban flood conditions', *Journal of Hydroinformatics*, 20 (3), 564-576. doi: https://doi.org/10.2166/hydro.2018.127.

Rubinato, M., Martins, R., Kesserwani, G., Leandro, J., Djordjević, S., Shucksmith, J. (2017) 'Experimental calibration and validation of sewer/surface flow exchange equations in steady and unsteady flow conditions', *Journal of Hydrology*, 552, pp.421-432. doi: 10.1016/j.jhydrol.2017.06.024.

Russo B., Sunyer D., Velasco M., Djordjević S. (2015) 'Analysis of extreme flooding events through a calibrated 1D/2D coupled model: The case of Barcelona (Spain)', J*ournal of Hydroinformatics*, 17 (3), pp. 473-491. doi: 10.2166/hydro.2014.063.

Russo B. (2009) 'Design of surface drainage systems according to hazard criteria related to flooding of urban areas', *PhD Thesis. Technical University of Catalunya*, Barcelona, Spain.

Russo, B. and Gómez, M. (2014) 'Diseño de sistemas de sumideros en medio urbano', *Book of Macharly.com*, in Spanish.

Russo, B. and Gómez, M. (2011) 'Methodology to estimate hydraulic efficiency of drain inlets', *Proceedings of the ICE - Water Management*, 164 (2), pp. 81–90. doi: 10.1680/wama.900070.

Russo, B., Gómez, M. and Tellez, J. (2013) 'Methodology to Estimate the Hydraulic Efficiency of Nontested Continuous Transverse Grates', *Journal of Irrigation and Drainage Engineering*, 139 (10), pp. 864–871. doi: 10.1061/(ASCE)IR.1943-4774.0000625.

Russam, K. (1969) 'The hydraulic efficiency and spacing of B.S. road gulleys', Ministry of Transport, RRL REPORT LR 277, Road Research Laboratory, Crowthorne, Berkshire. doi: 10.1017/CBO9781107415324.004.

Scarano, F. (2003) 'Theory of non-isotropic spatial resolution in PIV', *Experiments in Fluids*, 35 (3), pp. 268–277. doi: 10.1007/s00348-003-0655-4.

Schmitt, T. G., Thomas, M. and Ettrich, N. (2004) 'Analysis and modeling of flooding in urban drainage systems', *Journal of Hydrology*, 299 (3–4), pp. 300–311. doi: 10.1016/j.jhydrol.2004.08.012.

Seol, D., Bhaumik, T., Bergmann, C., Socolofsky, S. A. and Asce, M. (2007) 'Particle Image Velocimetry Measurements of the Mean Flow Characteristics in a Bubble Plume', *Journal of Engineering Mechanics*, 133 (6), pp. 665–676. doi: 10.1061/(ASCE)0733-9399(2007)133:6(665).

Sharma, N., Balan, S. and Naik, A. A. (2014) 'Video Processing Based Water Surface Velocity Measurement Using Spatial Cross Correlation Technique', *International Journal of Emerging trends & Technology in Computer Science (IJETTCS)*, 3 (2), pp. 233–236.

Smith, M. B. (2006) 'Comment on "Analysis and modeling of flooding in urban drainage systems"', *Journal of Hydrology*, 317 (3–4), pp. 355–363. doi: 10.1016/j.jhydrol.2005.05.027.

Sokoray-Varga, B. and Józsa, J. (2008) 'Particle tracking velocimetry (PTV) and its application to analyse free surface flows in laboratory scale models', *Periodica Polytechnica: Civil Engineering*, 52 (2), pp. 63–71. doi: 10.3311/pp.ci.2008-2.02.

Spaliviero, F., May, R. W. P., Escarameia, M. (2000) *Spacing of road gullies. Hydraulic performance of BS EN 124 gully gratings*, *HR walingford*. London, United Kingdom.

Stagonas, D. and Müller, G. (2007) 'Wave field mapping with particle image velocimetry', *Ocean Engineering*, 34 (11–12), pp. 1781–1785. doi: 10.1016/j.oceaneng.2006.12.006.

Stevens, C. and Coates, M. (1994) 'Applications of a maximised cross-correlation technique for resolving velocity fields in laboratory experiments', *Journal of Hydraulic Research*, 32, pp. 195–212. doi: 10.1080/00221689409498723.

Stucki, P. (1979) 'Advances in Digital Image Processing : Theory, Application Implementation', *Proceedins of the International Symposium in Digital Image Processing 1978*, Germany. doi: 10.1007/978-1-4615-8282-3.

Sutherland, B. R., Dalziel, S. B., Hughes, G. O. and Linden, P. F. (1999) 'Visualization and measurement of internal waves by "synthetic schlieren". Part 1. Vertically oscillating cylinder', *Journal of Fluid Mechanics*, 390, pp. 93–126. doi: 10.1017/S0022112099005017.

Takita, K., Aoki, T., Sasaki, Y., Higuchi, T. and Kobayashi, K. (2003) 'High-Accuracy Subpixel Image Registration Based on Phase-Only Correlation', *IEICE Transactions on Fundamentals of Electronics, Communications and Computer Sciences*, E86–A (8), pp. 1925–1934.

Takita, K., Muquit, M. A., Aoki, T. and Higuchi, T. (2004) 'A sub-pixel correspondence search technique for computer vision applications', *IEICE Transactions on Fundamentals of Electronics, Communications and Computer Sciences*, E87–A (8), pp. 1913–1923.

Tellez, J., Gómez, M., Russo, B., Redondo, J. M. (2016) 'Surface Flow Image Velocimetry (SFIV) for hydraulics applications', in *18th International Symposium on the Application of Laser and Imaging Techniques to Fluid Mechanics,* Lisbon, Portiugal.

Tellez, J., Gómez, M. and Russo, B. (2015) 'Metodología para determinar el campo de velocidades en los imbornales de captación.', in *Seminario Red de Laboratorios de Hidráulica de España Metodología*. pp. 2–3, Coruña, España.

Tellez, J., Gómez, M., Russo, B. and Redondo, J. M. (2015) 'A simple measuring technique of surface flow velocity to analyze the behavior of velocity fields in hydraulic engineering applications.', *Geophysical Research Abstracts - EGU General Assembly 2015*, Vienna, Austria.

Tellez, J., Gómez, M., Russo, B. and Redondo, J. M. (2016) 'Characterize the hydraulic behaviour of grate inlet in urban drainage to prevent the urban's flooding', *Geophysical Research Abstracts, EGU General Assembly 2016*, Vienna, Austria.

Thielicke, W. and Stamhuis, E. J. (2014) 'PIVlab – Towards User-friendly, Affordable and Accurate Digital Particle Image Velocimetry in MATLAB', *Journal of Open Research Software*, 2 (1), p. e30. doi: /10.5334/jors.bl.

Trivedi, N. (2004) 'PTU user's manual, internal report', *IIHR-Hydrosci. and Eng., Univ. of Iowa*, Iowa City, United States of America.

Tsubaki, R., Fujita, I. and Tsutsumi, S. (2011) 'Measurement of the flood discharge of a small-sized river using an existing digital video recording system', *Journal of Hydro-Environment Research*, 5 (4), pp. 313–321. doi: 10.1016/j.jher.2010.12.004.

Velasco, M., Cabello, A., & Russo, B. (2015) 'Flood damage assessment in urban areas. Application to the Raval district of Barcelona using synthetic depth damage curves', *Urban Water Journa*l, 13 (4), pp. 426-440, doi: 10.1080/1573062X.2014.994005.

User Manual Camera (2008) *'User Manual MV-D1280-640 CMOS Area Scan Camera'*. Swiss company Photonfocus.

Weitbrecht, V., Kühn, G. and Jirka, G. H. (2002) 'Large scale PIV-measurements at the surface of shallow water flows', *Flow Measurement and Instrumentation*, 13 (5–6), pp. 237–245. doi: 10.1016/S0955-5986(02)00059-6.

Weitbrecht, V., Socolofsky, S. a. and Jirka, G. H. (2008) 'Experiments on Mass Exchange between Groin Fields and Main Stream in Rivers', *Journal of Hydraulic Engineering*, 134 (2), pp. 173–183. doi: 10.1061/(ASCE)0733-9429(2008)134:2(173).

Westerweel, J., Dabiri, D. and Gharib, M. (1997) 'The effect of a discrete window offset on the accuracy of cross-correlation analysis of digital PIV recordings', *Experiments in Fluids*, 23 (1), pp. 20–28. doi: 10.1007/s003480050082.

Westerweel, J., Elsinga, G. E. and Adrian, R. J. (2013) 'Particle Image Velocimetry for Complex and Turbulent Flows', Annual Review of Fluid Mechanics, 45, pp. 409-436. doi: 10.1146/annurev-fluid-120710-101204.

Willert, C. (1997) 'Stereoscopic digital particle image velocimetry for application in wind tunnel flows', *Measurement Science and Technology*, 8 (12), pp. 1465–1479. doi: 10.1088/0957-0233/8/12/010.

Willert, C. E. and Gharib, M. (1991) 'Digital particle image velocimetry', *Experiments in Fluids*. Springer-Verlag, 10 (4), pp. 181–193. doi: 10.1007/BF00190388.

Wisner, P. E. and Kassam, A. M. (1983) 'OTTSWMM: A model for the analysis of dual drainage system', *IMPSWM urban drainage modelling procedures*, Department of Civil Engineering, University of Ottawa. Canada.

www.virtualdub.org.